Predicting Meniscus Mechanical Properties using Quantitative Magnetization Transfer Magnetic Resonance Imaging

A Thesis Submitted to the College of

Graduate and Postdoctoral Studies

In Partial Fulfillment of the Requirements

For the Degree of Master of Science

In the Department of Mechanical Engineering

University of Saskatchewan

Saskatoon

By

Brennan Berryman

Permission to use

In presenting this thesis/dissertation in partial fulfillment of the requirements for a Postgraduate degree from the University of Saskatchewan, I agree that the Libraries of this University may make it freely available for inspection. I further agree that permission for copying of this thesis/dissertation in any manner, in whole or in part, for scholarly purposes may be granted by the professor or professors who supervised my thesis/dissertation work or, in their absence, by the Head of the Department or the Dean of the College in which my thesis work was done. It is understood that any copying or publication or use of this thesis/dissertation or parts thereof for financial gain shall not be allowed without my written permission. It is also understood that due recognition shall be given to me and to the University of Saskatchewan in any scholarly use which may be made of any material in my thesis/dissertation.

Disclaimer

References in this thesis/dissertation to any specific commercial products, process, or service by trade name, trademark, manufacturer, or otherwise, does not constitute or imply its endorsement, recommendation, or favoring by the University of Saskatchewan. The views and opinions of the author expressed herein do not state or reflect those of the University of Saskatchewan, and shall not be used for advertising or product endorsement purposes.

Requests for permission to copy or to make other uses of materials in this thesis/dissertation in whole or part should be addressed to:

Head of the Department of Mechanical Engineering
57 Campus Drive
University of Saskatchewan
Saskatoon, Saskatchewan S7N 5A9
Canada

OR

Dean
College of Graduate and Postdoctoral Studies
University of Saskatchewan
116 Thorvaldson Building, 110 Science Place
Saskatoon, Saskatchewan S7N 5C9
Canada

Abstract

Osteoarthritis (OA) is a degenerative joint disease that affects the entire knee joint, afflicting approximately 13% of the Canadian population. The meniscus plays a key role in load bearing and stability of the knee joint, and its functionality is compromised throughout OA progression. Currently there does not exist a way to study the relationship between meniscal tissue degeneration and mechanical properties in vivo, but Quantitative Magnetization Transfer Magnetic Resonance Imaging (qMT MRI) is a quantitative MRI technique which may be a good candidate for this application. This is because qMT models soft tissues in a comparable way to how tissues are modeled mechanically, and qMT is dependent on water/macromolecule interactions similar to meniscal tissue functionality. The aim of this project is to assess whether qMT metrics – bound-pool fraction (f), magnetization exchange rate (k), and relaxation times of the free and bound pools (T1f, T2f, and T2b) – accurately predict experimentally-derived mechanical properties – aggregate modulus (Ha) and permeability (kp) – of excised meniscal samples.

Six human cadaver knee specimens were imaged using qMT MRI techniques in order to obtain imaging metrics of the menisci. Subsequent to imaging, 59 core meniscal samples were tested using a stress relaxation approach in a confined compression testing configuration in order to obtain *Ha* and *kp* of the samples as measures of mechanical properties. A Spearman's rho correlation was then performed on the mechanical properties and the imaging metrics of the core samples of the menisci to determine how well the imaging metrics predict the mechanical properties.

One correlation, albeit weak, was found between mechanical properties and qMT metrics (*Ha* and T_{2b}); however, this may be due to homogeneity in meniscal health of the specimens limiting the ability for correlations to be detected. Moderate to strong negative correlations between T_1 relaxation time and *f*, and *k* were found. These relationships should be further explored as T_1 is an often neglected imaging metric, and qMT in the meniscus is quite unexplored. T_1 was found to have a moderate correlation with T_2.

These results reinforce that qMT is viable to use in the meniscus, but that further work needs to be done in order to determine if it can be used as a non-invasive method of assessing meniscal tissue mechanical properties.

Acknowledgements

The number one person who I have to thank is my supervisor Dr. Emily McWalter who was there for me for the duration of my project and its many ups and downs. This project was not a simple undertaking, as she warned me from the beginning. Emily has always been good at motivating me, and she did this brilliantly awful-yet-helpful thing where she let me get stuck just the right amount before prodding me in the right direction. This caused me to think deeply about what I was doing, and to learn through adversity. Emily's friendly and approachable nature combined with her knowledge and ability to teach made my research an enjoyable experience.

Dr. Allan Dolovich has been an excellent advisor and mentor of mine for years going back to undergraduate studies, and this role has been amplified in my research. His unrelenting willingness to help combined with his rare mathematically inclined brain proved to be a deadly combination in helping me sift through some of the exceedingly "mathy" theory of biphasic materials. As any of his students could attest to, it would be easy to fill out pages and pages outlining just how valuable Allan is to academia, and his presence was certainly felt in this project. Without his guidance I surely would still be trying to figure this all out.

Dr. J.D. Johnston has been a great person to look up to as someone who leads by example. His unwavering dedication to his work and his students has permeated throughout our lab group which has created this culture of excellent and collaborative research. We all have high expectations of one another, and are willing to help each other, which has to be majorly attributed to his attitude. JD always had straight answers to my often difficult questions, and his influence on my project was immeasurable. His ICP code was a crucial piece to the puzzle that was my project, and I am grateful for everything he has done.

Lumeng Cui might be one of the MVP's of this project, coming in to save the day in an impossibly heroic feat of creating the qMT fitting code in such a short time-frame when I needed it the most. His MRI knowledge and willingness to help at pretty much anytime is something I am very appreciative of.

My good friend Duncan Boyes saved me from the clutches of the dreaded digitizer by helping me come up with the technique used in this project for converting basic photos to 3D models which were implemented in registration – one of the cruxes of this project.

Rob Peace was extremely valuable helping me with many technical aspects of my apparatus and experimental setup. His extremely practical mind was helpful for figuring out the simplest ways to get things done.

My family (as spread out as they are) have been a constant source of reassurance and support, for which I'm very grateful. Danke schön meine Mutter und Stiefvater aus Deutschland! Thanks to my brother for being my friend online from afar, and my grandma for always having me in mind. I am also grateful for my uncle Darren for being available whenever I need help.

Every single person in my lab group played a role in my project, whether it was directly helping with something in the lab, going out to DQ for blizzards, or simply being someone to play chess with. My thanks goes out to Chantal Kawalilak (your Halloween costume frightened me), Matthew Mcdonald (see you in the mosh pits), Dena Burnette (truly a mentor within the group), Lumeng Cui (unbelievably helpful), Mehrdad Hosseini (such a brilliant mind), Nima Ashjaee (Firouzja 2.0), Tim Gadzella (my partner in crime), Dustin Eichorn (a great example to follow), Mahdi Hosseinitabatabaei (level-headed and calculated), Amy Bunyamin (my true friend), Kadin Macher (Gryffindor personified), Kirstin Olsen (probably the most fun out of us), Ibukun Elebute (a creative spirit), Alvaro Espinosa (multi-talented enigma), Dylan Zaluski (very quick learner), Chelsey Thorson (I'm so grateful for your help in the lab!), Maddie Martel (bright student!), and Josje van Rens (without a doubt one of us).

I would like to thank the engineering machine shops for their expertise and quality of work. I never had a single issue communicating what I needed to them, and it always came out how I wanted in a timely manner.

I also would like to express my gratitude to Merle Friesen for providing bovine specimens for me to practice on in the lab, and obtain some preliminary data.

Last but not least, I want to thank my friends and roommates who have patiently waited for me to complete this marathon. I promise I can game more when this is all over.

Preface

Below are the roles of those involved in my project:

- Brennan Berryman: This is my M.Sc. research project. I was heavily involved in every step of the project, including literature review, experimental design, data collection, and data processing.
- Dr. Emily McWalter was my supervisor for this research project. She acquired funding making this project possible, and was involved in all major project decisions. She provided assistance in data collection and interpretation. Much of the equipment for this project was acquired by her. Dr. McWalter had a large role in developing the MR protocol for this project alongside Lumeng Cui.
- Dr. Allan Dolovich provided his mathematical expertise in the interpretation of Mow's biphasic theory, as well as other models for stress relaxation testing of soft-tissues. His guidance was useful for determining how to model the data in this project.
- Dr. J.D. Johnston gave advice on the experimental process of this project, including specific procedural techniques, and how to interpret the data statistically. He developed the ICP code which was used to register the MR images to point clouds to determine sample locations within the menisci. Much of the equipment used in this project was provided by him and his lab setup.
- Lumeng Cui had a major role for developing the MR protocol for this project. He operated the MR scanner during the image acquisition portion of the project. Lumeng developed the qMT code for this project, which used the MR data as an input and output the qMT parameters. Lumeng's expertise in MRI was used throughout the duration of this project.
- Rob Peace was the Mechanical Engineering Departmental Assistant during this project, and helped with a lot of the technical side of the project. He assisted with equipment configuration, resource allocation, and other miscellaneous problems that we encountered.
- Kirstin Olsen, Alvaro Espinosa, and Chelsey Thorson assisted with specimen dissections and preparations for MR scanning.

- Amy Bunyamin assisted in the lab during initial dissections of bovine specimens.
- Duncan Boyes provided access to 3D printers used for initial practice on image registration and expert recommendations on 3D modelling techniques and software.
- The Engineering Machine Shops constructed the confined compression rig for stress relaxation testing, as well as various other components used in this research.

Table of Contents

List of Figures

List of Tables

List of Abbreviations

- **ACL**: Anterior Cruciate Ligament
- **ADC**: Apparent Diffusion Constant
- **BLOKS**: Boston-Leeds Osteoarthritis Knee Score
- **dGEMRIC**: Delayed Gadolinium Enhanced Magnetic Resonance Imaging of Cartilage
- **GAG**: Glycosaminoglycan
- **MOAKS**: Magnetic Resonance Imaging Osteoarthritis Knee Score
- **MRI**: Magnetic Resonance Imaging
- **MT**: Magnetization Transfer
- **MTR**: Magnetization Transfer Ratio
- **OA**: Osteoarthritis
- **PBS**: Phosphate Buffered Saline
- **PG**: Proteoglycan
- **qMRI**: Quantitative Magnetic Resonance Imaging
- **qMT**: Quantitative Magnetization Transfer
- **RF**: Radio Frequency
- **TE**: Echo Time
- **TKA**: Total Knee Arthroplasty
- **TR**: Repetition Time
- **UTE-T_2**: Ultra-short Echo-Time T_2
- **WORMS**: Whole-Organ Magnetic Resonance Imaging Score

List of Terms

- **Aggregate Modulus (Ha)**: Mechanical property that measures the ability of the solid matrix of a biphasic material to resist compression.
- **Arthroscopy**: A surgical procedure where damaged parts of the meniscus or cartilage are carefully removed from the knee joint.
- **Articular Cartilage**: Soft tissue in the knee joint that is present on the ends of the bones and provides smooth surfaces for the bones to glide over one another.
- **Biomarker**: Something quantifiable in an organism that provides measures of disease progression.
- **Bound Pool Fraction**: The fraction of protons in the soft tissue that are bound to macromolecules.
- **Collagen**: A macromolecule that is very important for the structural integrity of soft tissues.
- **Confined Compression Testing**: A mechanical testing method in which a cylindrical core sample of biphasic material is compressed while in fluid within a confining chamber that prevents radial extrusion, yet allows axial compression, as well as flow of fluid through a porous platen.
- **Creep Testing**: A materials testing method in which a constant force is applied and the change in strain over time is monitored.
- **Dynamic Compressive Modulus**: A mechanical property that measures a material's response to dynamic changes in force.
- **Equilibrium Compressive Modulus**: A mechanical property that measures a material's ability to resist compression while in a state of equilibrium where there is no fluid flow.
- **Ex Situ**: Not in an intact tissue.
- **Ex Vivo**: Not in a living organism.
- **Femur**: The thigh bone; the longest bone in the leg.
- **Histology**: The analysis of micro structure of soft tissues.
- **Indentation Testing**: A mechanical testing method in which an indenter presses into an intact soft tissue at a direction normal to the surface of the tissue.
- **In Situ**: In an intact tissue.
- **In Vivo**: In a living organism.

- **Joint Space Narrowing**: The reduction in space between the femur and tibia commonly seen in osteoarthritis progression.
- **Meniscectomy**: The surgical removal of the meniscus, which is a common treatment for damaged menisci.
- **Meniscus**: A cartilaginous soft tissue of the knee that functions to facilitate smooth motion of the knee joint, as well as load bearing, and stability.
- **Osteoarthritis**: A degenerative joint disease that involves the degeneration of the soft tissues in the joint.
- **Patella**: The knee cap.
- **Permeability (kp)**: A mechanical property that measures the ease with which fluid flows through a material.
- **Proteoglycan (PG)**: A prominent macromolecule in cartilage and the meniscus.
- **Quantitative Magnetization Transfer (qMT)**: A quantitative MRI technique that indirectly provides measures of the macromolecules of soft tissues.
- **Relaxation Times**: MRI metrics which relate to the decay of induced current in a radio frequency coil following radio frequency pulses during image acquisition.
- **Stress Relaxation**: A mechanical testing method in which a strain is applied to a biphasic material, and the stress response is measured while fluid migrates out of the tissue.
- **Tibia**: The shin bone.
- **Total Knee Arthroplasty (TKA)**: A surgery that involves the replacement of the surfaces of the ends of the bones in the knee joint.
- **Unconfined Compression Testing**: A mechanical testing method in which a cylindrical core sample of biphasic material is compressed without any restrictions in lateral extrusion.

List of Symbols

- **B_0**: Permanent Magnetic Field of the MRI scanner
- **B_1**: Magnetism of the protons
- **CV_{RMS}**: Root-Mean-Square Coefficient of Variation
- **E_{eq}**: Equilibrium Compressive Modulus
- **E_{dyn}**: Dynamic Compressive Modulus
- **f**: Bound-Pool Fraction. This is the fraction of protons bound to macromolecules in the tissue
- **G***: Dynamic Shear Modulus
- **Ha**: Aggregate Modulus
- **h_0**: Original Specimen Height
- **k**: Magnetization exchange rate between bound and free pools
- **kp**: Permeability
- **m**: Number of samples
- **M_0**: Magnetic field of a group of protons
- **M_{0B}**: Magnetization of protons in the bound pool
- **M_{0F}**: Magnetization of protons in the free pool
- **M_{eff}**: Effective magnetic field of a group of protons
- **SD**: Standard deviation
- **t**: Time
- **t_0**: Time period in which tissue is compressed
- **t_i**: Stress-relaxation times
- **T_1**: Longitudinal relaxation time
- **T_{1b}**: T_1 relaxation time of the bound pool
- **T_{2b}**: T_2 relaxation time of the bound pool
- **$T_{1\rho}$**: Amount of time it takes for protons to decay after the spin lock pulse is released
- **T_{1gd}**: T_1 relaxation time in the presence of gadolinium contrast agent
- **T_2**: Transverse relaxation time
- **T_{2*}**: T_2, but including effects from magnetic field inhomogeneities.
- **TE**: Echo Time
- **TR**: Repetition Time

- $\boldsymbol{\alpha}$: Scan Power
- $\boldsymbol{\varepsilon}$: Strain
- $\boldsymbol{\varepsilon_0}$: Strain Rate
- $\boldsymbol{\sigma}$: Stress
- $\boldsymbol{\sigma_\infty}$: Equilibrium Stress

1.0 Introduction

The meniscus is an important cartilaginous tissue of the knee. It plays a role in both load bearing and stability [1, 2] and up to 80% of knee loads pass through the meniscus in certain conditions [2]. It is susceptible to degeneration in diseases such as osteoarthritis (OA), where its functionality is compromised.

OA is a degenerative joint disease that affects the entire knee joint, afflicting approximately 13% of the Canadian population [3]. People suffering from OA experience joint pain, stiffness, and mobility deficit and currently there is no cure.

While the entire joint is affected by knee OA, this study focuses on the meniscus which becomes damaged in the OA disease process. Both damage to the meniscus [4-9] and meniscectomies [8, 10-12] are known mechanical risk factors for OA. The meniscus is commonly treated in knee arthroscopy surgery, with almost 5000 procedures performed in Saskatchewan alone in the '15-'16 fiscal year [13]. With OA progression, mechanical integrity of the meniscus decreases. However, there currently is not a way to study the relationship between tissue degeneration and mechanical properties *in vivo*.

The most common way to model the meniscus and its mechanical properties is as a biphasic material, where the soft tissue is considered to be a porous solid matrix with fluid inside of it [14]. A major part of the functionality of the meniscus is to resist compressive forces. The mechanical properties of the tissue can be broken down into how the solid matrix helps resist compression from its geometry and composition, and how fluid flow through the pores causes drag to counteract compression as well.

Imaging techniques are commonly used to assess OA. The primary method of diagnosing OA clinically is via x-ray, which is relatively inexpensive. However, OA assessment using x-ray is limited in that it cannot directly assess changes in soft tissues, such as the meniscus. Magnetic resonance imaging (MRI) provides soft tissue contrast without exposing patients to radiation. It is relatively expensive though, so it is not routinely used clinically for OA, but is becoming a common tool in OA research. In addition to standard MRI techniques which provide us with pictures of the knee tissues, there are quantitative magnetic resonance imaging (qMRI) techniques which provide numerical values. These numerical values are related to proton

behaviour in a magnetic field, but have been linked to soft tissue health and, in a more limited manner, mechanical properties. qMRI techniques have been shown to be useful in OA research for both articular cartilage and the meniscus [15-17].

qMRI techniques have been implemented to explore the relationship between qMRI parameters and mechanical properties of soft tissues with the hope of finding imaging biomarkers for tissue mechanical properties. Most of these studies have been done on cartilage [15-31]. This is underexplored in the meniscus with only two such studies [18, 32], and only one of them being on human tissue [32].

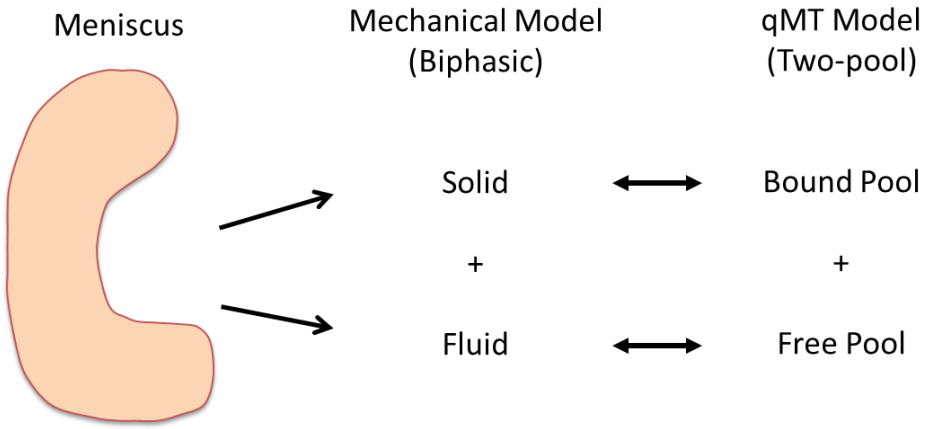

Figure 1.1 - Mechanical and qMT models of the meniscus are very similar. Mechanically, the meniscus is modeled as having a porous solid phase with a fluid phase within it. For qMT, there is a two-pool model which consists of a bound pool of protons (solid phase) and a free pool (fluid phase).

Quantitative magnetization transfer (qMT) is a qMRI technique that may be useful in studying meniscal degeneration and mechanical properties. The way qMT models the tissue is very similar to how we are modeling it mechanically (Figure 1.1); it treats the tissue as having a bound pool of protons attached to macromolecules (solid phase), and a free pool of protons associated with the fluid in the tissue (fluid phase), and probes the interactions between these two pools. Further, macromolecule content in the meniscus decreases with OA progression [33, 34] and water content is vital for normal tissue function due to its role in the tissue's osmotic swelling [35]. Since both qMT MRI and mechanical function are dependent on water/macromolecule interactions, I hypothesize that these parameters will provide an imaging biomarker for mechanical properties of the meniscus. ***The aim of this project is to validate qMT as a non-invasive method of assessing meniscal tissue mechanical properties, a measure of tissue function.***

2.0 Background

In this chapter, I review both healthy (2.1) and osteoarthritic (2.2) knee anatomy in order to understand the disease and its impact. I then review imaging options for the knee (2.3) to show the techniques previously implemented before showing how the technique I used – qMT MRI – is the only one that can assess the bound protons of the tissue which may provide measures more closely related to tissue mechanical properties. Finally, I explore mechanical testing options for assessing the mechanical properties of the meniscus (2.4).

2.1 Healthy Anatomy

In this study, we are focusing on the meniscus in the human knee joint as it is an important soft tissue for normal joint function which becomes compromised in the OA disease process. All of the experimentation in this thesis was done on human cadaver knees, but a basic understanding of healthy anatomy of the knee joint is important for putting this work into context. Here is an overview of the knee anatomy as a whole, as well as some additional attention to the articular cartilage and the meniscus.

2.1.1 General Knee Anatomy

The knee joint consists of two joints: the tibiofemoral joint, and the patellofemoral joint which facilitate flexion and extension motion, as well as some internal and external rotation. Many soft tissues are necessary for facilitating proper function of the knee (Figure 2.1). The knee joint has anterior and posterior cruciate ligaments, as well as lateral and medial collateral ligaments, which guide movement and provide stability. The joint capsule is lined with a synovial membrane, and filled with synovial fluid, which is responsible for delivery of nutrients to the primarily avascular soft tissues of the joint. Two soft tissues of particular importance for knee joint functionality in OA research and for this study are articular cartilage and meniscus.

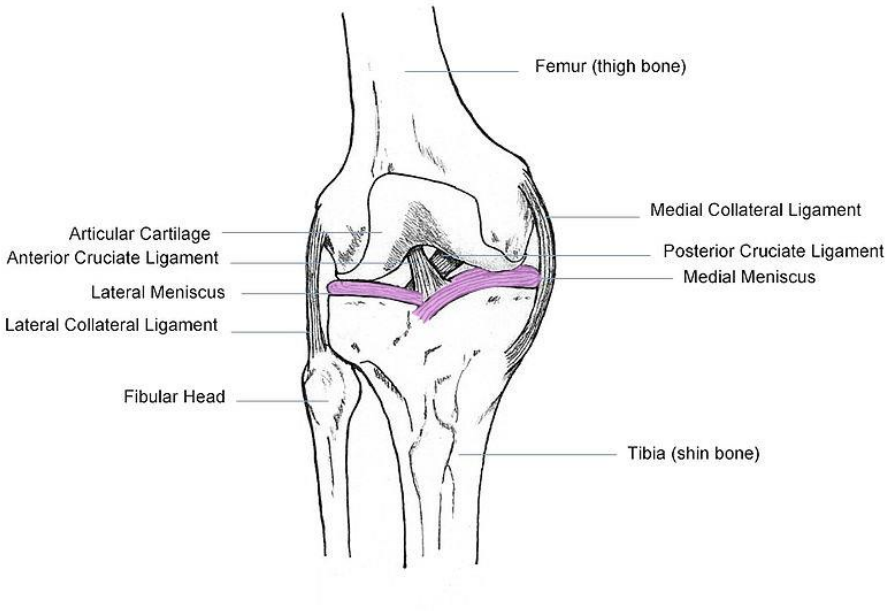

Figure 2.1 - Healthy Knee Anatomy with the Meniscus Highlighted [36]

2.1.2 The Meniscus

The meniscus is a cartilaginous soft tissue in the knee that is attached to the top of the tibial plateau, as shown in colour in Figure 2.1. The meniscus has lateral and medial halves, which are crescent shaped (Figure 2.2, Axial Cross-Section) and exhibit increasing thickness in the radially outward direction (Figure 2.2, Radial Cross-Section). The grey zone in the axial cross-section represents the more vascular region of the meniscus, while the white zone is predominantly avascular. The ability of the meniscus to heal is directly related to the vascularization of the tissue, meaning the radially outer portion of the meniscus has the highest capacity for healing [37]. The meniscus has an important role in both load bearing and stability [1, 2], and up to 80% of loading of the knee passes through the meniscus in certain conditions [2]. The meniscus is susceptible to injury, and commonly treated in knee arthroscopy surgery, with almost 5000 procedures performed in Saskatchewan in the ’15-’16 fiscal year [13].

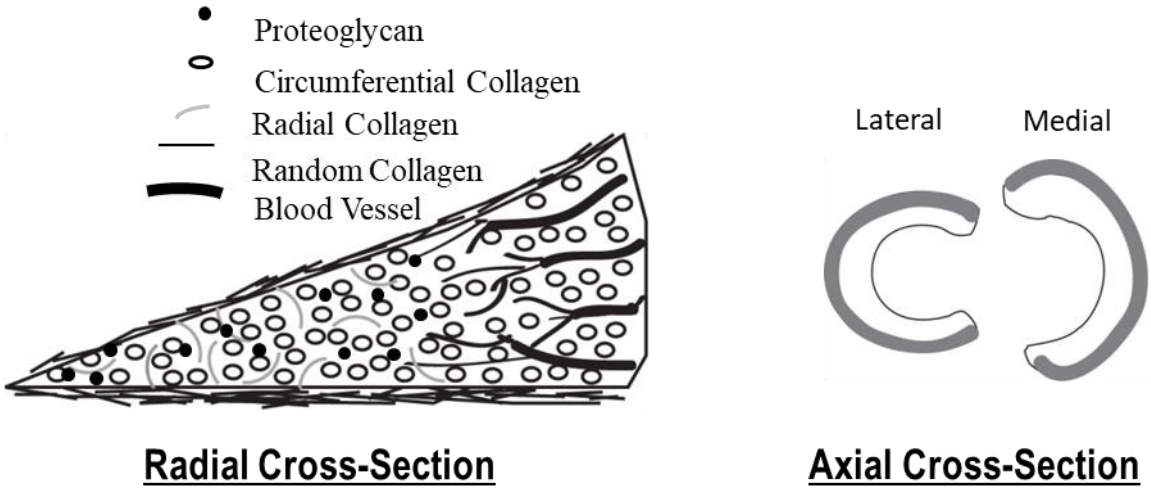

Figure 2.2 - The Meniscus (Courtesy of Emily McWalter)

The macromolecules and water content of the meniscus are crucial for the tissue's mechanical function [35]. Menisci are composed of approximately 60-70% water, 15-25% collagen (mostly type I), and 1-2% proteoglycans (PG's) (Table 2.1). Collagen fibres helps soft tissues resist both tensile and shear forces, while PG's repel each other due to their negative charges, which plays a role in resisting compression [35]. Proteoglycans also require counterions to maintain electroneutrality, which causes the ion concentration to be greater inside the tissue than its surroundings. This leads to osmotic pressure [35] which also contributes to compression resistance. The collagen is primarily oriented in the circumferential direction (Figure 2.2) which enables the tissue to resist hoop stresses enacted on it from axial loading, while the radially oriented tie fibres resist radial stresses and prevent the tissue from separating along circumferential lines (Figure 2.3).

Table 2.1 - Composition of Articular Cartilage and the Meniscus [35]

Component	Cartilage	Meniscus
Water	68-85%	60-70%
Collagen	10-20%	15-25%
Proteglycan	5-10%	1-2%

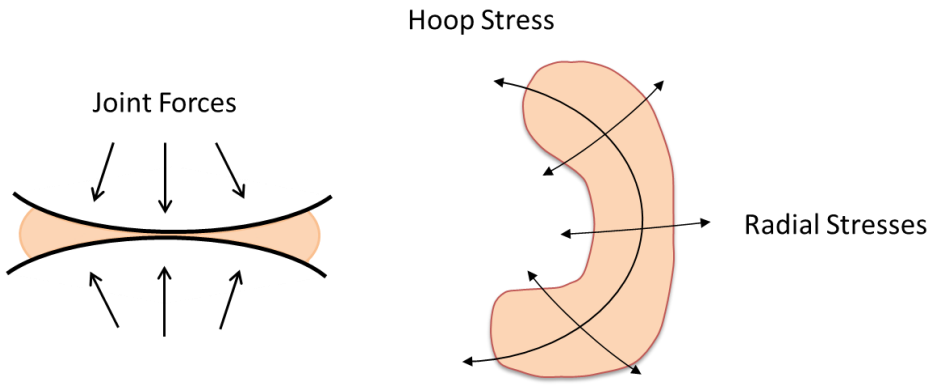

Figure 2.3 - Hoop Stresses and Radial Stresses in the Meniscus from Joint Forces

There are a few mechanical properties of the meniscus which are of interest in this study, including the aggregate modulus (*Ha*), and permeability (*kp*). *Ha* is a biphasic analog to the elastic modulus, but it only considers the solid phase's resistance to compression. *kp* is a measure of the ability of a fluid to flow through a material. A soft tissue with a low permeability – like the meniscus – will experience high drag forces when fluid flows through it. These drag forces are integral in the tissue's resistive quality to dynamic compressive forces.

2.1.3 Articular Cartilage

Articular cartilage covers the articulating surfaces of the knee including femoral condyles, the tibial plateau, and the patella. This is a smooth soft tissue that facilitates the movement of the joint while being responsible for load bearing of the knee joint. Articular cartilage is composed of approximately 68-85% water, 10-20% collagen (mostly type II), and 5-10% PG's [35]. There has been a considerable amount of work done on cartilage in this field, while work on the meniscus is limited. Since articular cartilage is similar to the meniscus in terms of composition and function, it is useful to study for research on the meniscus.

2.2 Osteoarthritis of the Knee

In this section I explore the relevant characteristics of OA so we can understand the effect it has on the healthy anatomy, as well as the impact it has on society.

2.2.1 Disease Characteristics

Throughout the OA process, many different tissues experience alteration. These include the meniscus, articular cartilage, bone, synovial membrane, ligaments, and muscles.

The meniscus is a key soft-tissue in the degenerative process of OA. Not only does the meniscus degenerate with OA [6], but meniscal damage can also lead to OA, as meniscal lesions have been found in 70% of early OA knees [38], and meniscus damage has been associated with the risk of cartilage loss [39]. Additionally, medial meniscus extrusion has been shown to predict radiographic knee OA [40]. The meniscus experiences a decrease in volume, and substance loss with OA progression [41], along with tears and lesions. PG and collagen content are also known to decrease in the degenerative process [33, 34].

During disease progression, thinning and cracking of articular cartilage occurs, and in extreme cases the cartilage wears down enough to expose the underlying bone (Figure 2.4). Early radiographic OA has been shown to be associated with lower cartilage volume [42], and OA severity has been linked with histological degeneration, including PG and collagen [43-45]. Collagen stiffness decreases along with an increase in tissue permeability [46], while total water content in OA cartilage has also been shown to increase by approximately 9% from normal cartilage [47].

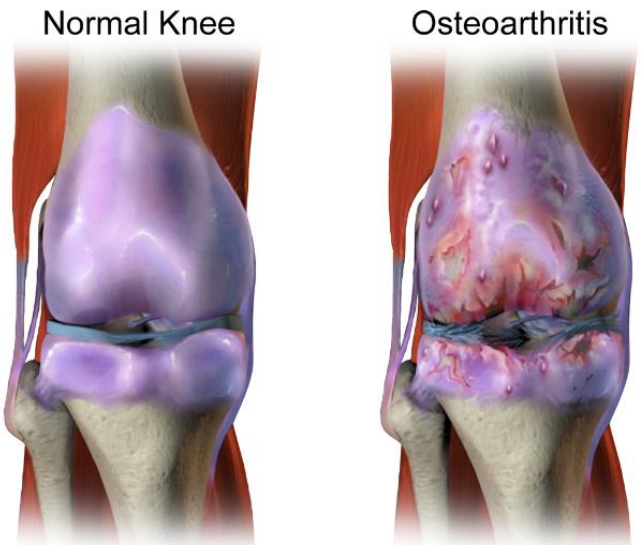

Figure 2.4 – Severely Osteoarthritic Knee [48]

With OA progression, there is often inflammation of the synovial membrane [49], as well as formation of bony protrusions called osteophytes in the subchondral bone [50]. The exact cause of osteophyte formation is unknown, however it may be that there is an association between presence of osteophytes and pain. This is presently under contention though, as there are studies that claim there is a correlation [51], and those that claim its absence [52].

2.2.2 Disease Impact on Mechanical Properties

A few tests have been done on the human meniscus to compare the mechanical properties between healthy and OA tissue. The general trend is that mechanical properties change with OA progression, reducing the ability of meniscus to transmit loads. Compressive moduli such as the equilibrium compressive modulus (E_{eq}) and instantaneous compressive modulus have been found to be lower in more osteoarthritic human menisci obtained as surgical waste from total knee arthroplasty procedures [53]. A decrease in compressive moduli has been shown to be associated with an increase in water content as well, with some cases showing a decrease in PG and collagen content [32]. Similar findings to the human studies have been found in animal OA models, with stiffness moduli decreasing with modeled OA progression in lapine knees along with decreased PG content [54-56].

Since there are so few related studies on the meniscus, we need to look to research on articular cartilage for clues as to how we might expect the meniscus to behave, as they are very similar tissues in terms of content, although organization differs. In articular cartilage, mechanical testing done on healthy and OA populations have shown distinctions between the group mechanical properties. In a review paper on changes in human cartilage with OA, a decrease in stiffness in tension, compression, and shear loading is prominent in OA cases compared to healthy [44]. These changes are accompanied with the deterioration of the collagen-proteoglycan solid network [44], indicating the relevance of macromolecules in tissue mechanical properties. Separately, a study found that OA severity had a strong negative correlation with cartilage elastic modulus [43]. Ovine OA models have previously been used to show that the dynamic shear modulus (G*) is strongly correlated with collagen content [57].

2.2.3 Risk Factors for Osteoarthritis

There are several known risk factors for OA, including body mass index [3-5, 7, 8], age [4], sex [4, 7], ACL reconstruction [8], damage to the menisci [4-9], and meniscectomies [8, 10-12].

The fact that damage to the meniscus and meniscectomies are risk factors for OA demonstrates its importance in the disease. It has been shown that 10-20 years after being diagnosed with meniscus or ACL tears, 50% of individuals will have OA with related pain and functional issues [9]. Additionally, meniscectomies lead to increases in cartilage-to-cartilage

contact area, as well as contact pressure in both cartilage and the meniscus [10]. It has also been shown that about 38% of patients that undergo arthroscopic partial medial meniscectomies either develop or advance in radiographic signs of OA [12].

2.2.4 Disease Impact on Society

OA of the knee is very costly to society, estimated to contribute to about $10 billion in direct health care costs, as well as approximately $17 billion in indirect costs annually [3]. People with OA experience pain and mobility issues, and currently there is no known cure. It is a serious problem for the Canadian workforce as well, with ~30% of workers having difficulty working due to OA [3]. A common intervention for OA is total knee arthroplasty (TKA), with degenerative arthritis being responsible for ~98% of all TKAs in Canada [58]. This is a last resort for patients who have already gone through the painful process of OA, when the joint is severely degenerated. There were over 61,000 TKA surgeries done in 2014-15, which was an increase of approximately 20% from 2009-10 [58].

2.3 Imaging

In this section I look at imaging options for the knee, including x-ray and MRI. I explore OA research findings using these techniques and build up to the quantitative MRI technique called Quantitative Magnetization Transfer (qMT), which this study employs.

2.3.1 X-ray

The primary imaging method for diagnosing OA clinically is via x-ray, which is relatively inexpensive. X-ray is useful in that it can provide morphological assessment of the bones in the knee joint (Figure 2.5). Here we can compare a normal knee to an osteoarthritic knee and clearly see joint space narrowing as well as some osteophytes, which are both characteristics of OA. Joint space narrowing indirectly assesses the cartilage and meniscus that fills the space between the bones, and some of the loss in joint space can be attributed to meniscal extrusion. This demonstrates that although x-ray cannot directly assess all of the soft tissues of the knee joint, radiographic images can still be used to evaluate some features of OA severity, highlighting its clinical usefulness.

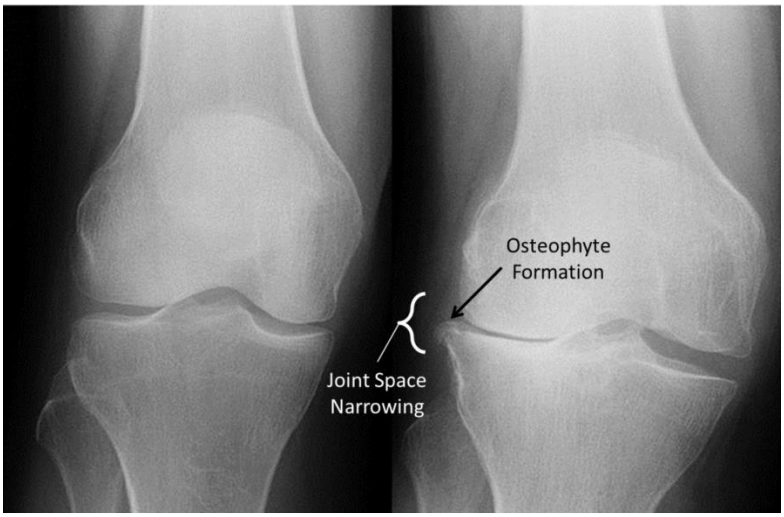

Figure 2.5 - X-rays of Normal (left) and Osteoarthritic (right) Knees. Modified from [59]

The Kellgren-Lawrence grading scheme is a semi-quantitative scoring system which grades radiographic images on a scale of 0-4 in terms of OA severity [60]; it is often used in OA research studies to classify the severity of the disease. The scale is based on osteophyte formation, joint-space-narrowing, and altered shape of bone ends [60]. This grading scheme is useful for assessment of OA severity. However, it does not detect changes in the knee related to OA that happen before gross morphological changes.

2.3.2 Magnetic Resonance Imaging

MRI is a useful imaging technique for assessing OA due to the soft tissue contrast it provides. With MRI, water (hydrogen protons, specifically) in the body is being measured, thus soft tissues – which are primarily composed of water – are visible. For example, the meniscus is composed of 60-70% water [35]. Below in Figure 2.6, the magnetization of a group of protons in MRI is represented. In MRI, protons in the soft tissue (i.e. water) are placed in a strong permanent magnetic field (B_0) which causes them to align with this magnetic fields (M_0) (Figure 2.6-A). A radiofrequency (RF) pulse is applied at hydrogen's resonance frequency which has its own magnetism (B_1) that "excites" the protons and tilts their magnetic fields (M_{eff}) towards the transverse plane at flip angle α (Figure 2.6-B). When the RF pulse is no longer applied, the M_{eff} "relaxes" back towards alignment with the B_0 field (Figure 2.6-C). This relaxation induces a current in the RF receive coils due to the magnetic flux. This process is repeated many times over the desired field of view. An image can be created by taking the spatial frequency data

acquired by the receive coil (k-space data) and converting it to image space using an inverse Fourier Transform.

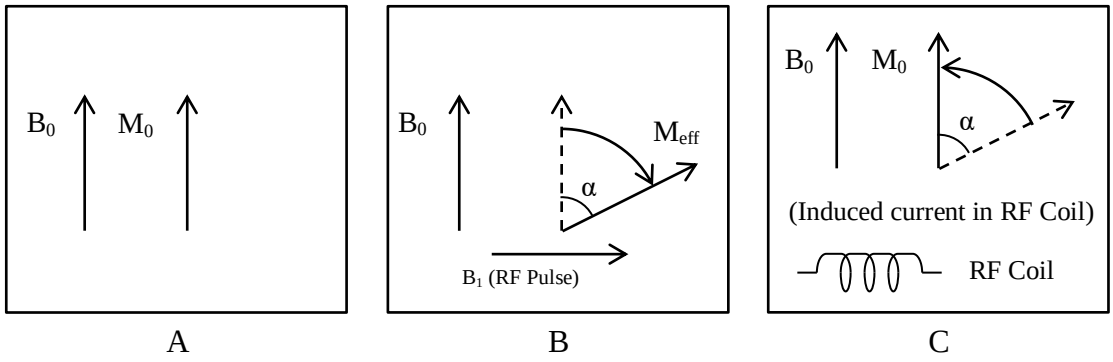

Figure 2.6 - Basic MRI Physics of a Group of Protons. A: The magnetic field of a group of protons (M_0) aligns with the permanent magnetic field of the MRI scanner (B_0). B: M_0 is subjected to a radio frequency (RF) pulse at the resonance frequency of a proton, causing the effective magnetic field of the protons (M_{eff}) to tilt toward the transverse plane at flip angle α. C: When the RF pulse is no longer applied, M_{eff} relaxes back to be in line with B_0. This induces a measurable current in the RF receiver coil. Images can be constructed from the RF coil signals resulting from multiple RF pulses.

By using various sequences of RF pulses, many different forms of contrast in the images can be created. Specific sequences that create strong contrasts between soft tissues are used for morphological assessment (2.3.2.1), while varying contrasts can be used to create quantitative maps of the tissues used in quantitative MRI (2.3.2.2).

2.3.2.1 Morphological Assessment of Osteoarthritis using Magnetic Resonance Imaging

Because of MRI's superior soft tissue contrast, it can enable morphological assessment of the various soft tissues of the knee joint (Figure 2.7). There are several semi-quantitative scoring systems available to evaluate images for OA severity. These scoring systems, such as MRI OA Knee Score (MOAKS), Boston-Leeds OA Knee Score (BLOKS), and Whole Organ MR Score (WORMS) base their scores off of morphological qualities such as osteophytes presence, size of bone marrow lesions and cysts, articular cartilage thickness, size and quantity of osteophytes, synovitis, extrusion, and morphological qualities in the meniscus such as tears [61-63]. These images may be more telling than standard radiography, but they lack the ability to detect early changes in the tissue before gross-morphological (i.e. structural) alterations.

Figure 2.7 - MRI Image of a Knee in the Sagittal Plane [64]

2.3.2.2 Quantitative Magnetic Resonance Imaging

In addition to standard MRI techniques, there are quantitative magnetic resonance imaging (qMRI) techniques that provide different information than morphologic images – they provide numerical values related to proton magnetic behaviour, which can yield useful information about tissue health and mechanical properties. This is valuable as it provides a metric that is not subjective, and not based on morphology, which is important because OA characteristics are present before morphological changes occur.

Several qMRI techniques are used to study musculoskeletal soft tissues such as cartilage and menisci. Some qMRI metrics implemented in OA research include cartilage thickness [65, 66]; T_1 [19], T_2 [65, 66], T_{2*} [18], $T_{1\rho}$ [66], and T_{1gd} [67] relaxation times; gadolinium concentration [68]; and sodium content [69, 70]. T_1 relaxation time is the amount of time it takes for the protons magnetic field to relax back to M_0 in the longitudinal direction (i.e. along the B_0 direction) after the removal of the RF pulse. T_2 relaxation time is similar to T_1, except that it accounts for relaxation in the transverse direction. Below in Figure 2.8 is an example of a qMRI colour map of a human meniscus, where the T_2 relaxation time is measured. T_{2*} is similar to T_2, although it includes the effects from the magnetic field inhomogeneities, and therefore is always shorter than T_2. $T_{1\rho}$ refers to a specific technique where the magnetization is subjected to a second RF pulse parallel to M_{eff} after the initial one, preventing phase decay, termed ‘spin lock’. $T_{1\rho}$ is the time it takes for the protons to decay after the “spin lock” pulse is released. In delayed gadolinium enhanced MRI of cartilage (dGEMRIC), T_1 is used in combination with gadolinium

(T_{1gd}). Gadolinium is a negatively charged intravenous MRI contrast agent which distributes inversely to the negatively charged glycosaminoglycans (GAGs) [68], which are the side-chains of proteoglycans. Sodium MRI is similar to conventional MRI, except it targets sodium atoms in the body rather than hydrogen. In order to do this, a special coil tuned to the Larmor frequency of sodium is required and therefore is not used often.

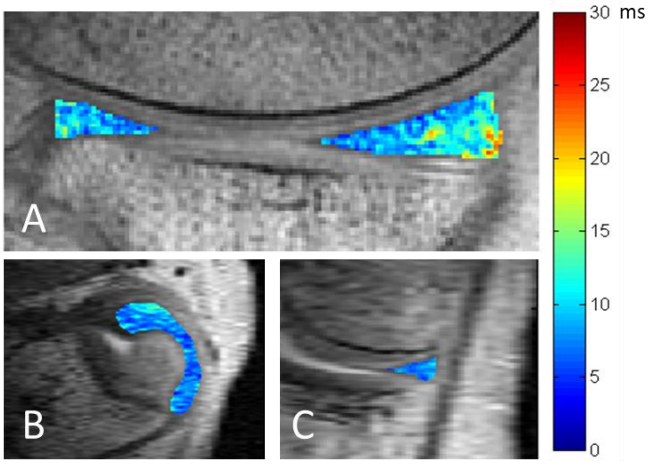

Figure 2.8 – Examples of qDESS T_2 maps of the meniscus in the sagittal (A), reconstructed axial (B), and coronal (C) planes.

The above described qMRI techniques have been implemented in several studies on cartilage and the meniscus in an attempt to correlate with biological materials with varying success (Table 2.2). The correlations found in these studies can be classified as very weak (correlation coefficient = 0 – 0.19), weak (0.2 – 0.39), moderate (0.4 – 0.59), strong (0.6 – 0.79), or very strong (0.8 – 1). To date, T_1 relaxation times have displayed primarily weak correlations [27]. T_2 relaxation times have been used extensively in the literature with a wide range of correlation strengths across various metrics. T_2 relaxation times have had very strong correlations with collagen organization [71], correlations ranging from moderate to very strong with water [32, 72, 73], and very weak to moderate with proteoglycans [32, 74, 75]. Higher cartilage T_2 relaxation times were present in ACL-injury patients 2-4 years post-meniscal repair (at high-risk for OA) compared to those with intact menisci [76]. T_2 has also been able to distinguish between healthy and osteoarthritic knee cartilage [77]. T_{2*} values have been shown to have weak correlations with water content [78], and found to be lower in healthy meniscal tissue in comparison to degenerate tissue [79]. Using *UTE*-T_{2*}, a variation of T_{2*} with a short echo-time, it was found that there were significant elevations of its values in menisci of ACL injured subjects

without clinical evidence of meniscal deficiency [79], which shows that *UTE-T_{2*}* can be useful for subclinical meniscal degeneration assessment. $T_{1\rho}$ has shown strong correlations with water content in the meniscus [32]. $T_{1\rho}$ was generally found to be less sensitive to PG content in the menisci than in cartilage [17, 32, 74, 75, 80], which is likely due to the considerably lower PG content in the meniscus. T_{1gd} can be used to infer the location of PG's [27, 81]. dGEMRIC has been also shown to correlate with collagen and proteoglycan content in cartilage [15]. Lower signal in sodium MRI has been correlated with a decrease in PG [82].

Table 2.2 - Key qMRI Correlations with Biological Materials

qMRI Metric	Biological Material	Correlation Strength				
		Very Weak	Weak	Moderate	Strong	Very Strong
T_1	Proteoglycans		[27]			
	Water					
$T_{1\rho}$	Proteoglycans		[32, 74]		[75]	[17, 80]
	Water				[32]	
T_2	Collagen Organization					[71]
	Water			[32]	[72]	[73]
	Proteoglycans	[32]	[74]	[75]		
T_{2*}	Water		[78]			
T_{1gd}	Proteoglycans				[27]	[81]
Gadolinium Concentration	Proteoglycans			[27]		
Sodium	Proteoglycans					[82]

2.3.2.2.1 Quantitative Magnetic Resonance Imaging and Mechanical Properties

Below in Table 2.3 is a summary of studies that examined relationships between qMRI metrics and mechanical properties of soft tissues. This table shows that there is a wide range of test configurations as well as metrics that have been explored, and a notable variation in correlation strengths.

Table 2.3 - Studies relating qMRI Parameters to Mechanical Properties

Study	Tissue	Tissue	Mech. Test	Mech. Properties	qMRI Parameters	Key Relationship
[21]	Cartilage	Human	Indentation	Stiffness	T_{1gd}	Stiffness-T_{1gd} (r_s=|0.72-0.97|)
[22]	Cartilage	Human	Indentation	E_{eq}, Relaxation Time	T_{1gd}, T_2, ADC	T_{1gd}-E_{eq} (r_s=0.81)
[83]	Cartilage	Human	Indentation	E_0	$T_{1\rho}$	-
[24]	Cartilage	Human	UC	E_{eq}, E_{dyn}	T_{1gd}, T_1, T_2	T_2-E_{eq} (r_s=-0.27) T_{1gd}-E_{eq} (r_s=0.57) T_{1gd}-E_{dyn} (r_s=0.5) [Gd-DTPA]-E_{eq} (r_s=-0.49) [Gd-DTPA]-E_{dyn} (r_s=-0.47)
[15]	Cartilage	Human	UC	E_{eq}, E_{dyn}	T_{1gd}, T_2	T_2-E_{eq} @1.5T (r_s=-0.4) T_2-E_{dyn} @ 1.5T (r_s=-0.45) T_{1gd}-E_{eq} @ 9.4T (r_s=0.43) T_{1gd}-E_{dyn} @ 9.4T (r_s=0.42)
[25]	Cartilage	Human	UC	E_{eq}, E_{dyn}	T_{1gd}, T_2	T_2-E_{eq} @1.5T (r_s=-0.4) T_2-E_{dyn} @ 1.5T (r_s=-0.46) [Gd-DTPA]-E_{eq} (r_s=-0.86) [Gd-DTPA]-E_{dyn} (r_s=-0.64) [Gd-DTPA]-Ha (r_s=-0.74)
[19]	Cartilage	Human Bovine	UC	E_{eq}, E_{dyn}	T_{1gd}, T_1, T_2	T_2-E_{eq} (r_s=-0.71) (Human) T_2-E_{dyn} (r_s=0.88) (Bovine)
[28]	Cartilage	Human	Indentation	E_{eq}, E_{dyn}	T_1, T_{1gd}, T_2, $T_{1\rho}$, MTR	T_2-E_{eq} (r_s=-0.65)
[29]	Cartilage	Human	UC	E_{eq}	ADC	-
[30]	Cartilage	Human	Indentation	Stiffness	T_{1gd}	Stiffness-T_{1gd} (r_s=0.9)
[31]	Cartilage	Human	Indentation	Peak force, Peak E_{dyn}, Energy Dissipation, Phase Angle	$T_{1\rho}$	Phase Angle-$T_{1\rho}$ (r_s=0.91)
[26]	Cartilage	Bovine	UC	E_{eq}, E_{dyn}, Ha	T_2, T_{1gd}	T_2-E_{eq} (r_s=-0.33) T_2-Ha (r_s=-0.34)
[16]	Cartilage	Bovine	Indentation	E_{eq}, Thickness	T_2	-
[17]	Cartilage	Bovine	CC	Ha, kp	$T_{1\rho}$	$T_{1\rho}$-Ha (r_s=|0.91|) $T_{1\rho}$-kp (r_s=|0.93|)
[20]	Cartilage	Porcine	Indentation	Viscosity, Relaxation Time	ADC	Viscosity-ADC (r_s=|0.87|) Relaxation Time-ADC (r_s=|0.83|)
[84]	Cartilage	Engineered	UC	E_{eq}, E_{dyn}	FCD	E_{eq}-FCD (r_s=|0.9|) E_{dyn}-FCD (r_s=|0.84-0.95|)
[85]	Cartilage	Engineered	UC	E_{eq}	T_1, T_2	E_{eq}-T_1 (r_s=-0.76) E_{eq}-T_2 (r_s=0.58)
[18]	Cartilage	Ovine	Tensile	Tensile Failure Load	T_2, T_{2*}	Increase in T_{2*} in torn menisci. Torn and repaired menisci had longer T_2 and lower force to failure in tension tests.
[78]	IVD	Human	Indentation	Residual Stress and Excised Strain	T_{2*}	Residual Stress-T_{2*} (r_s=0.35) Excised Strain-T_{2*} (r_s=0.41)
[86]	IVD	Human	CC	Ha, kp, Swelling Pressure	$T_{1\rho}$	Swelling Pressure- $T_{1\rho}$ (r_s=0.59)
[87]	IVD	Bovine	CC	Ha, kp	T_1, T_2, MTR	kp-T_1 (r_s=0.75) kp-T_2 (r_s=0.78)
[32]	Meniscus	Human	UC, TS	E_{eq}, E_{dyn}, G*	T_2, $T_{1\rho}$	$T_{1\rho}$-E_{eq} (r_s=-0.58) $T_{1\rho}$-E_{dyn} (r_s=-0.62) $T_{1\rho}$-G* (r_s=-0.57) T_2-E_{eq} (r_s=-0.5) T_2-E_{dyn} (r_s=-0.57) T_2-G* (r_s=-0.48)
[18]	Meniscus	Ovine	Tensile	Tensile Failure Load	T_2, T_{2*}	T_{2*} increases in torn menisci. Longer T_2 in torn and repaired menisci with lower force to failure in tension tests.

Legend:
E_{eq} = Equilibrium Compressive Modulus
E_{dyn} = Dynamic Compressive Modulus
Ha = Aggregate Modulus
kp = Permeability
G* = Dynamic Shear Modulus
dGEMRIC = Delayed Gadolinium Enhance Magnetic Resonance Imaging of Cartilage
E_0 = Initial Elastic Modulus MTR = Magnetization Transfer Ratio
UC = Unconfined Compression
CC = Confined Compression
TS = Torsional Shear
ADC = Apparent Diffusion Constant
IVD = Intervertebral Disc
FCD = Fixed Charge Density

Most of the studies that have examined relationships between qMRI metrics and mechanical properties of soft tissues have been on cartilage. T_2 relaxation times have been shown to have weak to strong negative correlations with the equilibrium compressive modulus (E_{eq}) in human tissue [15, 19, 24, 25, 28]. The same correlations were weak to moderate in bovine tissue [19, 26]. Similar correlations with the dynamic compressive modulus (E_{dyn}) have been shown in several of the same studies [19, 24, 25, 28]. This is consistent with expectations based on the previously established association of T_2 with the macromolecules of the tissue. $T_{1\rho}$ has also been very strongly correlated with *Ha* and *kp* [17]. dGEMRIC techniques have been implemented with some conflicting results. T_{1gd} has been shown to have weak to very strong positive correlations with tissue compressive resisting properties in humans such as E_{eq} [15, 22, 24], and E_{dyn} [24]. The concentration of the contrast agent in dGEMRIC in the tissue correlates strongly to very strongly negatively with E_{eq}, and *Ha* [26], which is expected as it negatively correlates with proteoglycan content.

Compared to articular cartilage, there have been few studies on the relationships between qMRI metrics and properties of the meniscus, and only two have involved mechanical properties [18, 32]. It has been shown that there was a significant increase and greater variability in T_{2*} values in the anterior regional menisci of ewes that have had their menisci surgically torn compared to those that had not [18]. Eight months post operation, torn and repaired menisci had longer T_2 values and tended to require lower biomechanical force to cause failure in tension tests compared to menisci that were not operated on [18]. Another study explored $T_{1\rho}$ and T_2 times and their association with human meniscus degeneration. They found that $T_{1\rho}$ and T_2, had moderate inverse relationships with mechanical properties E_{eq}, E_{dyn}, and G* assessed using an unconfined compression approach, as well as moderate and inverse correlations with collagen per wet mass, and moderate correlations with water content [32].

These studies indicate that qMRI shows great promise as a structural, functional and disease imaging biomarker, but further investigation is required, and currently the meniscus is underexplored. Part of the reason behind this is that the meniscus is difficult to image, with short relaxation times due to the bound macromolecules of the tissue. Some conventional qMRI techniques may not be suitable for the meniscus because of limited sampling before the MR signal decays. ***Since macromolecules play a large role in the mechanical properties of the***

meniscus, they may be important to study to understand how the meniscus and its mechanical properties change with OA. This is the reason that we have chosen to work with quantitative magnetization transfer MRI – a technique that can provide assessments of the bound protons of the tissue.

2.3.2.3 Quantitative Magnetization Transfer Magnetic Resonance Imaging (qMT MRI)

qMT MRI is a technique that assesses interactions between hydrogen protons associated with macromolecules and protons associated with the free water in the tissue. This provides an indirect measure of macromolecular content [88] that other qMRI techniques cannot because of very short relaxation times associated with bound protons (on the order of microseconds). The magnetization transfer (MT) effect can be modeled as a two-pool system as shown in Figure 2.9. The free pool consists of the water protons of the tissue with a net magnetization M_{0F}, and protons bound to macromolecules of the tissue with a net magnetization M_{0B}.

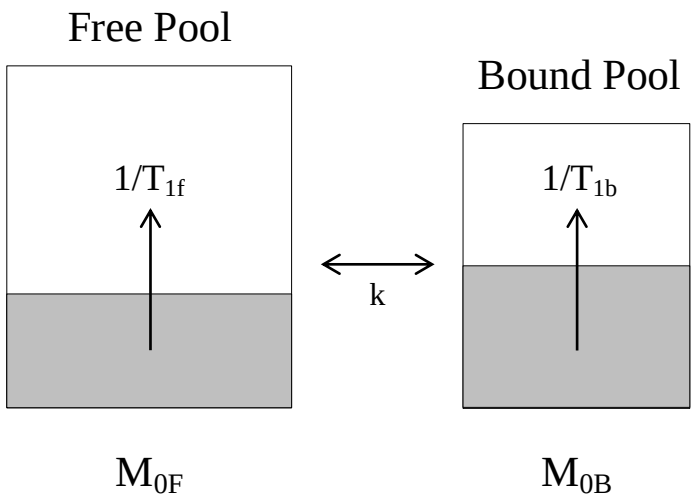

Figure 2.9 - This is a two pool qMT model which contains the protons in the water of the tissue (free pool) and the protons bound to the macromolecules (bound pool). The magnetization of protons in the free pool and bound pool are denoted by M0f and M0b respectively. Using off-resonance frequency RF pulses, the bound pool becomes saturated with magnetism, represented by the shaded portion of the pool. Due to the constant exchange of protons between the pools denoted by the magnetization exchange rate (*k*), the free pool will obtain excited protons, and lose protons aligned with the permanent magnetic field of the scanner, for a decrease in net magnetization. Modified from [88]

The bound pool can be selectively excited using off-resonance RF pulses. This is because the liquid pool is primarily susceptible to excitation from RF pulses near the resonance frequency, while the bound pool can be targeted for excitation at a wider frequency range than

the liquid pool (Figure 2.10) [88]. When the bound pool is saturated with excited protons – denoted by the shaded portion of the pool in Figure 2.9 – magnetization exchange between the pools causes an increase in excited protons in the free pool, thereby decreasing its net magnetization [88]. The MR images capture the magnetization of the free pool, which has been affected by the saturated protons of the bound pool. The relaxation rate of each pool, denoted by $1/T_{1f}$ and $1/T_{1b}$ respectively, are measures of the rates at which each pool reverts back to its normal longitudinal magnetization under the influence of the B_0 field after the RF pulses are no longer applied.

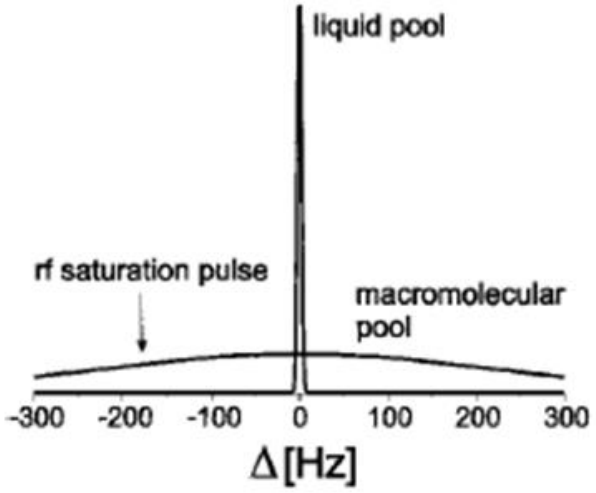

Figure 2.10 - Absorption susceptibility of the liquid and macromolecular pools of soft tissues [88].

The relaxation of the free pool can be interpreted to obtain information on the bound pool [88]. This is done by acquiring data at several off-resonance frequencies and multiple MT flip angles (MT flip angle is a term referring to the power of the RF pulses, opposed to flip angle α which is in regards to the proton's magnetization tilt into the transverse plane) to obtain images with varying MT weighting. These images are then used together to fit a mathematical model from which qMT parameters are obtained [89]. The key parameters found using qMT MRI are the magnetization exchange rate between the bound and free pools (k), the bound-pool fraction (f), and both the longitudinal and transverse relaxation times of the bound pool (T_{1b} and T_{2b}). In any sequence where magnetization transfer occurs, the Magnetization Transfer Ratio (MTR) can

also be calculated, which is a comparison of the signal in images with and without MT weighting [88].

There has already been some qMT research done on soft tissues. It has been shown that the qMT parameter *k* is sensitive to Alzheimer's Disease – another degenerative soft tissue disease from which macromolecules can be used as biomarkers [90] – showing significantly reduced values in Alzheimer's Disease patients [91]. qMT metrics have been compared to structural content of cartilage and found that *f* had a moderate correlation with proteoglycan content, while both *k* showed a moderate correlation with collagen [92]. It has also been found that *k* was significantly lower in patellar cartilage of OA patients compared to healthy, while T_{2b} was significantly higher [93]. Overall, these results have shown that qMT metrics are sensitive to macromolecular content and can distinguish between OA and healthy groups, making qMT a promising tool for assessing changes in soft tissue during early OA. To date, no study has related qMT to mechanical properties of soft tissues.

There has only been one qMT study done on the meniscus, and it was by collaborators at McGill University [89, 94]. This study successfully obtained qMT results in the meniscus and provided proof of concept that the meniscus demonstrates the MT effect and qMT parameters can be assessed for the meniscus. The qMT values from this study can be viewed in Table 2.4 below. It can be seen how much shorter T_{2b} times are than the other relaxation times, which is why this parameter needs to be determined using special techniques such as qMT.

Table 2.4 - qMT Values from Simard's Study

Tissue (n = 4)	f (%)	k (s^{-1})	T_1 (ms)	T_{1f} (ms)	T_{2b} (μs)
Lateral Meniscus	21.86 ± 2.51	2.26 ± 0.59	698.6 ± 120	783.1 ± 177.3	5.74 ± 0.74
Medial Meniscus	26.76 ± 2.82	2.67 ± 0.64	611.6 ± 85.9	661.0 ± 166.6	5.50 ± 0.95
Both Menisci	23.36 ± 2.41	2.38 ± 0.35	663.9 ± 90.9	736.2 ± 156.0	5.65 ± 0.81
Tibial Cartilage	16.24 ± 1.23	2.87 ± 0.58	763.0 ± 128.9	815.8 ± 189.5	4.97 ± 0.42
Femoral Cartilage	15.47 ± 0.68	3.11 ± 0.78	805.1 ± 128.9	881.5 ± 191.3	5.37 ± 0.36
Patellar Cartilage	12.99 ± 0.68	2.82 ± 0.64	904.5 ± 143.9	977.4 ± 225.5	5.56 ± 0.20
Whole Cartilage	15.19 ± 0.61	3.00 ± 0.69	813.3 ± 117.2	882.8 ± 186.2	5.30 ± 0.17

If there is a correlation found between the qMT parameters and mechanical properties of the meniscus and macromolecular content, it would yield an imaging biomarker for meniscal function. Biomarkers using qMT parameters would be particularly useful as they would be

associated with macromolecules of the tissue, providing a more direct link to tissue functionality and how it deteriorates with disease progression. Being able to monitor functional changes would enable the assessment of the efficacies of OA treatment strategies by evaluating their effect on the tissue's function over time.

2.4 Mechanical Testing of Soft Tissues

Mechanical testing of the meniscus is necessary in this project in order to see if qMT can be used to non-invasively assess mechanical properties of the tissue. When mechanically testing articular cartilage and meniscus, it is common to model them according to Mow's Biphasic Theory [14]. Similar to qMT, Mow's theory treats the tissue as having two phases: a solid porous phase, which is filled with a fluid phase. This is an important consideration to make, as there is a dynamic effect to take account of during testing where the fluid flows through the tissue, as well as exudes out of the slightly permeable solid phase, resulting in a resistive drag force. In this section I touch on the two main mechanical tests done on biological soft-tissues: creep and stress-relaxation testing, outlining why we have chosen the latter. Afterwards, I review the three testing configurations: indentation, unconfined compression, and confined compression testing, reasoning out why we have chosen the confined compression option.

2.4.1 Creep Testing

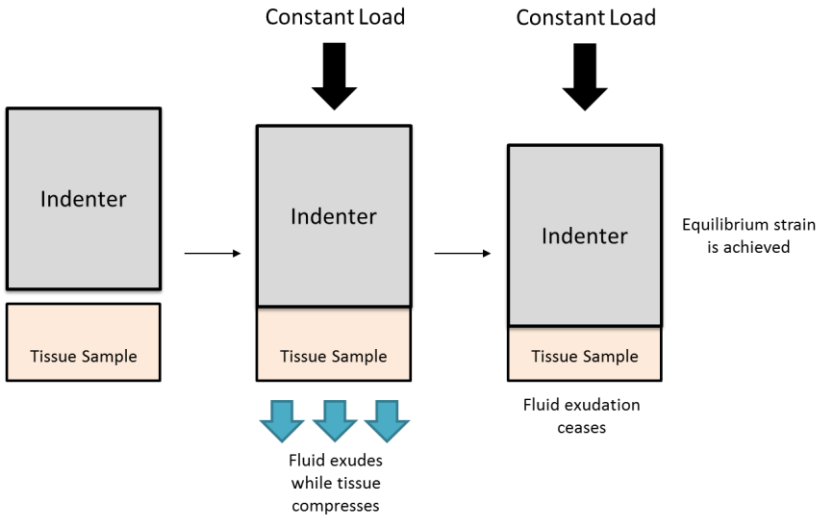

Figure 2.11 - Creep Testing

Creep testing is a force-controlled test (Figure 2.11), where the tissue is compressed with a defined load. This loading is maintained while fluid exudes out of the tissue, enabling further

compression until an equilibrium displacement is reached. The data from these tests can be fit to mathematical models to obtain physical parameters of the tissues being tested [95-97].

Implementing creep testing is somewhat challenging as it is not trivial maintaining a constant force on a sample. The load would be constantly changing as the fluid exudes out of the tissue, so the controller would have to update the actuator position to maintain the desired load. Continually updating the actuator position would introduce risks with damaging the sample, particularly because we only had access to an electrically controlled system which does not provide position control as fine as a hydraulic system would.

2.4.2 Stress-relaxation Testing

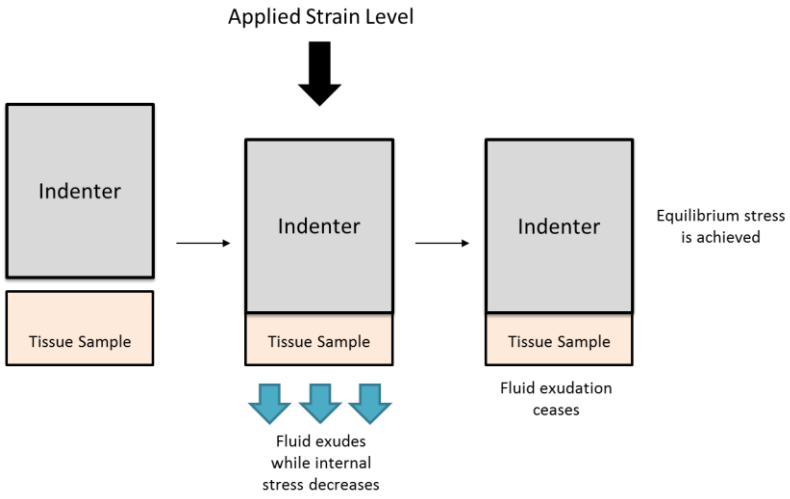

Figure 2.12 - Stress-Relaxation Testing

Stress-relaxation testing uses a position controlled test, where the tissue is compressed and held at a strain level (Figure 2.12). While held in place, the fluid exudes out reducing the stress in the tissue until an internal equilibrium stress is reached. Similar to creep testing, the data from a stress-relaxation test can be fit to mathematical models to obtain mechanical properties of the tissues being tested and it is often implemented in the relevant literature [19, 24, 32, 96, 98-105].

I opted to implement stress-relaxation over creep testing for simplicity and safety. It is simple because the actuator moves to a position and holds it there in place, compared to creep where the actuator would have to constantly adjust to be at the correct force level. It is safer because during creep testing it is possible for samples to be overloaded and damaged if the

actuator were to compress it too far during adjustments. For our system, if the actuator is off by 0.01mm from the target position, a warning will be given, which gives me confidence in the accuracy of the test.

2.4.3 Indentation Testing

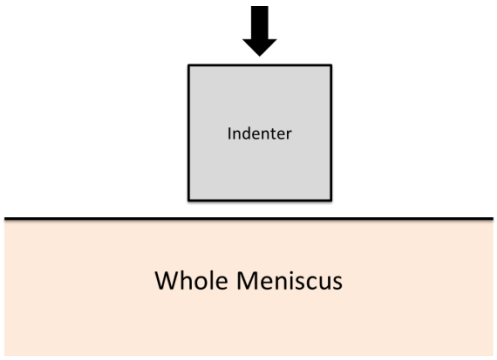

Figure 2.13 - Indentation Testing

Indentation testing involves pressing on the surface of an intact tissue with an indenter (Figure 2.13). Indentation testing is advantageous in that it involves testing on a tissue that is intact, opposed to core samples. It also has a fairly simple sample preparation process, as the tissue is left intact. Conversely, testing the tissue intact means that the boundary conditions for the test are rather complex and it is difficult to represent this mathematically, opposed to confined compression testing where there is a rigid cylinder surrounding the core sample defining the boundary. I have not found any studies addressing how far away from the indenter deformation would occur, and how this would affect the boundary conditions. Additionally, the indenter is required to be normal to the tissue surface during testing, which can be challenging to ensure without a specialized system or sample mounting device. It is another common method used to determine mechanical properties of soft-tissues [22, 31, 46, 95, 106].

2.4.4 Unconfined Compression Testing

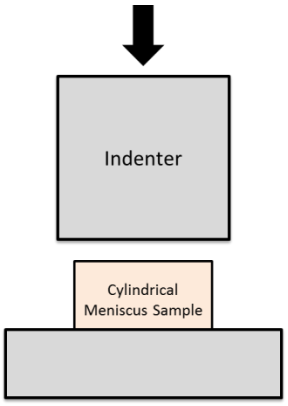

Figure 2.14 - Unconfined Compression Testing

Unconfined compression testing involves the testing of cylindrical core samples from the tissue. The sample sits on a flat testing platform and is compressed from above, while being allowed to expand outwards laterally (Figure 2.14). Unconfined compression testing has a relatively simple set-up, and is fairly easy to model mathematically due to the simple boundary conditions. It is also widely implemented in the literature [24, 32, 95, 101, 103, 107], so there is ample data to compare to. The main drawback of unconfined compression testing is that it is not an accurate representation of an in-situ tissue, as any core sample would have its lateral expansion resisted by surrounding tissue if it were still intact. I have chosen not to implement unconfined compression testing because of this reason.

2.4.5 Confined Compression Testing

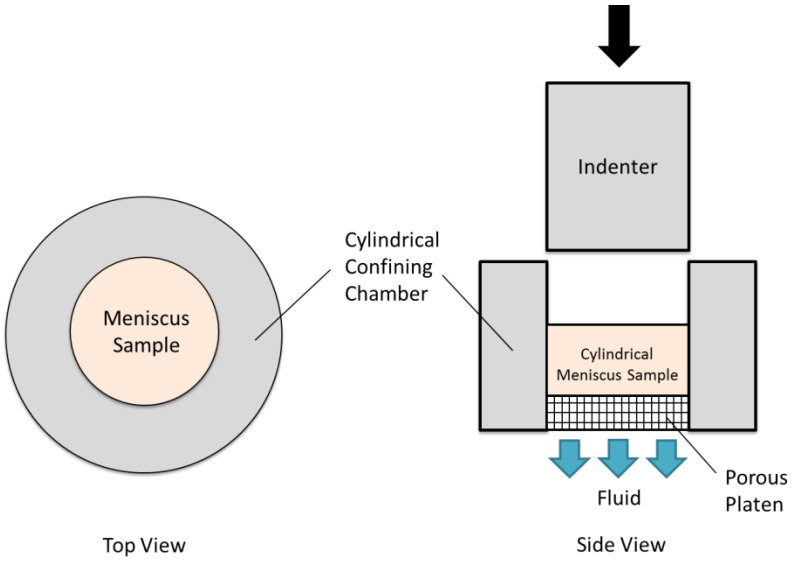

Figure 2.15 - Confined Compression Testing

Confined compression testing is similar to unconfined compression testing, except that the cylindrical samples are tested in a confining chamber (Figure 2.15). The cylindrical chamber has solid walls, preventing lateral expansion. The tissue sits on a porous platen which facilitates the fluid flow during compression. The main attractive quality of confined compression testing is that it is somewhat of a compromise between the other two testing methods; it is more representative of an in-situ environment than unconfined compression testing, while being easier to implement than indentation testing. Similar to unconfined compression, there is a significant amount of relevant literature to explore [96-100, 102, 104, 105, 107-109]. This is the mechanical testing method that I chose to implement in this study due to the positives mentioned above.

2.4.6 Data Models

The data obtained from confined compression testing had to be fit to a mathematical model in order to obtain physical meaning from them. Most of the models in the literature base their model off of Mow's biphasic theory [14], usually with some changes. The models explored for this project will be described in detail in the Methodology section.

2.5 Hypotheses

With tissues of varying health, I expect to see differences in tissue functionality being reflected in the mechanical properties of the meniscus, as well as the qMT metrics. With more

degenerated tissues, there will be lower *Ha* values as the solid matrix will be less able to resist compression. This should be accompanied by an increase in *kp*, as fluid flow will be less restricted by the further degenerated solid matrix. Since *f* describes the proportion of protons bound to macromolecules, I expect it to decrease with tissue degeneration because the solid matrix will be progressively damaged and the percentage of water content has been shown to increase with damage [47, 110]. Magnetization exchange (*k*) is both chemical and dipolar in nature and it is difficult to suggest and test how this parameter might change with tissue degeneration. T_2 relaxation times have been found to be significantly higher in OA cartilage samples compared to healthy samples [27, 111, 112]. T_1 relaxation times have both been shown to increase [27] and decrease [113] with degeneration, making it difficult to predict how this metric will behave, but it is possible T_1 is driven by similar macromolecules as T_2, so it could be they respond similarly. T_{1f}, T_{2f}, and T_{2b} relaxation times are likely to respond to degeneration similarly to T_1 and T_2. Because of the above reasoning, I hypothesize the correlation signs shown in Table 2.5.

Table 2.5 - Correlation Prediction

Independent Variable	Dependent Variable	Predicted Correlation Sign
Ha	kp	-
Ha	f	+
Ha	k	?
Ha	T_{1f}	-
Ha	T_{2f}	-
Ha	T_{2b}	-
kp	f	-
kp	k	?
kp	T_{1f}	+
kp	T_{2f}	+
kp	T_{2b}	+

2.6 Summary

OA of the knee is a degenerative joint disease that is prominent in Canada. Currently there is no cure for the disease, and treatment options for those afflicted by it are limited.

The meniscus is a soft-tissue that is important in the OA process, and comparable to articular cartilage in terms of composition. However, there has been comparatively little work investigating the potential of qMRI parameters as biomarkers for OA in the meniscus.

qMT is an MRI technique that has shown promise in having correlations with tissue macromolecules and hydration. It is the only qMRI technique that can properly assess bound protons of the meniscus as others are hindered by short relaxation times associated with the macromolecules of the tissue. Because macromolecule relative content and interactions with water are closely related to tissue mechanical properties, the measures closely related to macromolecules could be linked with tissue mechanical properties. Unlike other qMRI methods, qMT models the meniscus in a similar way to how I am modeling it mechanically (biphasic) which should give it a strong link to mechanical properties. This study investigates the potential of qMT parameters as biomarkers for meniscus functionality by relating qMT scan parameters to mechanical properties found via confined compression stress relaxation tests.

If there is a correlation found between the parameters and mechanical properties of the meniscus, it would yield an imaging biomarker for meniscal function. This has the potential to improve our understanding how tissue function deteriorates with disease progression. Importantly, being able to monitor mechanical properties of the meniscus non-invasively over time could help with the development and objective evaluation of OA treatment strategies.

2.7 Research Question & Objective

This study can be described in one research question: can qMT be implemented as a non-invasive method of assessing meniscal mechanical properties? To address this question, the objective of this research is to assess whether qMT metrics (e.g., f, k, T_{1b}, and T_{2b}) accurately predict experimentally-derived mechanical properties (e.g., Ha and kp) of excised meniscal samples.

3.0 Methodology

Figure 3.1 below represents the methodology pipeline for this project for each of the six cadaver knees. The aim of this project was to determine if qMT can be used to predict mechanical properties of the meniscus. In order to do this, for every knee I needed to obtain qMT parameters for each core sample, and perform a correlation with the mechanical properties.

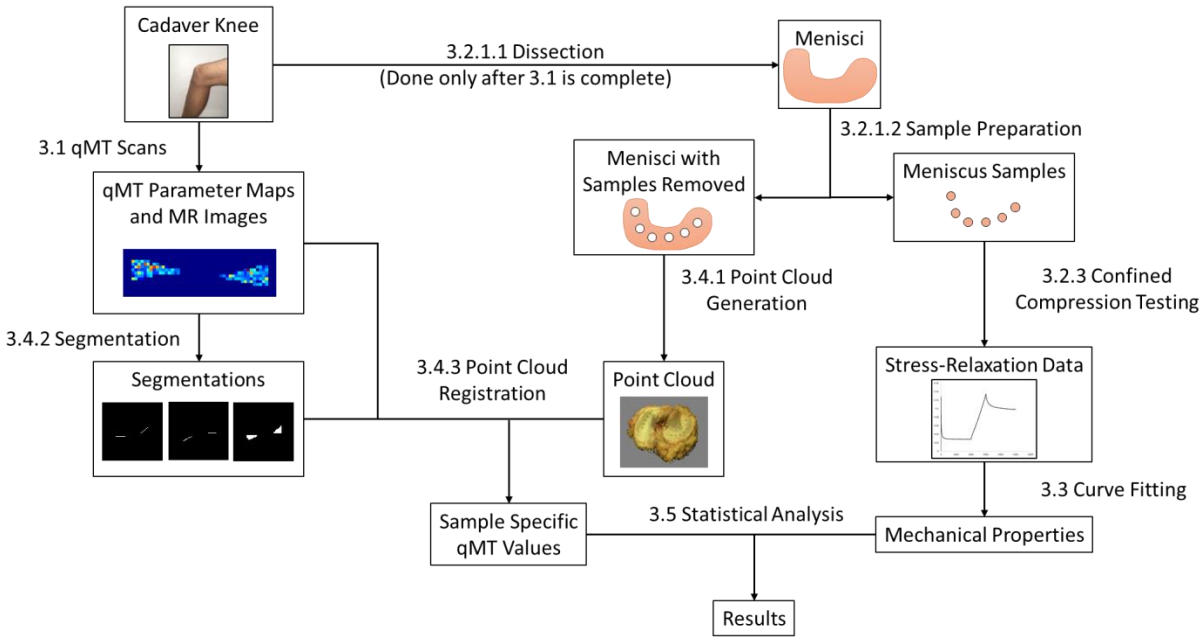

Figure 3.1 - Project Pipeline

This process began by acquiring a series of MRI scans on intact cadaver knee joints to obtain qMT parameter maps of menisci (3.1). These images were subsequently segmented to give the meniscus masks necessary for determining sample specific parameter values and for registration purposes (3.4.2). After scanning, the knees were dissected to provide access to the meniscus (3.2.1.1). Small cylindrical core samples were then procured from the tissue (3.2.1.2), which provided both the samples and the meniscus with the samples removed from it. The samples themselves went through mechanical testing in order to obtain their mechanical properties (3.2.3, and 3.3). The remaining menisci were photographed at many different angles and packaged software was used to create a point cloud of the tissue (3.4.1). This point cloud was then registered with the qMT parameter maps (3.4.3). After registration, relationships

between qMT parameters and mechanical properties were assessed using a Spearman's rho analysis (3.5).

3.0.1 Specimens

In this study, meniscus samples were procured from 6 cadaver knees (Science Care, Inc., Phoenix, AZ) for testing. Of the knees tested, 3 were male and 3 female, 3 were left knees and 3 were right, while the mean age was 70.3 ± 9.3 years. The knees had no history of injury or surgery.

3.1 MRI Scans and Image Processing

All MRI scans were carried out on a 3T system (MAGNETOM Skyra, Siemens Healthcare, Erlangen, Germany). Scans were acquired to carry out qMT and T_2 relaxation time mapping.

To acquire the required scans for qMT parameter mapping a custom sequence was required. A PhD student from our group (Lumeng Cui) developed the sequence using a product GRE sequence as its basis in vendor specific software (IDEA, Siemens Healthcare, Erlangen, Germany). This allowed us to acquire images with MT contrast; specifically we were able to modify the duration of the MT pulse, modify the MT flip angle (also known as "power", and different from flip angle α), and modify the frequency offset. The MR imaging protocol involved a series of scans:

1. Scans for T_1 relaxation time mapping: 4 scans were acquired with 4 different flip angles (α = 5°, 10°, 20°, and 30°) using a Spoiled Gradient Recalled Echo (SPGR) sequence, with FOV = 160x160mm^2, Repetition Time and Echo Time (TR/TE) = 26/3.22ms, a 256 x 256 matrix, and 0.625mm x 0.625mm x 3mm voxel size at 3.0T.
2. MT scans: 10 scans were acquired with 2 different MT flip angles (142° and 426°) and 5 offsets (433Hz, 1087Hz, 2732Hz, 6862Hz, and 17235Hz), with FOV = 160x160mm^2, TR/TE = 48/3ms, a constant flip angle α = 10°, a 256 x 256 matrix, and 0.625mm x 0.625mm x 3mm voxel size at 3.0T. The low and high MT flip angles were performed alternately to avoid exceeding Specific Absorption Rate (SAR) limitations. Scans without MT pulse were done at the beginning, middle, and end of the experiment to monitor the potential drift in the data due to scanner heating. The scan protocol can be seen in **Error! Reference source not found.** in ppendix A – qMT Sequence.

3. Scans for B_1 mapping: 2 scans we acquired with 2 different flip angles (α = 60°, and 120°) using an SPGR sequence, with FOV = 160x160mm^2, TR/TE = 6000/3.58ms, a 256 x 256 matrix, and 0.625mm x 0.625mm x 3mm voxel size at 3.0T.
4. Scans for T_2 mapping: One custom multi-echo steady state sequence (MEDESS) [114] was used with FOV = 160x160mm^2, TR = 17.85ms, four echo times of TE = 3.03, 6.92, 8.88, 12.72ms, ΔTE = 2ms, a constant flip angle α = 30°, a 256 x 256 matrix, and 0.625mm x 0.625mm x 3mm voxel size at 3.0T.

Image Processing

The T_1 relaxation maps were obtained using a variable flip angle technique called Driven Equilibrium Single Pulse Observation of T_1 (DESPOT1) [115]. In this technique, T_1 is determined from a series of SPGR images using multiple flip angles with a constant TR. The following signal model is used:

$$\frac{SI_{SPGR}}{\sin\alpha} = \frac{SI_{SPGR}}{\tan\alpha}E_1 + M_{leq}(1 - E_1)$$

$$E_1 = \exp(-\frac{TR}{T_1})$$

where SI_{SPGR} = Signal Intensity, α = Flip Angle, and M_{leq} = Factor proportional to the equilibrium longitudinal magnetization. Plotting $SI_{SPGR}/\sin\alpha$ versus $SI_{SPGR}/\tan\alpha$ allows T_1 to be calculated from the slope of this line as:

$$T_1 = -\frac{TR}{\ln(slope)}$$

qMT parameter maps (k, f, T_{1f}, T_{2f} and T_{2b}) were modeled using methods reported previously [89]. Briefly, data from the ten MT contrast images were fit to both Super-Lorentzian and Gaussian line shapes (Figure 3.2). Most often Super-Lorentzian line shapes are used; however, in some cases Gaussian line shapes may be more appropriate for the macromolecules of the bound pool [116, 117]. Therefore, both analyses were done and the results from both models were assessed. The equations for both line shapes can be seen in Appendix G – qMT

Line Shapes. I assumed T_{1b} = 1s, as this is commonly done to provide a more robust fitting to the other qMT parameters and has been shown to have negligible effect on the model [118].

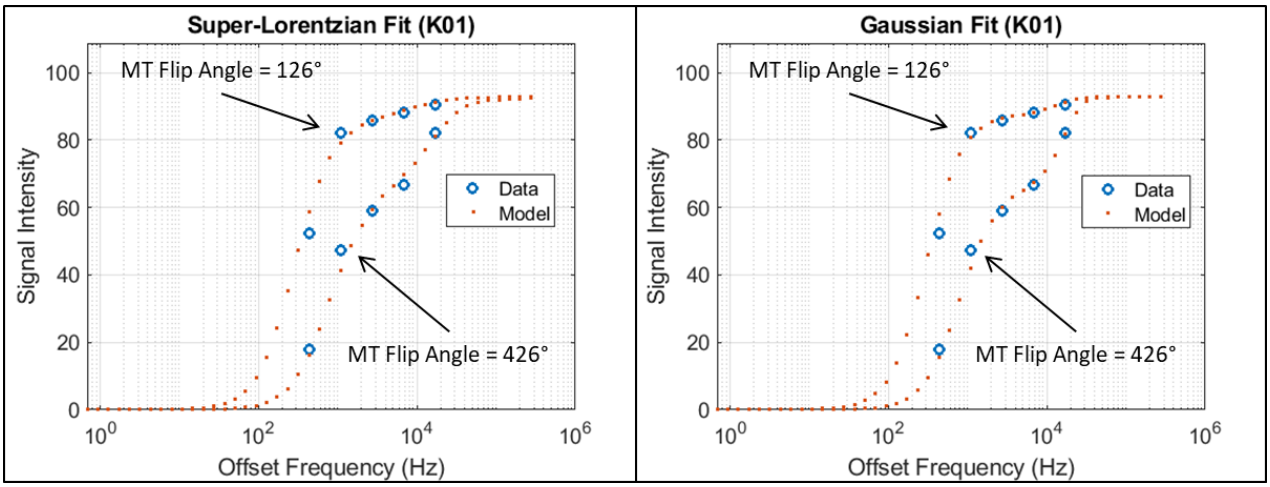

Figure 3.2 – Comparison of Super-Lorentzian and Gaussian Line Shape Fits on Specimen K01. The upper set of data on each figure has MT Flip Angle = 126°, while the lower set of data has MT Flip Angle = 426°.

With T_1 maps acquired and T_{1b} set to 1 second, the remaining qMT parameters T_{1f}, T_{2f}, T_{2b}, k, and f were obtained by fitting data to the two pool model [89] using custom software (Matlab, MathWorks, Natick, MA) written by a PhD student in our group (Lumeng Cui).

In order to obtain the Magnetization Transfer Ratio (*MTR*), the image with the greatest MT effect (MT flip angle of 426° and an MT frequency offset of 433 Hz) was used along with the MT-off image. *MTR* is defined for each voxel as:

$$MTR = \frac{M_0 - M_{sat}}{M_0},$$

where M_0 = the voxel's signal without magnetization saturation, and M_{sat} = the voxel's MT-weighted signal [88].

B_1 maps were obtained to correct for any errors in the flip angle in the qMT parameter fitting process. The B_1 field refers to the magnetic field introduced by the applied radio frequency pulses in the scanner. These values have inhomogeneities in their fields which needed to be quantified. In order to account for B_1 field inhomogeneities, a standard double angle technique [119] was implemented to obtain an adjustment factor for each individual voxel.

The T_2 relaxation time maps were created by using the MEDESS technique [114]. In this technique, each TR yields two echoes before (S^+) and two echoes after (S^-) an effective spoiler

gradient. The TR is then repeated with an offset of ΔTE. The two TRs are run alternately, to yield eight images with differing contrast (four S^+ and four S^-). T_2 relaxation times can be estimated using S^+ and S^- pairs (for example: pulses 1 and 8 together) with the following model:

$$T_2 = \frac{TE_{S^+,1} - \left(TR + TE_{S^-,8}\right)}{\log\left(\frac{S_{-,8}}{S_{+,1}}\right)}$$

3.2 Mechanical Testing

For mechanical testing, considerations had to be made for how the samples were procured (3.2.1), how the tests were configured (3.2.2), and how the tests were carried out (3.2.3).

3.2.1 Sample Procurement

The sample procurement can be broken down into the initial dissection where the menisci were exposed and the sample preparation where the core samples were prepared.

3.2.1.1 Dissection

In order to procure samples from the specimens, I dissected the knee joint thereby exposing the meniscus. Dissection occurred the morning after the qMT scans were performed, with the knee joint being stored in the fridge at 4°C overnight. The first step was to locate the patella. The surrounding tissue was then resected in order to expose and remove the patella. Next, the femur and tibia were separated. To do this, muscles and ligaments connecting them had to be severed. After the femur and tibia were separated, the menisci were exposed. The meniscal attachments to the tibial plateau were retained.

3.2.1.2 Sample Preparation

Figure 3.3 - Bovine Menisci with Core Samples Removed

A 4mm biopsy punch was used to procure samples from the menisci. When doing this, the punch was kept as normal to the tibial plateau as possible, and pushed through the entire meniscus. It is notable that the meniscus is thicker near the horns, and more difficult to punch all the way through. The sample usually adhered to the interior of the biopsy punch, and therefore a thin probe was often inserted into the punch from the back end to push it out. A dissected bovine stifle joint with core samples removed from the menisci can be seen above in Figure 3.3.

Figure 3.4 - Bovine Meniscus Core Sample (Uncut)

When samples were procured, they were longer than required for testing (Figure 3.4). Each sample was cut down to approximately 2mm using a custom-made core sample cutter. There are four slots on the core sample cutter for razor blades. For the 2mm cut to be relatively

accurate, all four blades were placed in the slots. An ideal cut would take the sample from the middle of the core, while removing the angled surface layer. After putting the sample in the 4mm groove (Figure 3.5A), I placed razor blades into the outer two spots of the rig in a downward position, possibly cutting off the ends of the sample (Figure 3.5B). To line up the cuts accordingly, the middle two razor blades were put in their slots in the vertical position. The blades were then lowered to a position which enabled a visual assessment of the line-up of the cut (Figure 3.5C). When the tissue was aligned as desired, the razor blades were guided down into their slots to make the cut (Figure 3.5D). The part of the tissue between the middle blades was the sample to be tested. Each sample was placed into a vial with a 1X PBS solution containing protease inhibitors 5mM ethylenediaminetetraacetic acid and 5mM Benzamidine HCl [19], which are important for slowing down tissue degeneration. We expected 1X PBS to be appropriate as samples are not expected to have excessive swelling at this concentration [120]. Samples were stored in the fridge at 4°C to allow them time to equilibrate before mechanical testing.

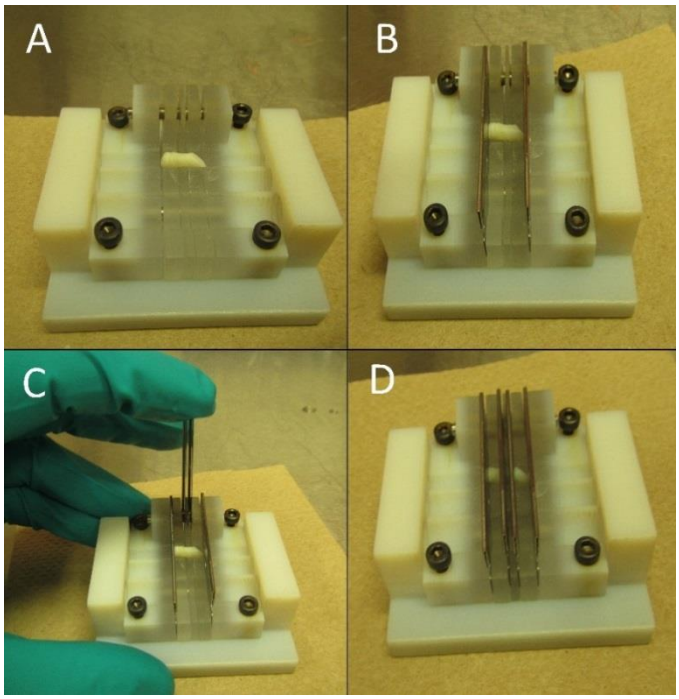

Figure 3.5 - Cutting a Meniscus Core Sample with the Core Sample Cutter: A) Sample in Position; B) Outer Blades Down; C) Inner Blades Vertical; D) Sample Cut

3.2.2 Apparatus

The components that make up the testing apparatus include the confined compression rig and the Zwick materials testing machine (Zwick Z010, Zwick Roell Group, Ulm, Germany) (Figure 3.6).

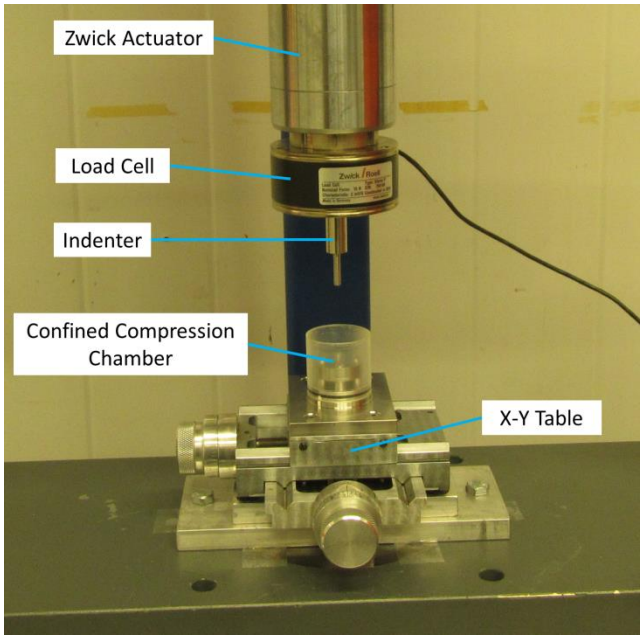

Figure 3.6 - Apparatus

3.2.2.1 Confined Compression Rig

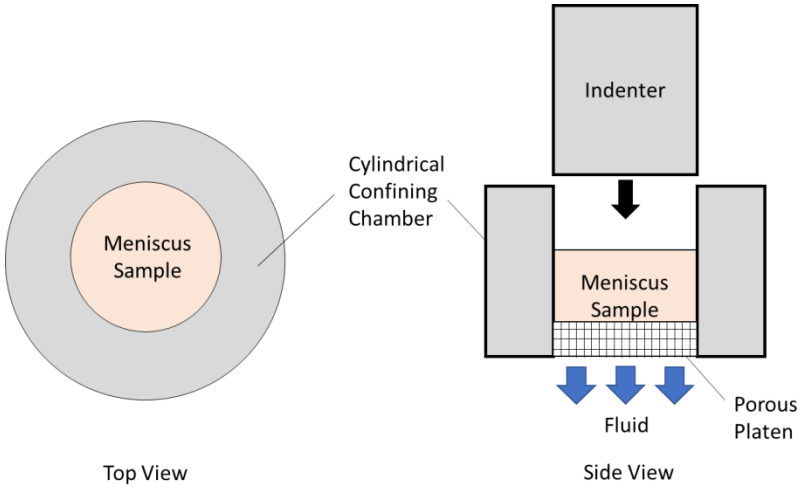

Figure 3.7 - Confined Compression Testing Configuration

For a confined compression test, it was necessary that core samples of soft tissue could be compressed in the axial direction but that they were prevented from expanding out laterally. To

achieve this, samples were tested in a confined compression chamber, designed by a member of our group (Josef Beug). The chamber is cylindrical, with the walls made of stainless steel that prevent lateral extrusion of the tissue. The bottom of the chamber is a porous platen that supports the sample, but also facilitates fluid flow. This platen was carefully selected by a member of our group (Dr. Emily McWalter) to ensure fluid flowed was not restricted through it. The tissue was compressed from above by an indenter that is also made of stainless steel and attached to the load cell. During testing fluid flow would mostly be restricted to pass through the porous platen. A representation of this setup can be seen above in Figure 3.7.

The confining chamber sits on stilts above a reservoir, and this setup was encased in an acrylic tube. The acrylic tube was sealed with an O-ring at the base so that it can be filled with a 1X PBS solution to keep the tissue hydrated during testing. The base secures onto an X-Y table, which allows for fine horizontal adjustments in order to align the indenter with the confined compression chamber. The actual confined compression rig setup can be seen in Figure 3.8.

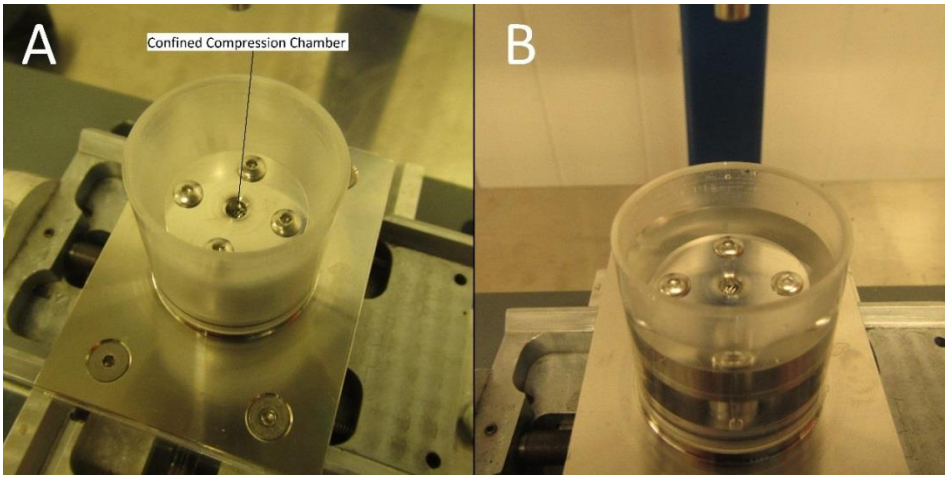

Figure 3.8 - Confined Compression Rig: A) Without 1X PBS; B) With 1X PBS

3.2.2.2 Zwick Materials Testing Machine

The Zwick materials testing machine along with packaged software (testxpertII, Zwick Roell, Ulm, Germany) was used for displacement-controlled testing. I equipped it with a 10 N load cell with an error of up to ± 1% at the lowest forces within the measurement range, and a custom made indenter for testing. When used for position control, the actuator is directed by a controller that has an error of ± 0.01mm. Before tests could be carried out, the indenter had to be properly configured.

3.2.2.3 Indenter Alignment

Before mechanical testing could be done, the indenter had to be properly aligned with the confining chamber. It was important that the indenter did not touch the confining walls during testing, as the resulting friction would skew the force data. In order to do this, the actuator was first lowered to a few millimeters above the confining chamber using manual controls. The indenter was then aligned with the confining chamber hole as best as possible by hand using the x-y table.

A custom-made 'testxpertII' sequence was implemented to lower the indenter very slowly (10mm/min). If a force greater than 0.01N was detected by the load cell, then the indenter was automatically retracted and the x-y table was adjusted. If the indenter could travel into the chamber without a force greater than 0.003N, then the indenter was considered properly aligned.

3.2.2.4 Indenter Zeroing

After the indenter was properly aligned, it had to be configured properly so that when it was at the bottom of the confining chamber, the tool separation was set to 0mm. To do this, a custom-made 'testxpertII' sequence was implemented to lower the indenter until a force of 0.1N was detected, upon which the actuator will retract to the starting position of the test. This was done 3 times into the confining chamber void of fluid, and the data for each test was exported to excel. The tool separation vs. force data was analyzed to determine the tool separation at which the indenter contacted the bottom of the confining chamber. This measure was averaged over the 3 tests to determine the zeroing point to properly configure the Zwick.

3.2.3 Confined-Compression Testing

In order for the samples to be properly tested, I first needed to know the specimen heights before stress-relaxation testing.

3.2.3.1 Sample Height Measurement

After being left in the fridge overnight to reach equilibrium, the samples were taken out one at a time for height measurements. The sample being measured was removed from its vial, and dabbed on a paper towel before being placed in the confining chamber. Samples that needed to be forced into place likely swelled a lot in the 1X PBS solution. These samples were deemed to be too large for testing, and were discarded.

A custom-made sequence in 'testxpertII' was developed to perform sample height measurements. The actuator of the Zwick was lowered onto the sample, compressing it until the load cell detects 0.01N of force, after which the sample was unloaded. This procedure was done 3 times, and each set of data was exported to excel. The force-displacement data was analyzed similarly to it was for indenter zeroing. The 'Tool Separation' read out value that corresponds with the increase in force is the sample height. The average of the 3 measures of sample height was the one used. After the height measurements were made, the sample was put back into the fridge with the exception of first sample being tested.

3.2.3.2 Stress-Relaxation Testing

After the sample height was determined, stress-relaxation testing was carried out. Before being tested each sample was left out for approximately 90 minutes to be certain that it was at room temperature. The confining chamber was filled with the 1X PBS solution in order to keep the tissue hydrated during testing (Figure 3.8B). A custom 'testxpertII' program was made to control the stress-relaxation testing. Before initiating the sequence, the indenter was lowered to a tool separation of 5mm and the force readout was zeroed. From there, the indenter was lowered to a tool separation of the sample height, and the test was started. The tissue was compressed to 10% of its original height at strain rate of 50%/min and held for 2000s. Next it was compressed to 15% of its original height at a strain rate of 0.3%/min and held for 2000s. The data was sampled at 1Hz, and the 15% strain data was analyzed for curve fitting. Fifteen percent was chosen for the stress-relaxation curve because initial testing with bovine samples gave the most robust data for fitting, and it is close to 11.6% axial strain which was found to be physiologically normal for porcine menisci at 200% body weight [121].Ten percent was chosen for preloading because the 5% strain increase to 15% was found to be a sufficient amount to provide a pronounced stress-relaxation effect. The stress-relaxation period was set 2000s because it is approximately that of the Bursac's stress-relaxation period, which I ultimately ended up using (details to follow in section 3.3).

3.3 Curve Fitting

The data obtained from confined compression testing had to be fit to a mathematical model in order to obtain estimates of the mechanical properties. Most of the models in the literature are based on Mow's biphasic theory [14]. Below are the models that were considered

for use in this study. Other models that were investigated can be seen in Appendix B – Other Models for Curve Fitting.

3.3.1 Seitz Model [104]

The Seitz model is a poroelastic, biphasic model for soft tissue samples undergoing confined compression testing. It takes one-dimensional fluid flow into consideration, and its origins lie in Mow's biphasic theory, although in a simplified manner.

$$\sigma = \sigma_\infty + 2\varepsilon H_A e^{-\left(\frac{\pi}{h_0}\right)^2 H_A k_p t}$$

Where $\sigma =$ stress in the tissue, $\sigma_\infty =$ equilibrium stress at a given strain-level, $\varepsilon =$ strain-level for stress-relaxation, $H_A =$ aggregate modulus, $h_0 =$ original specimen height, $k_p =$ tissue permeability, and $t =$ test time.

Fits for this model were achieved using the curve-fitting application in Matlab (Matlab, MathWorks, Natick, USA). R^2 values for these fits were fairly high (~0.97) but a quick visual assessment indicated that the model did not fit well at the start or finish of the curve (Figure 3.9).

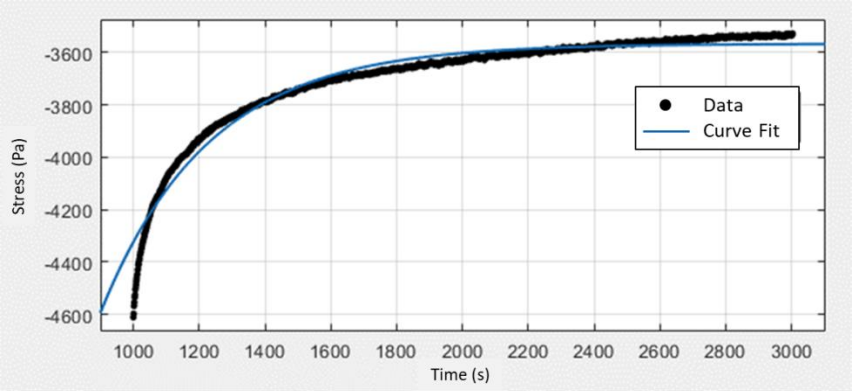

Figure 3.9 - Seitz Model Fit on Bovine Meniscus Tissue

This model has the advantages of including both *Ha*, and *kp*, which are useful tissue properties for describing both the static and dynamic compressive behaviors of soft tissues. However, this model is limited in that it does not include the strain rate applied to the tissue sample. The applied strain rate is an important parameter, as the stress-relaxation period is dependent on how long the strain is applied, and this affects the curve shape. This was the first model I explored, but it became clear that it is not the right one to use as it does not fit the data well enough.

3.3.2 Bursac Model [108]

Similar to the Seitz model, the Bursac model is a poroelastic, biphasic model for the confined compression of soft tissue samples. This model is a bit more complex than the Seitz model though, and may better reflect the physical response of the soft tissue samples.

$$\sigma = H_A \dot{\varepsilon}_0 t_0 - \frac{2\dot{\varepsilon}_0 h_0^2}{\pi^2 k_p} \sum_{n=1}^{\infty} \frac{e^{-\frac{nt}{\tau'}} - e^{-\frac{n^2(t-t_0)}{\tau'}}}{n^2}$$

$$\tau' = \frac{h_0^2}{\pi^2 H_A k_p}$$

Where $\dot{\varepsilon}_0$ = applied strain rate, and t_0 = time period during which the tissue is compressed.

This is the model that I implement in this study. Fits for this model were achieved using a custom-made Matlab script that optimized the fit based on minimizing sum of squares. The fit found using this script was much better than any fit found using the Seitz model, achieving very high R^2 values of 0.9849 ± 0.0149 (mean ± standard deviation) with a median of 0.9902, a minimum R^2 of 0.9469 and a maximum of 0.9991 for a range of 0.0522 during the precision study. This model includes both *Ha* and *kp* as the Seitz model does, but it also includes the applied strain rate.

While I have achieved good fits with this model, it was not simple to get to this point. Initially, I had been performing tests with an applied strain rate of 50%/min, which is similar to what can be seen in most stress-relaxation tests in the literature. However, the best fits I could get with this strain rate had R^2 values in the 0.87 range, and visually they did not look appropriate. Eventually I decided to implement a much lower strain rate of 0.3%/min which was what was implemented in Bursac's study, which led to the results shown here (Figure 3.10).

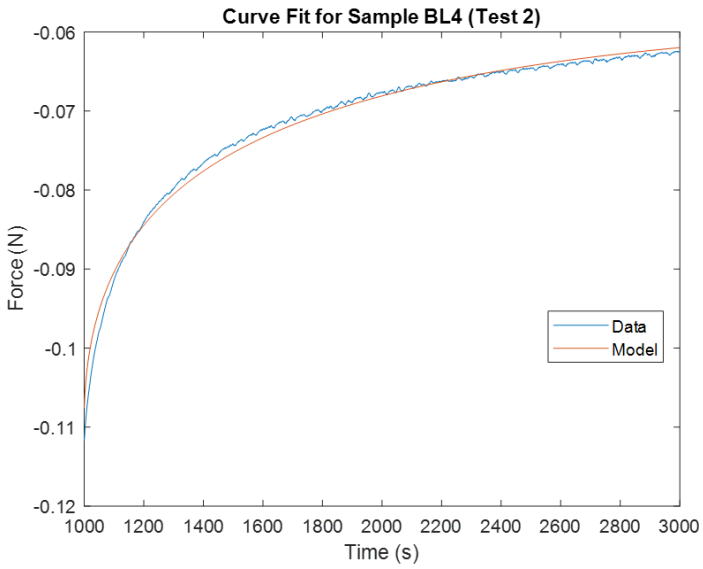

Figure 3.10 – A Typical Bursac Model Fit on Bovine Meniscus Tissue

Additionally, I had to consider the number of terms in the summation term to include. In order to decide this, I performed curve fitting on all of the samples using the model from n=1 up to n=25 terms. Most samples converged by n=20 terms, where the R^2 value remains the same beyond this point when considering 3 decimal points of precision, and all of them did by 25 terms. I chose to go with 25 terms, which is also what was used in Bursac's study. A more in-depth discussion on this can be seen in Appendix D – Bursac Model's Sensitivity to Parameter n.

Due to the high R^2 values of 0.9849 ± 0.0149 for this fitting method using this model, in this study any samples that have an R^2 less than 0.9 will be excluded from the study.

3.3.3 Andrews Model [98]

Rather than originating from biphasic theory, the Andrews model seems to be a model that was fabricated to fit the data.

$$\sigma = \sigma_\infty + \sum_{i=1}^{3} \sigma_i e^{-\frac{t}{t_i}}$$

where σ_i = Maxwell spring constants, and t_i = stress-relaxation times.

Fits for this model (Figure 3.11) were achieved using Matlab's curve fitting application with a Levenberg-Marquardt optimization algorithm. While it is apparent that the fit is nearly

perfect (R^2~0.99), it is not obvious what the model parameters mean physically. Also, this model has only been used by one group which limits cross-referencing capabilities of results.

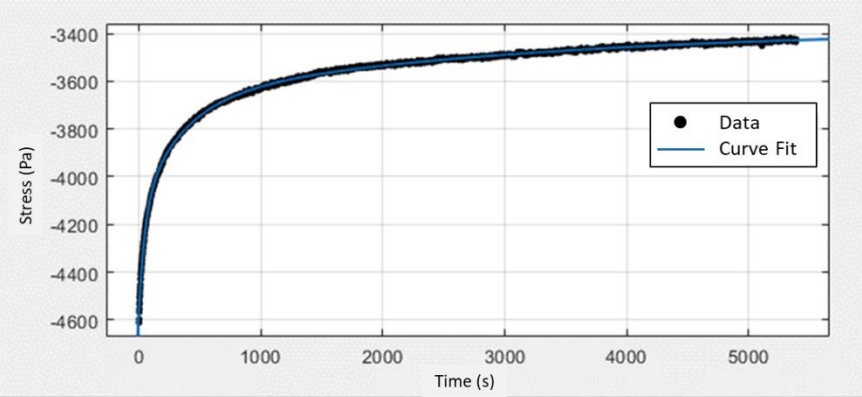

Figure 3.11 – Andrews Model Fit on Bovine Meniscus Tissue

3.4 Image Processing

After obtaining mechanical testing outcomes, I needed to see if there was a correlation between qMT metrics and the mechanical testing outcomes. To do this, I needed to know which qMT values in the parameter maps correspond to the samples tested. In other words, I needed to know where within the qMT maps the samples would be located. In order to do this, I wanted a point cloud of the meniscus with samples removed, which could then be registered over the qMT maps to find the sample locations.

3.4.1 Point Cloud Generation

In order to obtain a point cloud of the menisci, I used dedicated packaged software (Agisoft Photoscan, Agisoft LLC, St. Petersburg, Russia). This software works by processing a number of photos of an object taken from different angles, and recognizing common reference points between the images. It can then construct a point cloud of the object.

In order to create a good point cloud of the menisci, several things had to be done to help the software recognize common reference points between images. Talcum powder was gently applied to the surface of the menisci and surrounding tissue to help reduce shine so that it would not interfere with the common point recognition. For similar reasons, the lighting in the room had to be somewhat even without any harsh direct lighting. Distinct markings were made on the potting to help the imaging software with recognizing common points between images for point

cloud production. I typically wrote letters with a point beside them surrounding the joint indicating the sides of the knee, along with random markings (Figure 3.12). It is also important to note that the images were taken in a room with objects in the background. I placed a one 25.4mm wide calibration block in the frame to allow scaling of the model later in the process.

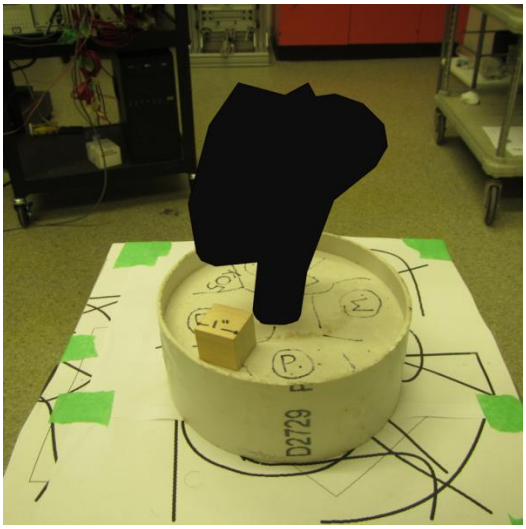

Figure 3.12 - Potted Human Knee (Censored) Prepared for Point Cloud Generation

The photo-taking process was done immediately after sample procurement. It consisted of taking approximately 100 photos using a standard digital camera from various different angles and distances from the object, while generally keeping the whole knee joint in frame.

These photos were then uploaded into software, which created a dense point cloud of the object. This dense point cloud could then be turned into a textured 3D model (Figure 3.13). Since the model is textured, I was able to manually delete the points of the mesh that were associated with the holes where the samples were removed. This is important for determining the sample locations after registration.

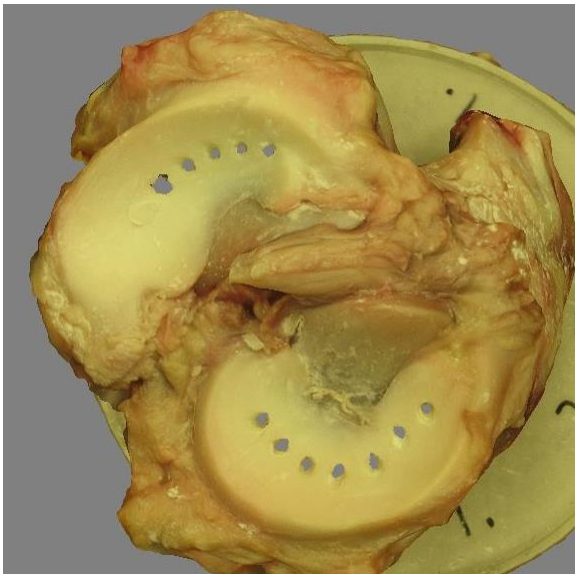

Figure 3.13 – 3D Model of a Dissected Bovine Knee

After the samples were removed from the model, I uploaded the model into packaged solid modeling software (Geomagic, Geomagic, Morrisville, USA) for scaling. Since the calibration block was 25.4mm wide, I could scale the model to the appropriate size. Once scaled, I deleted everything in the model that was not the top surface of the menisci (Figure 3.14). Each meniscus was saved as its own .stl file to be registered individually.

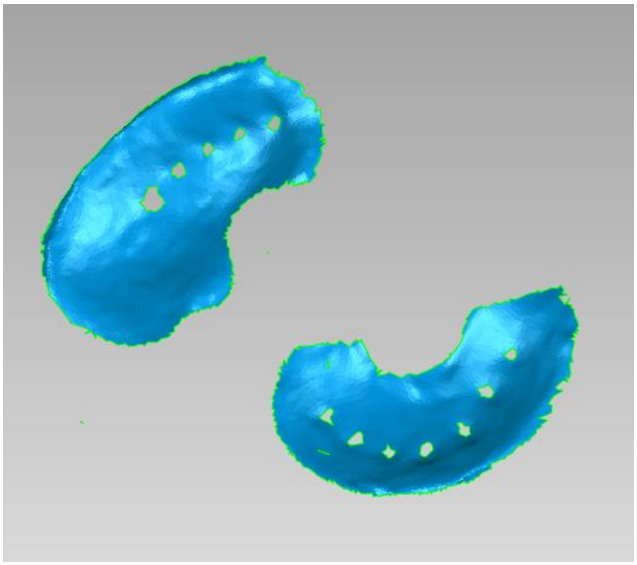

Figure 3.14 - Scaled and Cropped 3D Models of Bovine Menisci

3.4.2 Image Segmentation

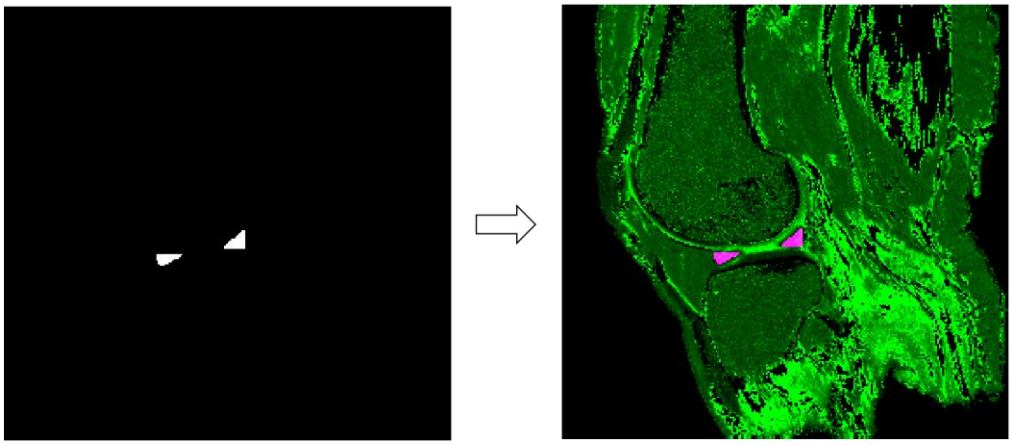

Figure 3.15 - A Single Slice of a Meniscus Mask Overlaid on a Parameter Map

After obtaining the point cloud, a few different segmentation masks were needed to perform registration. First, packaged image processing software (Analyze 10.0, Mayo Clinic, Rochester, USA) was used to segment and create a mask of both menisci. This mask was overlaid on parameter maps in order to get parameter values for the menisci (Figure 3.15). Additionally, segmentations of only the bottom and top surfaces of the menisci were created (Figure 3.16). The top surface mask of the meniscus was also exported as a .stl and scaled to its appropriate physical size in Geomagic for registration purposes.

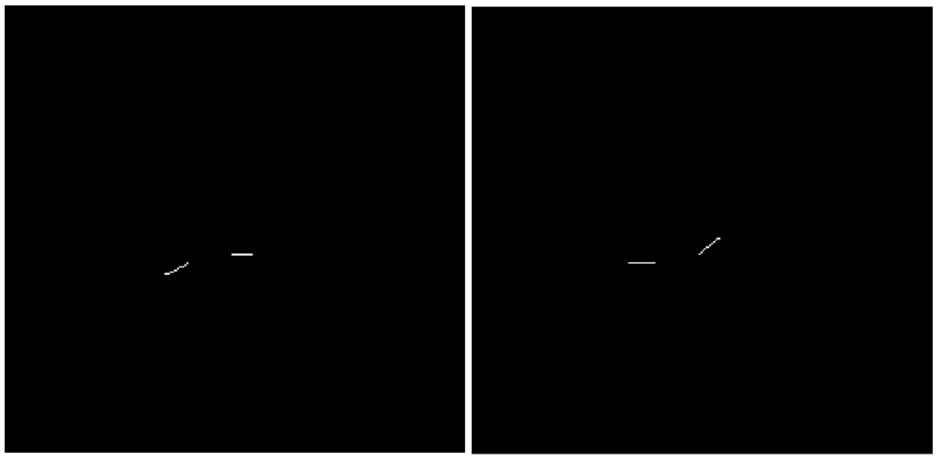

Figure 3.16 - Segmentations of the Bottom (left) and Top (right) Surfaces of the Menisci

3.4.3 Point Cloud Registration

Next, the top surface mask .stl and the Agisoft model were read into Matlab (Matlab R2017b, MathWorks, Natick, Ma) and viewed at the same time to compare their orientations (Figure 3.17). I separated the .stl files such that I was only manipulating their vertices, which effectively acted as point clouds. The point clouds were expected to have entirely different positions, but it was desired to have their orientations be similar to help the registration process. If their orientations were too different, I would take the Agisoft model back into Geomagic and rotate it until it was similar enough like shown in the figure below. It was important to rotate the Agisoft model and not the segmented model from Analyze, as the Analyze model has a physical location that is in line with the parameter maps which I wanted to stay the same.

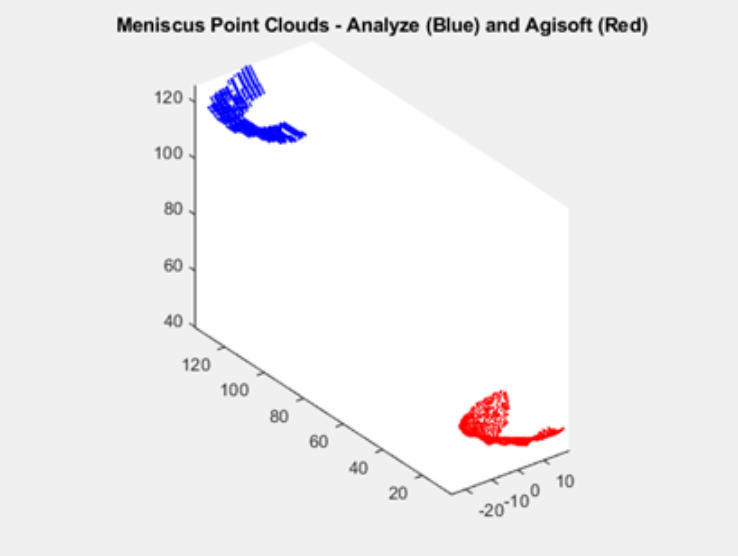

Figure 3.17 - Meniscus Point Clouds Viewed Together in Matlab - Analyze Point Cloud (Blue), Agisoft Point Cloud (Red)

Once orientations were similar enough, I would upload the Agisoft model into modeling software (Fusion 360, Autodesk, San Rafael, USA). I created cylinder models to pass through the sample hole locations to represent the samples that were removed from the meniscus (Figure 3.18). I did this for every sample and each model was exported as its own .stl file, which could then be read into Matlab as a point cloud.

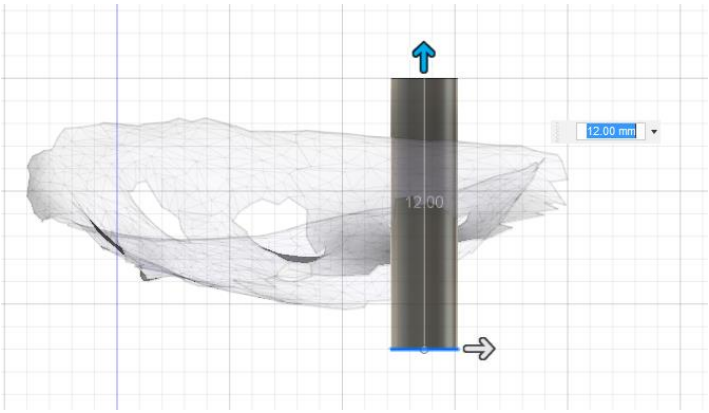

Figure 3.18 - Cylinder Model in Fusion 360

Using an Iterative Closest Points function [122, 123] in Matlab developed by a member of our group (Dr. James Johnston), the Agisoft point cloud was then registered to the Analyze point cloud. The translation and rotation that was applied to the Agisoft point cloud through the registration process was then applied to the sample cylinder point cloud to find out where the sample cylinder intersects with the Analyze point cloud (Figure 3.19).

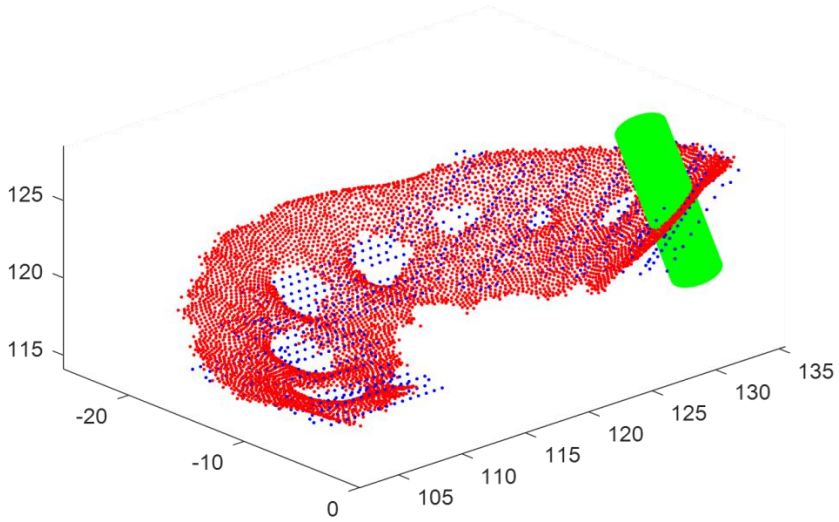

Figure 3.19 - Point Cloud Registration Results - Agisoft Point Cloud (Red), Analyze Point Cloud (Blue), Cylinder Point Cloud (Green)

This took into consideration the cylinder and the meniscus surface (Figure 3.20 – a), and isolated the intersection of the two (Figure 3.20 – b). However, this did not yield where it would be located throughout the depth of the meniscus. In order to find that, I wrote a custom function in Matlab that took this intersection in the same space as the bottom surface of the meniscus (Figure 3.20 – c), and extended it down toward the bottom meniscus surface segmentation that I made previously to define the sample boundaries within the meniscus. It then was filled in to define the punch out of the sample (Figure 3.20 – d). To define the core sample, the middle three rows of voxels below the sloped portion of the sample were taken (Figure 3.20 – e). Some samples were too short and were only able to provide one or two rows of voxels. This process was done slice by slice until I had a full mask for the sample of the meniscus.

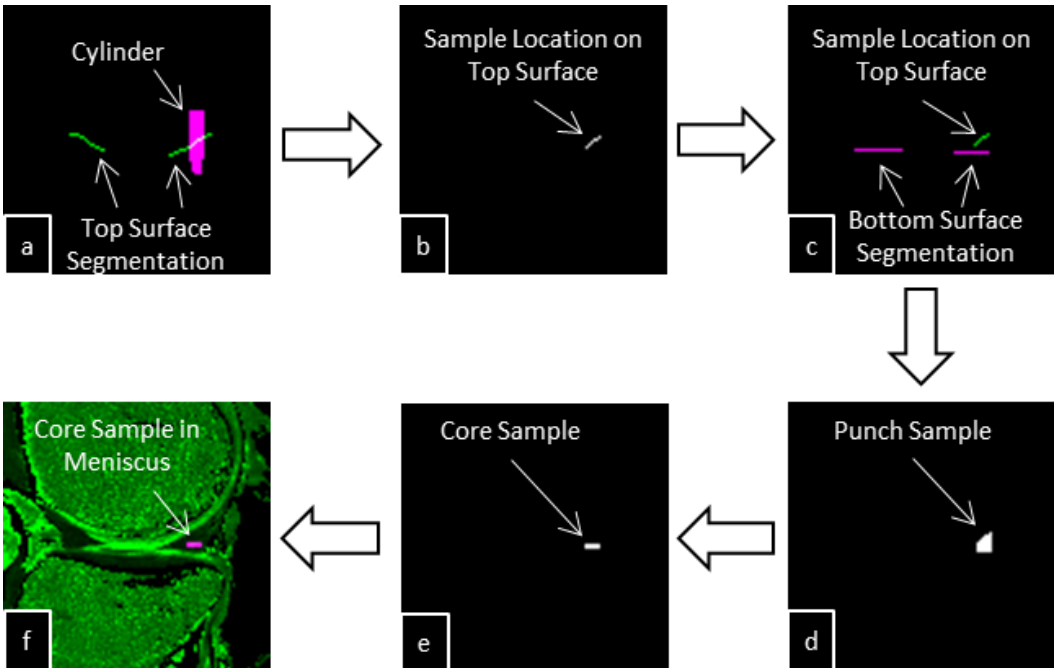

Figure 3.20 – Locating Core Sample Locations in MR Images. a) The cylinder and the meniscus surfaces are placed in the same imaging space in order to find their intersection as shown in b). c) The intersection previously found is put in the same space as the bottom meniscus surface segmentations. These boundaries are implemented to define the punch sample as shown in d) which is further reduced to the core sample shown in e) by taking up to three of the middle voxel rows below the slanted meniscus surface. An example core sample within its respective meniscus is shown in f).

3.5 Precision Study

Before beginning the main study, a precision study was done on the mechanical testing protocol for this project, including the confined compression testing and curve fitting necessary to obtain the aggregate modulus and permeability of the samples. This study was performed on

14 samples from 3 bovine stifle joints in order to find root-mean-square coefficient of variation (CV_{RMS}) for each parameter. Each sample was tested 2 times, and was given time overnight after each test to re-equilibrate in 1X phosphate buffered saline (PBS) containing protease inhibitors 5mM ethylenediaminetetraacetic acid and 5mM Benzamidine HCl [19] before being tested again.

The coefficient of variation for sample i is calculated as:

$$CV_i = \frac{SD_i}{\bar{x}_i} * 100$$

where SD_i is the standard deviation of the measured parameter for sample i after repeated measures, and $\bar{x}_i$ is the mean value [124].

The root-mean-square coefficient of variation is:

$$CV_{RMS} = \sqrt{\sum_{i=1}^{m} CV_i^2 / m}$$

where m is the total number of samples tested [124]. CV_{RMS} values were found to be 10.47% and 7.25% for *Ha* and *kp* respectively. These results can be seen tabulated in Table 3.1 below.

Table 3.1 - Precision Study Results

Sample	Knee	Meniscus	CV%	
			Ha (%)	kp (%)
1	0	Lateral	7.68	2.09
2	0	Lateral	2.68	4.88
3	0	Lateral	0.12	2.40
4	0	Medial	11.41	7.06
5	1	Lateral	9.36	7.56
6	1	Lateral	5.35	4.13
7	1	Lateral	1.54	11.14
8	1	Medial	6.24	6.50
9	1	Medial	2.99	3.68
10	2	Lateral	3.64	10.36
11	2	Lateral	2.43	12.94
12	2	Medial	29.68	10.23
13	2	Medial	15.90	0.66
14	2	Medial	4.20	4.29
CVrms			10.47	7.25

3.6 Association Analysis

Spearman's rho correlations were implemented to determine how well qMT metrics were associated with the mechanical properties using packaged software (SPSS, IBM Corp., Armonk, NY). I did not use a Pearson product-moment correlation because it would assume a normal distribution and homoscedasticity while a Spearman's rho correlation makes no such assumptions. Since this is the first study of the associations between qMT and mechanical properties, I did not have the necessary data to test the assumptions; thus, I chose the Spearman's rho correlation. The metrics correlated using Spearman's rho can be grouped into the categories: Mechanical Properties (*Ha*, *kp*), qMT Parameters (T_{1f}, T_{2f}, T_{2b}, *f*, *k*), and Other Parameters (T_1, T_2, *MTR*) (Table 3.2). The primary correlations I was interested in were between mechanical properties and qMT parameters, while all of the other correlations were secondary outcomes. A correlation was determined to be significant if it had a p-value less than 0.05. The correlations found in this study adhered to the following classification scheme: very weak (correlation coefficient = 0 – 0.19), weak (0.2 – 0.39), moderate (0.4 – 0.59), strong (0.6 – 0.79), or very strong (0.8 – 1). Each individual sample was considered its own individual measurement even though many samples were taken from the same menisci. This is an appropriate assumption because there is expected to be plenty of variation within each individual meniscus [32].

Table 3.2 - Metrics Analyzed using a Spearman's rho Analysis

Primary Correlations		Secondary Correlations	
Independent Variables	Dependent Variables	Independent Variables	Dependent Variables
Mechanical Properties	qMT Parameters	Mechanical Properties	Other Parameters
		Mechanical Properties	Mechanical Properties
		qMT Parameters	Other Parameters
		qMT Parameters	qMT Parameters
		Other Parameters	Other Parameters
Mechanical Properties: Ha, kp || **qMT Parameters**: T_{1f}, T_{2f}, T_{2b}, f, k || **Other Parameters**: T_1, T_2, MTR			

4.0 Results

In total, 59 samples were used in the final analysis. From the 6 cadaver knees, 106 meniscus samples were procured. Out of the 106 samples, 32 were excluded from the study from either being damaged during procurement or being misshapen and unable to fill out the confined compression chamber. Eight more samples were excluded for swelling too much to fit in the testing chamber. From the 66 remaining samples, 5 were excluded for having an R^2 value below 0.9 for the stress-relaxation data curve fitting, and 2 more were excluded for being outside of the segmented region of the image. Below I go into detail on the mechanical testing and imaging parameter results, followed by the correlations found in this study.

4.1 Mechanical Testing Results

The mean *Ha* for the samples was 22.64 ± 19.65kPa, while the mean *kp* was 1.03E-13 ± 1.42E-13m^4/Ns (Table 4.1). There is a large range of values for *Ha*, with a difference of 100.93kPa between the largest and smallest values. The model curve fitting R^2 values for the 59 samples were 0.9815 ± 0.0213 (mean ± standard deviation). The median curve fit can be seen in Figure 4.1. More curve fitting results can be seen in Appendix C – Curve Fitting Results.

Table 4.1 - Summary of Mechanical Parameters

	Ha (kPa)	kp * 10^{15} (m^4/Ns)
mean	22.64	103.48
std	19.65	142.47
max	102.19	702.90
min	1.26	7.40
range	100.93	695.50

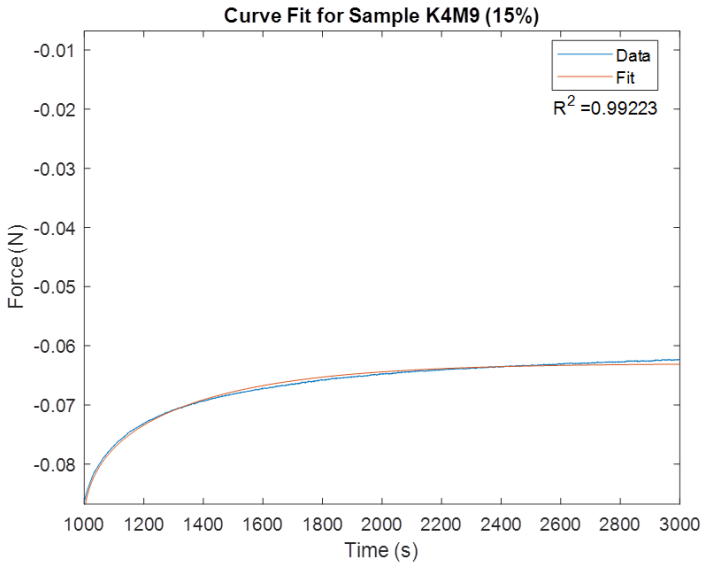

Figure 4.1 – Median Curve Fit Example for a Specimen at 15% Strain

4.2 Imaging Parameter Results

The qMT analysis of all samples was done with both a Super-Lorentzian line shape, and a Gaussian line shape. Using a Super-Lorentzian line shape yielded mean values for T_{1f} of 577.01 ± 110.90ms, T_{2f} of 6.95 ± 3.22ms, T_{2b} of 5.47 ± 0.91μs, f of 29.22 ± 5.38%, and k of 2.93 ± 0.77s^{-1} (Table 4.2). Using a Gaussian line shape returned mean values for T_{1f} of 598.11 ± 104.32ms, T_{2f} of 5.73 ± 2.48ms, T_{2b} of 16.10 ± 1.47μs, f of 23.53 ± 4.25%, and k of 3.03 ± 1.19s^{-1}.

Table 4.2 - Summary of qMT Parameters for both Super-Lorentzian and Gaussian Line Shapes

		T_{1f} (ms)	T_{2f} (ms)	T_{2b} (μs)	f (%)	k (1/s)
Super Lorentzian	mean	577.01	6.95	5.47	29.22	2.93
	std	110.90	3.22	0.91	5.38	0.77
	max	967.17	16.89	7.45	41.13	5.81
	min	351.14	1.83	2.96	14.97	1.27
	range	616.03	15.06	4.49	26.16	4.54
Gaussian	mean	598.11	5.73	16.10	23.53	3.03
	std	104.32	2.48	1.47	4.25	1.19
	max	968.34	14.66	19.38	33.40	7.77
	min	372.49	1.67	12.27	13.34	1.18
	range	595.86	12.99	7.11	20.06	6.59

The mean T_1 relaxation time was 666.35 ± 74.45ms and the mean T_2 relaxation time was 14.82 ± 2.46ms (Table 9). The mean *MTR* was 76.80 ± 4.69% (Table 9). Below in Figure 4.2 are some qMT parameter maps of the medial meniscus of specimen K02 that are good representations of the data outlined in Table 4.2 for the Gaussian line shape model, and more qMT parameter maps for each knee can be found in Appendix F – qMT Maps of Each Knee.

Table 4.3 - Summary of Other qMRI Parameters

	T_1 (ms)	T_2 (ms)	MTR (%)
mean	666.35	14.82	76.80
std	74.45	2.46	4.69
max	842.63	22.52	87.76
min	482.06	8.44	63.70
range	360.57	14.07	24.06

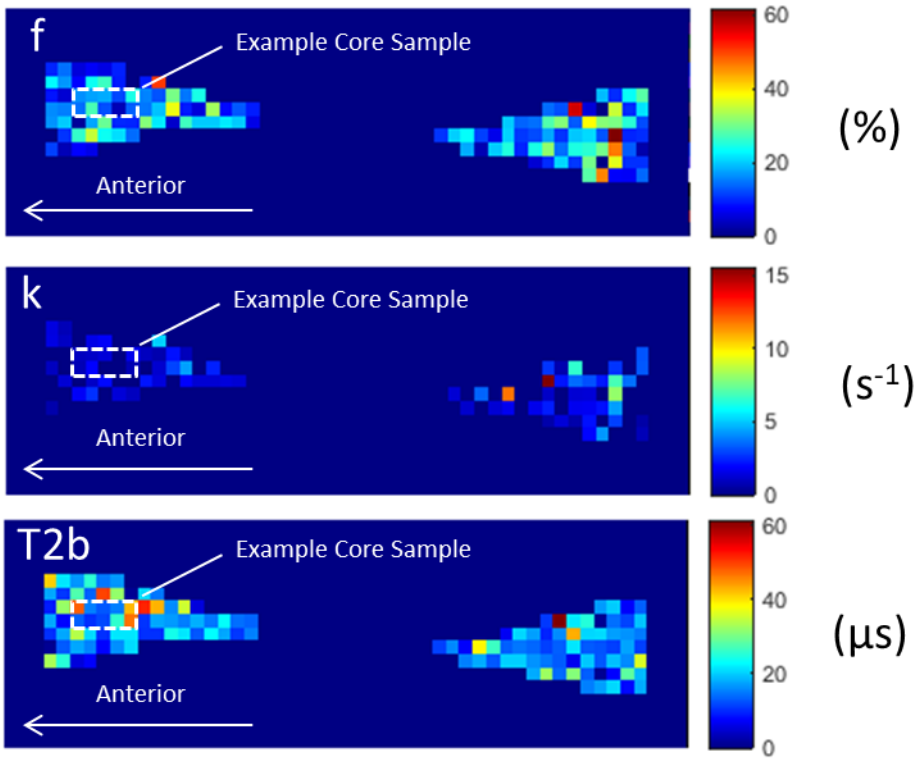

Figure 4.2 - qMT Parameter Maps (Gaussian line shape) of the lateral meniscus of specimen K02 viewed in the sagittal direction. An example of the size of a core sample within the meniscus is shown in white outline.

4.3 Correlations

The image registration using the Iterative Closest Points function was fairly successful, as measured by the shape match error. For every point in the data set, the distance between that point and the closest point in the model set was calculated, and the shape match error is the average of those distances. For all 12 of the registrations, there is an average shape match error of 0.676 ± 0.056mm.

Spearman's rho correlation analyses were done for both Super-Lorentzian (Table 4.4) and Gaussian line shapes (Table 4.5). I found that *Ha* and *kp* have a strong negative correlation (r_s=-0.686, p <0.01) but there was only one significant correlation between mechanical properties and any imaging metrics, which was between *Ha* and T_{2b} (r_s=-0.336, p<0.01) when using a Super-Lorentzian line shape. T_1 relaxation time did show significant correlations with qMT metrics, notably with *f* (r_s=-0.757, p<0.01) only when using a Super-Lorentzian line shape, and *k* (r_s=-0.542, p<0.01) when using a Gaussian line shape.

Table 4.4 - Spearman's rho Correlation Table (Super-Lorentzian Line Shape). The only correlation between mechanical properties and qMT parameters is highlighted in yellow.

Super Lorentzian Line Shape		Ha	kp	T_1	T_2	T_{1f}	T_{2f}	T_{2b}	f	k	MTR
Ha	Correlation Coefficient		-.686**	0.001	0.133	-0.037	-0.204	-0.336**	0.063	0.183	0.206
	Sig. (2-tailed)		p < 0.001	0.995	0.314	0.783	0.12	0.009	0.633	0.165	0.118
kp	Correlation Coefficient	-.686**		-0.027	0.007	0.029	0.202	0.206	-0.073	-0.206	-0.236
	Sig. (2-tailed)	p < 0.001		0.841	0.959	0.825	0.126	0.117	0.582	0.117	0.072
T_1	Correlation Coefficient	0.001	-0.027		.456**	.979**	.705**	0.196	-.757**	-.406**	.427**
	Sig. (2-tailed)	0.995	0.841		p < 0.001	p < 0.001	p < 0.001	0.137	p < 0.001	0.001	0.004
T_2	Correlation Coefficient	0.133	0.007	.456**		.463**	.551**	.285*	-.447**	-0.1	-.483**
	Sig. (2-tailed)	0.314	0.959	p < 0.001		p < 0.001	p < 0.001	0.029	p < 0.01	0.453	p < 0.01
T_{1f}	Correlation Coefficient	-0.037	0.029	.979**	.463**		.697**	0.225	-.833**	-.476**	-.405**
	Sig. (2-tailed)	0.783	0.825	p < 0.001	p < 0.001		p < 0.001	0.086	p < 0.001	p < 0.001	0.001
T_{2f}	Correlation Coefficient	-0.204	0.202	.705**	.551**	.697**		.484**	-.489**	-0.022	-.863**
	Sig. (2-tailed)	0.12	0.126	p < 0.001	p < 0.001	p < 0.001		p < 0.001	0.008	0.869	p < 0.001
T_{2b}	Correlation Coefficient	-0.336**	0.206	0.196	.285*	0.225	.484**		-0.146	0.028	-.494**
	Sig. (2-tailed)	0.009	0.117	0.137	0.029	0.086	0		0.271	0.833	0
f	Correlation Coefficient	0.063	-0.073	-.757**	-.447**	-.833**	-.489**	-0.146		.621**	0.195
	Sig. (2-tailed)	0.633	0.582	p < 0.001	p < 0.001	p < 0.001	0.008	0.271		p < 0.001	0.138
k	Correlation Coefficient	0.183	-0.206	-.406**	-0.1	-.476**	-0.022	0.028	.621**		-0.137
	Sig. (2-tailed)	0.165	0.117	0.001	0.453	p < 0.001	0.869	0.833	p < 0.001		0.299
MTR	Correlation Coefficient	0.206	-0.236	.427**	-.483**	-.405**	-.863**	-.494**	0.195	-0.137	
	Sig. (2-tailed)	0.118	0.072	0.004	p < 0.001	0.001	p < 0.001	p < 0.001	0.138	0.299	

** Correlation is significant at the 0.01 level (2-tailed).	Correlation Legend	Very Weak (0-0.19)	Weak (0.2-0.39)
* Correlation is significant at the 0.05 level (2-tailed).	Moderate (0.4-0.59)	Strong (0.6-0.79)	Very Strong (0.8-1)

Table 4.5 - Spearman's rho Correlation Table (Gaussian Line Shape)

Gaussian Line Shape		Ha	kp	T_1	T_2	T_{1f}	T_{2f}	T_{2b}	f	k	MTR
Ha	Correlation Coefficient		-.686**	0.004	0.133	-0.007	-0.182	-0.221	0.151	0.142	0.206
	Sig. (2-tailed)		p < 0.001	0.978	0.314	0.96	0.168	0.093	0.253	0.282	0.118
kp	Correlation Coefficient	-.686**		-0.003	0.007	0.003	0.195	0.185	-0.165	-0.075	-0.236
	Sig. (2-tailed)	p < 0.001		0.98	0.959	0.98	0.138	0.16	0.213	0.571	0.072
T_1	Correlation Coefficient	0.004	-0.003		.456**	.903**	.715**	.317*	-.535**	-.542**	-.374**
	Sig. (2-tailed)	0.978	0.98		p < 0.001	p < 0.001	p < 0.001	0.015	p < 0.001	p < 0.001	0.004
T_2	Correlation Coefficient	0.133	0.007	.456**		.458**	.572**	.369**	-0.256	-.302*	-.483**
	Sig. (2-tailed)	0.314	0.959	p < 0.001		p < 0.001	p < 0.001	0.004	0.051	0.02	p < 0.001
T_{1f}	Correlation Coefficient	-0.007	0.003	.903**	.458**		.730**	.295*	-.681**	-.701**	-.387**
	Sig. (2-tailed)	0.96	0.98	p < 0.001	p < 0.001		p < 0.001	0.024	p < 0.001	p < 0.001	0.002
T_{2f}	Correlation Coefficient	-0.182	0.195	.715**	.572**	.730**		.511**	-.343**	-.397**	-.830**
	Sig. (2-tailed)	0.168	0.138	p < 0.001	p < 0.001	p < 0.001		p < 0.001	0.008	0.002	p < 0.001
T_{2b}	Correlation Coefficient	-0.221	0.185	.317*	.369**	.295*	.511**		-0.123	-0.206	-.425**
	Sig. (2-tailed)	0.093	0.16	0.015	0.004	0.024	p < 0.001		0.353	0.117	0.001
f	Correlation Coefficient	0.151	-0.165	-.535**	-0.256	-.681**	-.343**	-0.123		.665**	0.045
	Sig. (2-tailed)	0.253	0.213	p < 0.001	0.051	p < 0.001	0.008	0.353		p < 0.001	0.736
k	Correlation Coefficient	0.142	-0.075	-.542**	-.302*	-.701**	-.397**	-0.206	.665**		0.16
	Sig. (2-tailed)	0.282	0.571	p < 0.001	0.02	p < 0.001	0.002	0.117	p < 0.001		0.227
MTR	Correlation Coefficient	0.206	-0.236	-.374**	-.483**	-.387**	-.830**	-.425**	0.045	0.16	
	Sig. (2-tailed)	0.118	0.072	0.004	p < 0.001	0.002	p < 0.001	0.001	0.736	0.227	

** Correlation is significant at the 0.01 level (2-tailed).	Correlation Legend	Very Weak (0-0.19)	Weak (0.2-0.39)
* Correlation is significant at the 0.05 level (2-tailed).	Moderate (0.4-0.59)	Strong (0.6-0.79)	Very Strong (0.8-1)

Scatter plots provide better visual representation of the correlations found from the Spearman's rho correlation analysis (Figure 4.3 to Figure 4.6). In Figure 4.3, permeability's negative correlation with the aggregate modulus is illustrated. The spread of permeability values was quite noticeable when aggregate modulus was on the low end. Since T_{2b} correlated with *Ha* for a Super-Lorentzian line shape is the only correlation found between mechanical properties and imaging parameters, I have shown the scatter plots for both line shapes in Figure 4.4 for comparison. In Figure 4.5 are scatter plots showing how imaging parameters correlate with permeability. There are no obvious correlations visible from the scatter plots, but it is particularly notable how much data clustering there is. T_1 relaxation time had some of the strongest correlations in this study, and these correlations are represented by scatter plots in Figure 4.6. T_1 relaxation times' correlations are particularly noticeable with *f* and *k*. Correlation scatter plots between *Ha* and qMT parameters, as well as T_2 relaxation time correlations can be seen in Appendix E – Additional Correlations Scatter Plots.

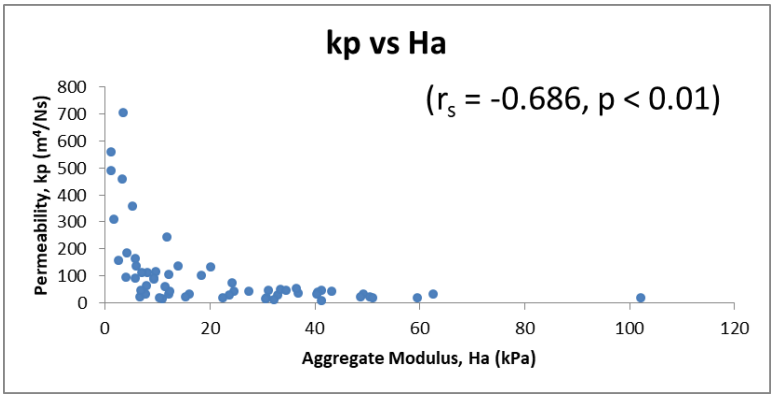

Figure 4.3 – Permeability Correlation with Aggregate Modulus

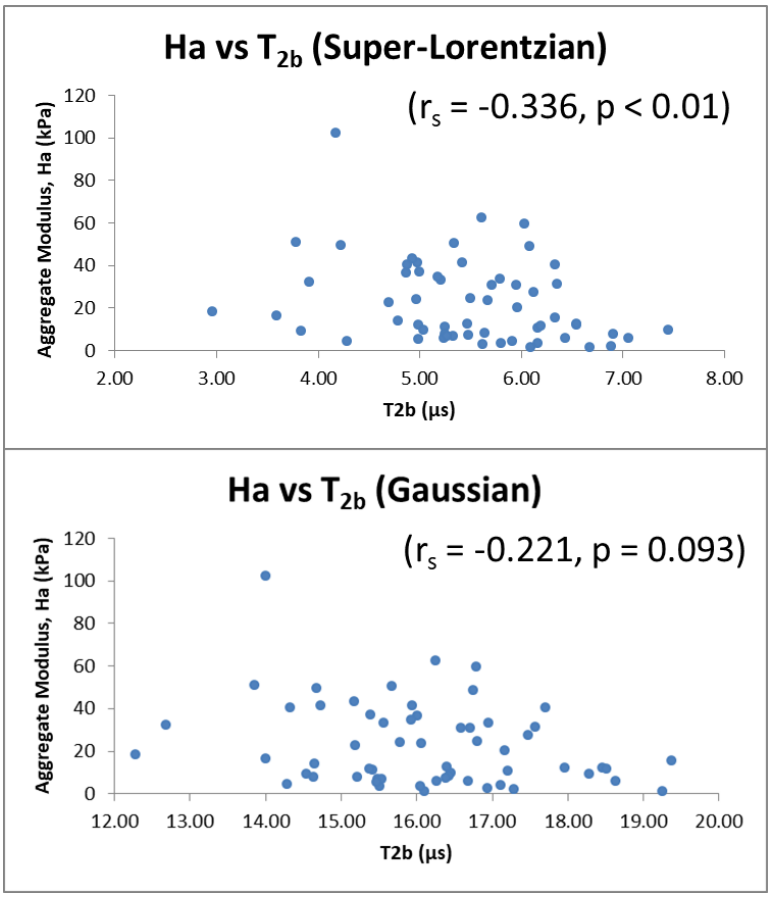

Figure 4.4 - T_{2b} Correlation with Aggregate Modulus

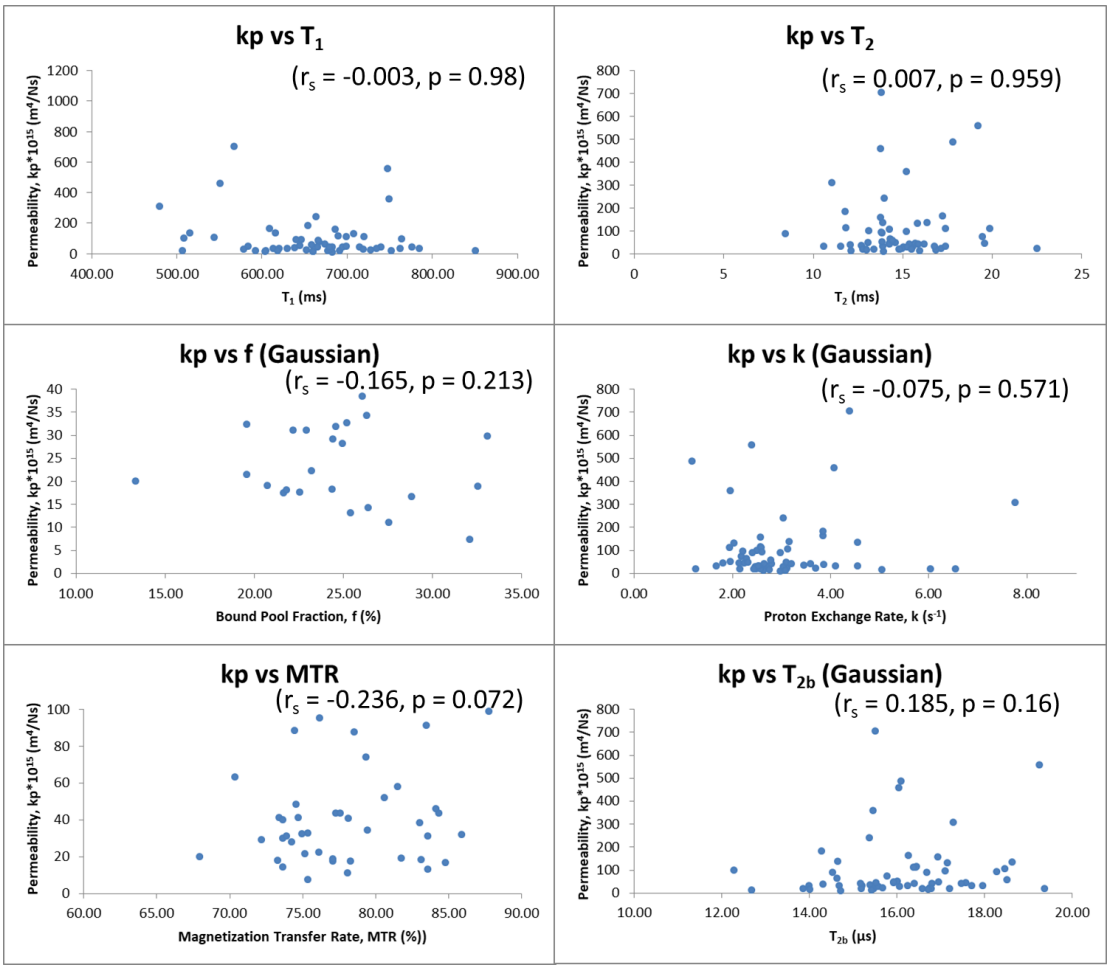

Figure 4.5 - Imaging Metrics Predicting Permeability (Gaussian Line Shape)

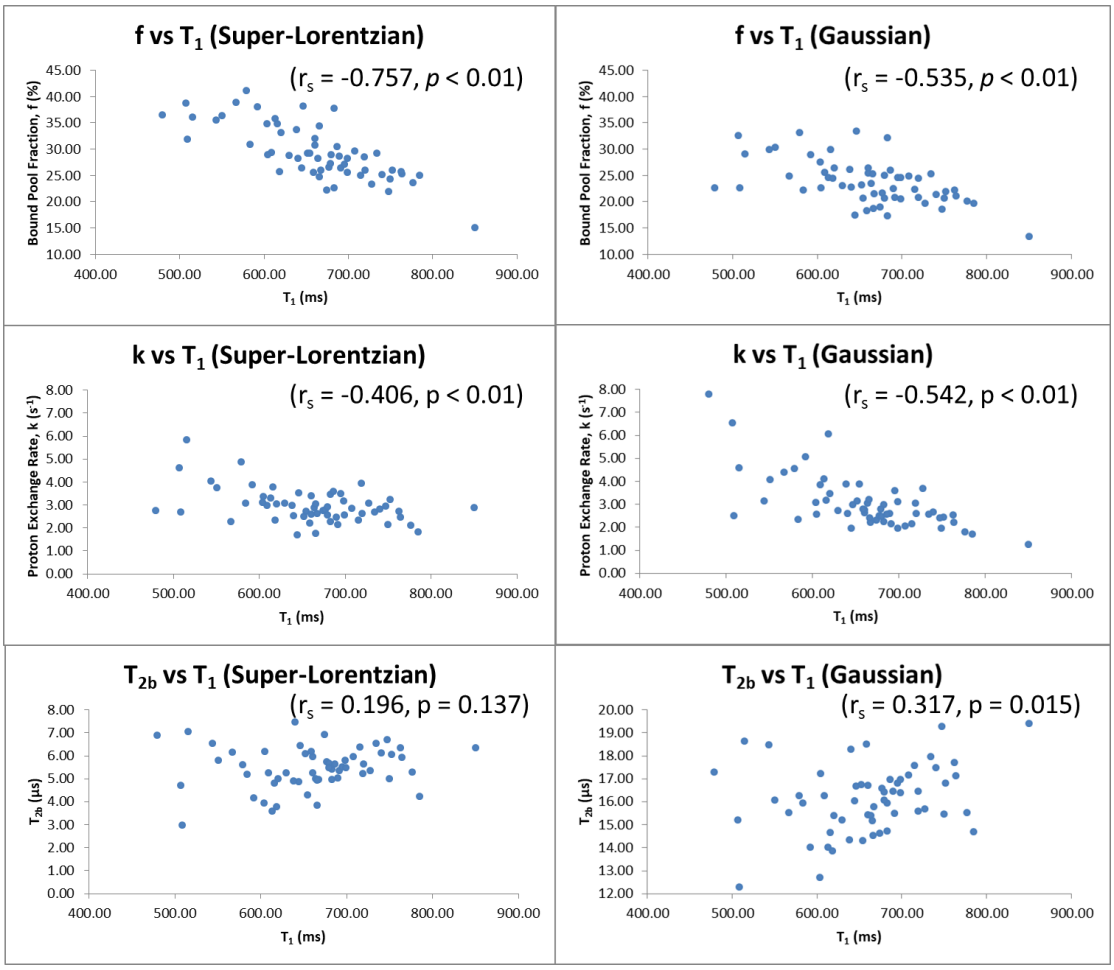

Figure 4.6 - T_1 Correlating with qMT Parameters for both Line Shapes

5.0 Discussion

In this section I am going to focus on five points of discussion. The focus of this study was on the potential correlations between meniscal mechanical properties and qMT parameters, but only one correlation was found and the reasons for this will be addressed first (5.1). While more key relationships were not uncovered, there were other correlations I did find between imaging metrics which I discuss next (5.2). I will then discuss the difficulties involved with mechanical testing of the meniscus (5.3), and Super-Lorentzian versus Gaussian line shapes in qMT models (5.4). Finally, I will compare qMT values between cartilage and the meniscus in the literature (5.5) before moving on to strengths and limitations of this study (5.6).

5.1 Why did we not Capture More Correlations between Mechanical Properties and qMT Parameters?

In the background section, I explained that I expected correlations between the mechanical properties of the meniscus and qMT parameters, but only one correlation was found between *Ha* and T_{2b} (r_s=-0.336, p<0.01) when using a Super-Lorentzian line shape. I expected to find these correlations because both qMT and mechanical function are dependent on water/macromolecule interactions, and qMT models the tissue as a biphasic material, similar to how I model the mechanical testing data. Why did we not find more of these correlations?

For the most part, the results trended in the way I expected. The mechanical properties behaved as I anticipated, with *Ha* having a significant and strongly negative correlation with *kp* from a Spearman's rho analysis (r_s=-0.686). The thought process here is that as the tissue gets weaker, its capability to resist compression should be reduced (*Ha*) and fluid flow through the tissue should become less resisted (*kp*). I also predicted that with tissue degeneration, *f* would decrease, and relaxation times would increase in general. All of the correlations indicate that this could be what is happening. It could be that these correlations exist, but they were not found in this particular study.

If more of these correlations exist but I am not capturing them, it may be because of a narrow range of health for specimens tested. Viewing the scatter plots in the results section (Figure 4.3 to Figure 4.6), it should be noted how "clumped" the data appear. Looking at some of the results more closely, it can be seen how the range of values is quite small. T_2 relaxation time for example was found to be 14.82 ± 2.46ms. This is a small standard deviation which is an

indication that the samples were quite similar. Without a wider range of values between specimens, it is difficult to find correlations. But, it is also possible that the correlations do not exist. In order to determine this, further similar studies would need to be done with a sample set that has a wide range of health between specimens.

Investigating the literature to see how standard deviations for T_2 compare to the current results, even in the most similar study the standard deviations are much higher [32]. In that study they took core samples from the meniscus and compared T_2 relaxation times for them regionally and even among the same regions the standard deviations ranged from approximately 3 to 8ms. If the samples were compared across all regions the standard deviation would likely be even higher. There are other studies that analyze T_2 times regionally in menisci which have some standard deviations similar to those reported here (ranging from 0.95 to 2.08ms) [125] and some higher than those reported here (ranging from 1.45 to 4.51ms) [126]. These values are not ideal comparisons to the current study as they measure entire meniscus regions instead of core samples, and I would expect the standard deviations of regions to be lower than specimens as outlier values get averaged out in larger regions.

Voxel size is another consideration to make when attempting to find correlations. Our sample sizes were 4mm in diameter, but our slice thickness was 3mm which introduces the possibility of the partial-voluming effect, where a voxel would represent both inside and outside the region-of-interest. Almost every sample was across two image slices, which is 6mm compared to the 4mm sample diameter. This means that some partial voluming was occurring, which could have hindered our ability to find correlations.

5.2 qMRI Correlations

T_1 relaxation times had significant correlations with every qMT metric, including a strongly negative correlation with f using a Super-Lorentzian line shape. While I did not work with degenerated or diseased specimens, it is useful to think about how metrics behave in degeneration to make sense of the correlations present in this study. T_1 relaxation times have previously been shown to increase in cartilage with tissue degeneration [27]. The more degenerated a tissue is, the lower f should be, therefore a negative correlation with T_1 is intuitive. It is interesting that T_1 correlated better with qMT metrics than T_2, considering T_1 is an often neglected parameter in the musculoskeletal literature while T_2 is quite commonly implemented.

T_2 had some correlations with qMT metrics, most notably a moderate negative correlation with f when using a Super-Lorentzian line shape.

T_1 and T_2 were found to have a moderately positive correlation. These two metrics being positively correlated could be because they are influenced by the same macromolecules. In one study, T_1 and T_2 correlated very strongly in the human meniscus ex vivo [127], while in another study, T_1 was found to have a moderate correlation with T_2 in human patellar cartilage, but this relationship did not exist in bovine or porcine specimens [19]. In a study involving rabbit intervertebral discs, there was no significant relationship between T_1 and T_2 [128]. It was also found that $T_{1\rho}$ and T_2 were very strongly correlated in the human meniscus [32], which is another indication that correlations between qMRI parameters do occur, and that some parameters may be influenced by certain macromolecules more than others. This is particularly important when considering how qMRI metrics may behave differently in some tissues than others, as different tissues have different macromolecular compositions. Additionally, in degenerative processes some macromolecules may be affected more greatly than others, which could be why some imaging metrics are sensitive to degeneration while others are not. This correlation should be further explored as it is not completely understood and could vary between species.

5.3 Challenges Involving Mechanical Testing the Meniscus

This project is a good demonstration of how difficult mechanical testing the meniscus is. It is challenging to know the optimum approach as there are many different techniques for every step of the whole process and little consistency throughout the literature. Testing procedures in the literature implement either stress relaxation [32, 96, 98, 99, 104, 108] or creep [83, 95, 96] testing methodologies for confined compression [96, 98, 99, 104, 108], unconfined compression [24, 32, 95], or indentation setups [22, 31, 83, 95]. For stress relaxation, there are different strain levels which samples are tested at, as well as different applied strain rates when compressing the samples (Table 5.1). Core samples can be procured in a variety of ways and from varying locations within the menisci. These samples can be a range of sizes in terms of diameter, thickness and procurement location along the depth which affects the mechanical testing force magnitudes. Further, they are stored in different enzyme inhibitor solutions which can affect how degenerated the tissues become. There are also many different mechanical properties that a study can choose to measure which are often model dependent. Preloading is something some

studies do to deal with potential residual stresses in the samples [98, 99], while others – including the current study – do not [32, 53, 96, 108].

Table 5.1 - Various testing parameters used in the literature for stress-relaxation tests. Strain rates reported as %/min, normalized for a sample height of 2mm.

Study	Year	Tissue	%/min	Strain Levels (%)	Core Diameter (mm)
Seitz [104]	2013	Meniscus	100.000	10, 15, 20	4.6
Son [32]	2013	Meniscus	6.000	5, 10, 15, 20	4
Ateshian [99]	1997	Cartilage	0.750	10, 20, 30, 40, 50	6.35
Perie [107]	2005	Intervertebral Discs	0.600	5, 10, 15, 20	5
Bursac [108]	1999	Cartilage	0.345	3,6, 9, 12, 15	4.5
Current	2020	Meniscus	0.300	15	4

Data modeling is an extremely difficult part of this process that does not seem to be appropriately discussed in the literature. While many models for determining *Ha* and *kp* originate from the same source [14], almost every researcher went with their own simplified versions of it [96, 99, 104, 107-109] as the original is difficult to model due to its complexity and large number of terms. Having such a wide variety of models makes it difficult to know if results are comparable, and in the case of this project it was challenging getting the models to fit our data. Many studies gloss over how difficult this is and do not go into detail on what they had to do to make this work. I tested many different bovine specimens using varying testing parameters, models, and curve fitting methods before I had one I was satisfied with. I tested samples of 4mm and 6mm in diameter, at strains ranging from 5% to 30% with a wide range of strain rates, and varying stress relaxation times. I found that the most sensitive variables were the strain rates and strain levels, and carefully adjusting these led to very high quality fits with an average R-Square of 0.98.

The applied strain rate in this study is slower than any of the similar tests in the literature, with most being over twice as fast. I found that the applied strain rate influences the shape of the curve of the mechanical testing data, meaning it is important to have an appropriate strain rate for the model used. The strain rate used is not as important as how the data fits the model. If the desired outcomes are obtained and can be compared to outcomes from other studies, it should not matter specifically how they were obtained.

There is limited literature on mechanical testing of the meniscus. When it is narrowed down to human menisci with *Ha* and *kp* outcomes, the comparisons are reduced to only a few studies, most of which used different methodologies. The mechanical testing outcomes are compared for the medial meniscus in Table 5.2. Compared to the literature, our *Ha* values are much smaller. However, the studies that implemented creep testing had considerably higher values than those that used stress relaxation. My permeability values are quite a bit higher than those in the literature in general, which could be due to tissue health differences, or the differences in mechanical testing models and procedures.

Table 5.2 - Mechanical Testing Outcomes in the Literature for Human Medial Menisci. Medial Menisci were compared as that is all that was tested for each study.

Medial Meniscus Mechanical Testing Outcomes						
Study	Year	Setup	Methodology	Ha (kPa)	kp * 10^{15} (m^4/Ns)	R-Square
Seitz [104]	2013	Confined Compression	Stress Relaxation	64.00	3.93	0.73
Sweigart [129]	2004	Indentation	Creep	120	1.78	Unknown
Joshi [130]	1995	Confined Compression	Creep	230	1.99	Unknown
Hacker [131]	1992	Confined Compression	Creep	230	0.88	Unknown
Current	2020	Confined Compression	Stress Relaxation	20.84	110.48	0.98

When compared closely to the only other study that used stress relaxation [104], some key differences are found in the testing approaches. My applied strain rate for compressing the sample was 0.3%/min, while in that study they used an applied strain rate of 100%/min, which is over 300 times faster. Since the model used in this study does not account for applied strain rate, this could be an important factor in the testing outcomes. Higher strain rates cause higher peak forces which alter the shapes of the relaxation curves and ultimately altering the magnitudes of the mechanical properties. Samples were also tested at strain levels of 10, 15, and 20% compared to the current study which only tested at 15%. This should not make a difference though, as I only compared their 15% results to ours, and between strain levels they gave 90 minutes for the sample to fully relax which is even more than the 2000 seconds (33.3 minutes) I gave ours after the initial loading to 10%. This study does not explicitly report the force values of their tests, but from inspecting the figures it can be approximated that our relaxed force values are under half of

theirs, which explains the differences in *Ha*. Differences in forces could also be attributed to many things such as differences in specimen storage in terms of temperature and storage solution composition, length of time allowed tissues were allowed to be unfrozen before testing, location of sample procurement, size of the individual samples, and general tissue health. My *kp* values are also quite larger than in this paper. The CV_{RMS} values obtained from our precision study were 10.55% and 8.36% for *Ha* and *kp* respectively, which do not explain the differences in our findings alone. The differences in methodologies could be a source of variation between our results, in particular the completely different strain rates used and how their model does not account for this testing parameter.

In the precision study we tested bovine menisci, and the resulting *Ha* values were much closer to the literature (Table 5.3). Seeing a large range of *Ha* values here, even though the number of studies is low, indicates that this metric is quite variable in the literature in general, meaning that our values found are not necessarily invalidated by being different. The permeability values I found are much larger than those in the literature here as well, meaning either our model under-estimates this metric, or it is generally over-estimated in the literature.

Table 5.3 - Aggregate Modulus and Permeability for Bovine Meniscus in the Literature

Study	Year	Ha (kPa)	$kp*10^{15}$ (m^4/Ns)
Joshi [130]	1995	13	3.18
Proctor [132]	1989	41	0.81
Sweigart [129]	2004	14	5.57
Danso [133]	2018	252	-
Current	2020	30	81.8

Ultimately, our mechanical testing outcomes are quite different from the literature, but there is such a variety in how these studies are done that comparison is difficult. A standard approach to how this testing is done is much needed in this field. I suggest the model I used from Bursac's study, as I have proven it can have very good fits to experimental data, strain rate is taken into consideration, and the parameters have physical meaning, compared to some models which determine arbitrary coefficients.

5.4 Super-Lorentzian or Gaussian?

In this study, both Super-Lorentzian and Gaussian line shapes were used during qMT modeling. It has been previously suggested to fit both line shapes [88], but most studies use Super-Lorentzian and do not implement Gaussian [89, 92]. Previously in one study there were conflicting results on which line shape is better. They found that a Super-Lorentzian line shape had better results for their in-vitro specimens, while a Gaussian line shape was better for their in-vivo specimens [116].

Table 5.4 - Fit Quality Comparison: Super-Lorentzian versus Gaussian Line Shapes

Fit Quality (Normalized RMS)		
Specimen	Super-Lorentzian	Gaussian
K01	0.8602	0.8790
K02	0.8410	0.8569
K03	0.9134	0.9332
K04	0.9232	0.9412
K05	0.8874	0.9012
K06	0.9006	0.9208
Mean	0.8876	0.9054

We found that the Gaussian line shape had better fits, but only marginally (Table 5.4). A Super-Lorentzian line shape yielded quite different T_{2b} results than Gaussian, and had different correlations, which means these modeling techniques could be useful in different ways. Because these line shapes have not been thoroughly compared in the literature, it is unknown as to how sensitive each metric is to the fit quality. Both line shapes appear to be appropriate, but it is not clear which is better. Below in Figure 5.1 is a visual representation of both line shape fits side-by-side. Probing differences in results due to curve fitting is beyond the scope of this thesis; future work in this area is discussed in section 6.1.

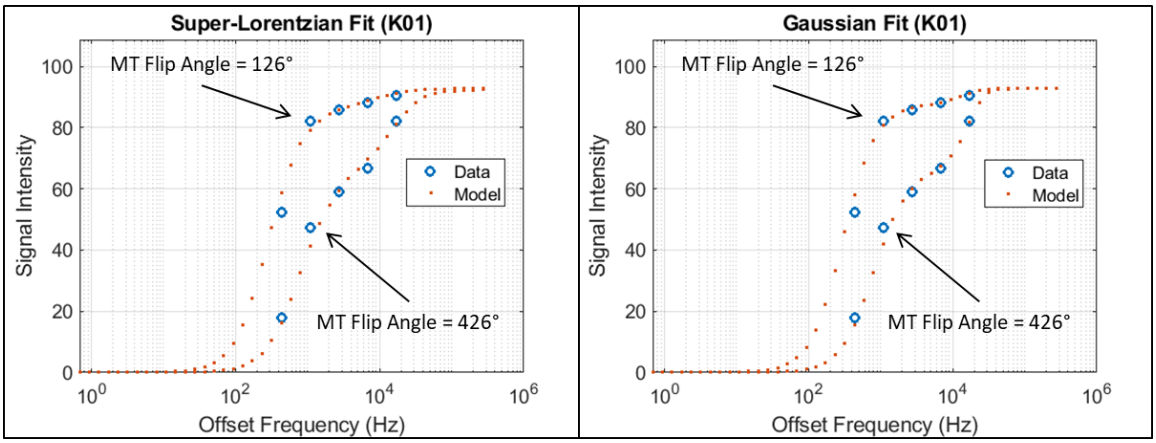

Figure 5.1 - Comparison of Super-Lorentzian and Gaussian Line Shape Fits on Specimen K01

5.5 Comparing qMT Measures in Cartilage and the Meniscus

The MT effect can be demonstrated with signal suppression on images acquired with MT. Looking at Figure 5.2 below, it can be seen that signal varies greatly with offset frequency, which shows signal suppression is occurring. This demonstrates the MT effect in the meniscus. This has been shown previously [134], and in Simard's study the MT effect was demonstrated and qMT measures were obtained [89]. However this is something that has not been thoroughly explored and this study further demonstrates that qMT studies are viable in the meniscus.

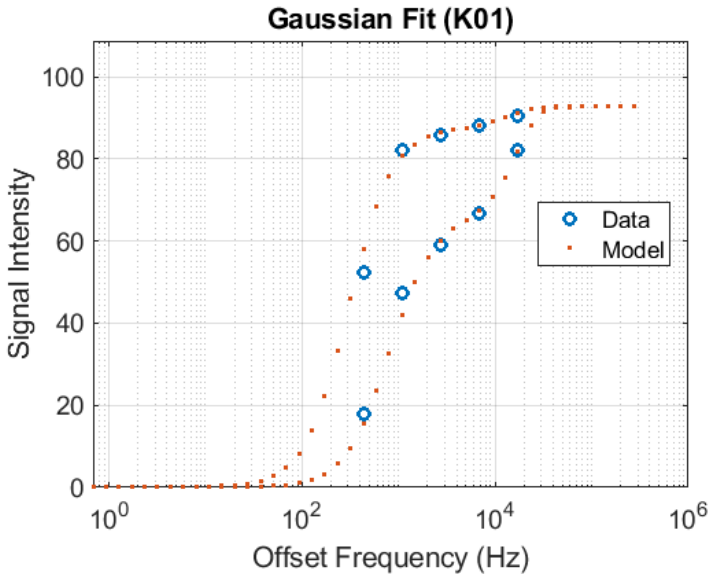

Figure 5.2 - MT Effect of Specimen K01 Shown with a Gaussian Line Shape Fit

Comparing *f* and *k* values of the current study to the only other qMT study on the meniscus shows strong similarities [89] (Table 5.5). The biggest difference is in T_{2b} when using a Gaussian line shape, which is approximately three times as long in this study as in Simard's. It is unclear as to why there is such a large discrepancy in T_{2b} between line shapes.

Table 5.5 - qMT Values in Cartilage and the Meniscus

qMT Values in Cartilage and Meniscus							
	Cartilage				Meniscus		
	Sritanyaratana [93]		Stikov [92]	Simard [89]	Simard [89]	Current	
	(Asymptomatic)	(OA)				Super-Lorentzian	Gaussian
f (%)	12.46	12.8	25*	15.19	23.36	29.22	23.53
k (s^{-1})	7.22	6.13	1.8*	3	2.38	2.93	3.03
T_{2b} (μs)	6.49	6.8	-	5.3	5.65	5.47	16.1
T_{1f} (ms)	-	-	-	882.8	736.2	577.01	598.11
*Values not directly reported and were estimated from figures.							

It is useful to compare qMT measure between cartilage and the meniscus as they are similar soft tissues. As can be seen in Table 5.5, *f* is typically larger in the meniscus. This indicates that cartilage has a higher percentage water composition than the meniscus, which is consistent with what was previously discussed (Table 2.1) [35]. *k* is a metric that is a bit less consistent in cartilage with some values being larger, some smaller, and some in the same range as those measured in the meniscus. This is an indication that we need more data on this metric to get a sense for how it behaves in these soft tissues. T_{2b} is another metric that needs to be further assessed to find trends in these tissues. At 16.1μs in the current study, T_{2b} while using a Gaussian line shape is considerably larger than in any of the previous measures with the second closest being 6.8 μs in OA cartilage [93]. It may be that this difference is due to the line shape used, as Simard used a Super-Lorentzian line shape and had similar values to ours. T_{1f} does not yet have enough measures available in the literature to find any trends.

5.6 Strengths and Limitations

The primary strength of this study is that it implemented an MRI technique which models soft tissues in the same way that they are physically modeled. Since they both model soft tissues as being biphasic, qMT provides metrics related to macromolecules of the tissue which are

responsible for tissue functionality. This is the first study to correlate qMT parameters to mechanical properties in the meniscus, and the second study to correlate qMRI parameters with meniscal mechanical properties. Since the meniscus is a key soft tissue in the OA process, it is important that this relationship be further explored. The second strength of this study was that it used a novel approach in its image registration process, starting with the point cloud generation techniques. This approach is time effective and provides highly detailed point cloud models which led to high quality registration with low shape match errors (considering the qMRI resolution limitations). The third strength is the data modeling implemented in this study, which had very robust fits and outputs that theoretically have physical meaning directly related to tissue functionality.

The primary limitation of this study is that the cadaver specimens were too homogeneous. If there was a wider range of tissue health in terms of age and level of disease then I might have found more correlations. I only worked with 6 cadaver knees that had no history of knee surgery or disease, but if I had utilized more or if I had used trypsin to degrade tissues selectively, it is possible I could have had better variation.

Another limitation of this study is from qMRI image resolution limiting image registration capabilities. This is a common challenge in OA research, as there is no simple way to approach this problem. The metric that indicates the quality of registration is the shape match error, which ended up being very close to the in-plane image resolution. Also, If the image resolution was better, the shape match error would likely have been lower. Manual segmentation of the menisci is another source of error that compounds with this one. A study measuring interobserver reproducibility in manual segmentation of the meniscus found that the root mean square interobserver reproducibility error was 5.4% for medial meniscus volume [135]. Segmentation capabilities are limited by the image resolution, but there is a trade-off because increasing the resolution will decrease the signal to noise ratio, and there needs to be enough signal within the voxel in order to adequately fit the qMRI parameters.

Sample locations in the images are a concern as well, even beyond image registration challenges. When the samples were procured from the menisci by hand, they were intended to be taken from the soft tissue at a direction normal to the tibial plateau. This is an assumption that was made when defining the sample locations in the menisci after registration, so if the samples

procured were not perpendicular to the tibial surface then there would be a mismatch in the sample location in the images and the physical menisci. To mitigate this source of error, the samples themselves were 4mm in diameter, but the samples in the images were made to be only 3mm in diameter which allows for some variance in sample procurement angle. Additionally, the 3D modeled cylinders that represent the samples and were created in Fusion360 were lined up with the holes in the meniscus surface models by hand, as well as those holes being cut by hand. There is human error involved in this process which is difficult to quantify.

The partial-voluming effect is another limitation to consider. Each sample was 4mm thick, and spanned two image slices which are 3mm thick each. This means that a 4mm diameter sample is being represented over 6mm, and some of the information for those voxels has to come from outside the region-of-interest. This could have limited our ability to find correlations.

Preloading of meniscal samples before mechanical testing was not implemented in this study. It is possible that residual stresses exist in core samples from being cut which could increase the variability of the data of the mechanical tests. I did not implement preloading to avoid damaging the samples from unnecessary loading. There are many studies that implement preloading [98, 99], and many which do not [32, 53, 96, 108], and it is something that should be considered for future studies.

6.0 Conclusions

The aim of this study was to assess whether qMT metrics (e.g., f, k, T_{1f}, T_{2f}, and T_{2b}) accurately predict experimentally-derived mechanical properties (e.g., *Ha* and *kp*) of excised meniscal samples. This assessment yielded one weak correlation between the mechanical properties and qMT metrics (*Ha* and T_{2b} using a Super-Lorentzian line shape); however, more may exist and were not detected because the specimens were too similar and did not provide a range of tissue health for correlations to be derived from. Or, it is possible that more of these correlations do not exist and qMT cannot be used for assessing mechanical properties.

There are a number of useful findings resulting from this research. The correlations found between T_1 and other imaging metrics is an interesting finding as it is something not commonly found in the literature and this could indicate that T_1 is an important metric for the meniscus. It was also shown that that there is a qMT effect in the meniscus, reinforcing what was found by Simard [94]. Additionally, this study has provided a large amount of qMT data which can be used for context in future studies.

6.1 Future Work

Due to the nature of qMT modeling soft tissues in the same way they are physically modeled, there are strong possibilities that this imaging technique could provide insight into tissue functionality at all stages of degeneration. My recommendation is to have more studies similar to the current study with the meniscus, but with an emphasis on having a wider range of specimen health. Additionally, it would be valuable to study the relationship between qMT metrics and cartilage mechanical properties. While cartilage is similar to the meniscus, the macromolecular composition differs and qMRI metrics have had different correlations in both tissues. There is a large body of literature on cartilage and qMRI to work off of and any studies of this type would have other studies to compare results to, providing insight into the bigger picture. It is also still unclear as to which line shape is more appropriate to use – Super-Lorentzian or Gaussian. It is important to investigate which line shape is better, and to determine how sensitive measures are to the fit quality. Both accuracy and repeatability should be considered and this might require a study that employs spectroscopy or a synchrotron to better characterize the macromolecules present.

In similar future studies, larger core sample sizes should be considered. Larger regions of interest would have more voxels within them and would be less susceptible to influence from outlier values. Selectively degenerating samples using trypsin could be a method to introduce variability in tissue degeneration to help find correlations. Additionally, the Andrews model explored in this study could be worth investigating further even if the parameters in it are not directly related to specific tissue properties, as the model fit the data almost perfectly and the parameters can be compared between samples.

References

[1] M. Djurasovic, J. W. Aldridge, R. Grumbles, M. P. Rosenwasser, D. Howell, and A. Ratcliffe, "Knee joint immobilization decreases aggrecan gene expression in the meniscus," *Am J Sports Med,* vol. 26, pp. 460-6, May-Jun 1998.

[2] P. S. Walker, S. Arno, C. Bell, G. Salvadore, I. Borukhov, and C. Oh, "Function of the medial meniscus in force transmission and stability," *J Biomech,* vol. 48, pp. 1383-8, Jun 01 2015.

[3] A. A. o. Canada. (2011, January 16, 2017). *The Impact of Arthritis in Canada: Today and Over the Next 30 Years*. Available: http://www.arthritisalliance.ca/en/impactquick

[4] C. Ding, J. Martel-Pelletier, J. P. Pelletier, F. Abram, J. P. Raynauld, F. Cicuttini, *et al.*, "Meniscal tear as an osteoarthritis risk factor in a largely non-osteoarthritic cohort: a cross-sectional study," *J Rheumatol,* vol. 34, pp. 776-84, Apr 2007.

[5] M. Englund, A. Guermazi, F. W. Roemer, P. Aliabadi, M. Yang, C. E. Lewis, *et al.*, "Meniscal tear in knees without surgery and the development of radiographic osteoarthritis among middle-aged and elderly persons: The Multicenter Osteoarthritis Study," *Arthritis Rheum,* vol. 60, pp. 831-9, Mar 2009.

[6] M. Englund, F. W. Roemer, D. Hayashi, M. D. Crema, and A. Guermazi, "Meniscus pathology, osteoarthritis and the treatment controversy," *Nat Rev Rheumatol,* vol. 8, pp. 412-9, May 22 2012.

[7] J. P. Pelletier, J. P. Raynauld, M. J. Berthiaume, F. Abram, D. Choquette, B. Haraoui, *et al.*, "Risk factors associated with the loss of cartilage volume on weight-bearing areas in knee osteoarthritis patients assessed by quantitative magnetic resonance imaging: a longitudinal study," *Arthritis Res Ther,* vol. 9, p. R74, 2007.

[8] M. V. Smith, J. J. Nepple, R. W. Wright, M. J. Matava, and R. H. Brophy, "Knee Osteoarthritis Is Associated With Previous Meniscus and Anterior Cruciate Ligament Surgery Among Elite College American Football Athletes," *Sports Health,* vol. 9, pp. 247-251, May/Jun 2017.

[9] L. S. Lohmander, P. M. Englund, L. L. Dahl, and E. M. Roos, "The long-term consequence of anterior cruciate ligament and meniscus injuries: osteoarthritis," *Am J Sports Med,* vol. 35, pp. 1756-69, Oct 2007.

[10] J. Y. Bae, K. S. Park, J. K. Seon, D. S. Kwak, I. Jeon, and E. K. Song, "Biomechanical analysis of the effects of medial meniscectomy on degenerative osteoarthritis," *Med Biol Eng Comput,* vol. 50, pp. 53-60, Jan 2012.

[11] C. Hoser, C. Fink, C. Brown, M. Reichkendler, W. Hackl, and J. Bartlett, "Long-term results of arthroscopic partial lateral meniscectomy in knees without associated damage," *J Bone Joint Surg Br,* vol. 83, pp. 513-6, May 2001.

[12] C. Rangger, T. Klestil, W. Gloetzer, G. Kemmler, and K. P. Benedetto, "Osteoarthritis after arthroscopic partial meniscectomy," *Am J Sports Med,* vol. 23, pp. 240-4, Mar-Apr 1995.

[13] G. o. Saskatchewan. (2016, Annual Statistical Report for 2015-2016.

[14] V. C. Mow, S. C. Kuei, W. M. Lai, and C. G. Armstrong, "Biphasic creep and stress relaxation of articular cartilage in compression? Theory and experiments," *J Biomech Eng,* vol. 102, pp. 73-84, Feb 1980.

[15] E. Lammentausta, P. Kiviranta, M. J. Nissi, M. S. Laasanen, I. Kiviranta, M. T. Nieminen, *et al.*, "T2 relaxation time and delayed gadolinium-enhanced MRI of cartilage (dGEMRIC) of human patellar cartilage at 1.5 T and 9.4 T: Relationships with tissue mechanical properties," *J Orthop Res,* vol. 24, pp. 366-74, Mar 2006.

[16] M. T. Nieminen, J. Toyras, J. Rieppo, J. M. Hakumaki, J. Silvennoinen, H. J. Helminen, *et al.*, "Quantitative MR microscopy of enzymatically degraded articular cartilage," *Magn Reson Med,* vol. 43, pp. 676-81, May 2000.

[17] A. J. Wheaton, G. R. Dodge, D. M. Elliott, S. B. Nicoll, and R. Reddy, "Quantification of cartilage biomechanical and biochemical properties via T1rho magnetic resonance imaging," *Magn Reson Med,* vol. 54, pp. 1087-93, Nov 2005.

[18] M. F. Koff, P. Shah, S. Pownder, B. Romero, R. Williams, S. Gilbert, *et al.*, "Correlation of meniscal T2* with multiphoton microscopy, and change of articular cartilage T2 in an ovine model of meniscal repair," *Osteoarthritis Cartilage,* vol. 21, pp. 1083-91, Aug 2013.

[19] M. J. Nissi, J. Rieppo, J. Toyras, M. S. Laasanen, I. Kiviranta, M. T. Nieminen, *et al.*, "Estimation of mechanical properties of articular cartilage with MRI - dGEMRIC, T2 and T1 imaging in different species with variable stages of maturation," *Osteoarthritis Cartilage,* vol. 15, pp. 1141-8, Oct 2007.

[20] T. Aoki, A. Watanabe, N. Nitta, T. Numano, M. Fukushi, and M. Niitsu, "Correlation between apparent diffusion coefficient and viscoelasticity of articular cartilage in a porcine model," *Skeletal Radiol,* vol. 41, pp. 1087-92, Sep 2012.

[21] M. Baldassarri, J. S. Goodwin, M. L. Farley, B. E. Bierbaum, S. R. Goldring, M. B. Goldring, *et al.*, "Relationship between cartilage stiffness and dGEMRIC index: correlation and prediction," *J Orthop Res,* vol. 25, pp. 904-12, Jul 2007.

[22] V. Juras, M. Bittsansky, Z. Majdisova, P. Szomolanyi, I. Sulzbacher, S. Gabler, *et al.*, "In vitro determination of biomechanical properties of human articular cartilage in osteoarthritis using multi-parametric MRI," *J Magn Reson,* vol. 197, pp. 40-7, Mar 2009.

[23] K. E. Keenan, S. Pal, D. P. Lindsey, T. F. Besier, and G. S. Beaupre, "A viscoelastic constitutive model can accurately represent entire creep indentation tests of human patella cartilage," *J Appl Biomech,* vol. 29, pp. 292-302, Jun 2013.

[24] J. E. Kurkijarvi, M. J. Nissi, I. Kiviranta, J. S. Jurvelin, and M. T. Nieminen, "Delayed gadolinium-enhanced MRI of cartilage (dGEMRIC) and T2 characteristics of human knee articular cartilage: topographical variation and relationships to mechanical properties," *Magn Reson Med,* vol. 52, pp. 41-6, Jul 2004.

[25] E. Lammentausta, P. Kiviranta, J. Toyras, M. M. Hyttinen, I. Kiviranta, M. T. Nieminen, *et al.*, "Quantitative MRI of parallel changes of articular cartilage and underlying trabecular bone in degeneration," *Osteoarthritis Cartilage,* vol. 15, pp. 1149-57, Oct 2007.

[26] M. T. Nieminen, J. Toyras, M. S. Laasanen, J. Silvennoinen, H. J. Helminen, and J. S. Jurvelin, "Prediction of biomechanical properties of articular cartilage with quantitative magnetic resonance imaging," *J Biomech,* vol. 37, pp. 321-8, Mar 2004.

[27] M. J. Nissi, J. Toyras, M. S. Laasanen, J. Rieppo, S. Saarakkala, R. Lappalainen, *et al.*, "Proteoglycan and collagen sensitive MRI evaluation of normal and degenerated articular cartilage," *J Orthop Res,* vol. 22, pp. 557-64, May 2004.

[28] J. Rautiainen, M. J. Nissi, E. N. Salo, V. Tiitu, M. A. J. Finnila, O. M. Aho, *et al.*, "Multiparametric MRI assessment of human articular cartilage degeneration: Correlation with quantitative histology and mechanical properties," *Magn Reson Med,* vol. 74, pp. 249-259, Jul 2015.

[29] J. G. Raya, A. P. Arnoldi, D. L. Weber, L. Filidoro, O. Dietrich, S. Adam-Neumair, *et al.*, "Ultra-high field diffusion tensor imaging of articular cartilage correlated with histology and scanning electron microscopy," *MAGMA,* vol. 24, pp. 247-58, Aug 2011.

[30] J. T. Samosky, D. Burstein, W. Eric Grimson, R. Howe, S. Martin, and M. L. Gray, "Spatially-localized correlation of dGEMRIC-measured GAG distribution and mechanical stiffness in the human tibial plateau," *J Orthop Res,* vol. 23, pp. 93-101, Jan 2005.

[31] S. Y. Tang, R. B. Souza, M. Ries, P. K. Hansma, T. Alliston, and X. Li, "Local tissue properties of human osteoarthritic cartilage correlate with magnetic resonance T(1) rho relaxation times," *J Orthop Res,* vol. 29, pp. 1312-9, Sep 2011.

[32] M. Son, S. B. Goodman, W. Chen, B. A. Hargreaves, G. E. Gold, and M. E. Levenston, "Regional variation in T1rho and T2 times in osteoarthritic human menisci: correlation with mechanical properties and matrix composition," *Osteoarthritis Cartilage,* vol. 21, pp. 796-805, Jun 2013.

[33] J. Herwig, E. Egner, and E. Buddecke, "Chemical changes of human knee joint menisci in various stages of degeneration," *Ann Rheum Dis,* vol. 43, pp. 635-40, Aug 1984.

[34] M. L. Killian, D. I. Isaac, R. C. Haut, L. M. Dejardin, D. Leetun, and T. L. Donahue, "Traumatic anterior cruciate ligament tear and its implications on meniscal degradation: a preliminary novel lapine osteoarthritis model," *J Surg Res,* vol. 164, pp. 234-41, Dec 2010.
[35] V. C. Mow, *Basic Orthopaedic Biomechanics and Mechano-Biology*, 2005.
[36] From Wikimedia Commons: By Kari Stammen - Sent to me personally, Public Domain, https://commons.wikimedia.org/w/index.php?curid=24863847.
[37] S. P. Arnoczky and R. F. Warren, "Microvasculature of the human meniscus," *Am J Sports Med,* vol. 10, pp. 90-5, Mar-Apr 1982.
[38] T. Karachalios, A. Zibis, P. Papanagiotou, A. H. Karantanas, K. N. Malizos, and N. Roidis, "MR imaging findings in early osteoarthritis of the knee," *Eur J Radiol,* vol. 50, pp. 225-30, Jun 2004.
[39] D. J. Hunter, Y. Q. Zhang, J. B. Niu, X. Tu, S. Amin, M. Clancy, *et al.*, "The association of meniscal pathologic changes with cartilage loss in symptomatic knee osteoarthritis," *Arthritis Rheum,* vol. 54, pp. 795-801, Mar 2006.
[40] K. Emmanuel, E. Quinn, J. Niu, A. Guermazi, F. Roemer, W. Wirth, *et al.*, "Quantitative measures of meniscus extrusion predict incident radiographic knee osteoarthritis--data from the Osteoarthritis Initiative," *Osteoarthritis Cartilage,* vol. 24, pp. 262-9, Feb 2016.
[41] K. Bloecker, W. Wirth, A. Guermazi, W. Hitzl, D. J. Hunter, and F. Eckstein, "Longitudinal change in quantitative meniscus measurements in knee osteoarthritis--data from the Osteoarthritis Initiative," *Eur Radiol,* vol. 25, pp. 2960-8, Oct 2015.
[42] G. Jones, C. Ding, F. Scott, M. Glisson, and F. Cicuttini, "Early radiographic osteoarthritis is associated with substantial changes in cartilage volume and tibial bone surface area in both males and females," *Osteoarthritis Cartilage,* vol. 12, pp. 169-74, Feb 2004.
[43] R. U. Kleemann, D. Krocker, A. Cedraro, J. Tuischer, and G. N. Duda, "Altered cartilage mechanics and histology in knee osteoarthritis: relation to clinical assessment (ICRS Grade)," *Osteoarthritis Cartilage,* vol. 13, pp. 958-63, Nov 2005.
[44] L. A. Setton, D. M. Elliott, and V. C. Mow, "Altered mechanics of cartilage with osteoarthritis: human osteoarthritis and an experimental model of joint degeneration," *Osteoarthritis Cartilage,* vol. 7, pp. 2-14, Jan 1999.
[45] A. Lahm, E. Mrosek, H. Spank, C. Erggelet, R. Kasch, J. Esser, *et al.*, "Changes in content and synthesis of collagen types and proteoglycans in osteoarthritis of the knee joint and comparison of quantitative analysis with Photoshop-based image analysis," *Arch Orthop Trauma Surg,* vol. 130, pp. 557-64, Apr 2010.
[46] J. T. Makela, S. K. Han, W. Herzog, and R. K. Korhonen, "Very early osteoarthritis changes sensitively fluid flow properties of articular cartilage," *J Biomech,* vol. 48, pp. 3369-76, Sep 18 2015.
[47] H. J. Mankin and A. Z. Thrasher, "Water content and binding in normal and osteoarthritic human cartilage," *J Bone Joint Surg Am,* vol. 57, pp. 76-80, Jan 1975.
[48] From Wikimedia Commons: By BruceBlaus - Own work, CC BY-SA 4.0 International, https://commons.wikimedia.org/w/index.php?curid=44968165.
[49] D. L. Goldenberg, M. S. Egan, and A. S. Cohen, "Inflammatory synovitis in degenerative joint disease," *J Rheumatol,* vol. 9, pp. 204-9, Mar-Apr 1982.
[50] R. Altman, E. Asch, D. Bloch, G. Bole, D. Borenstein, K. Brandt, *et al.*, "Development of criteria for the classification and reporting of osteoarthritis. Classification of osteoarthritis of the knee. Diagnostic and Therapeutic Criteria Committee of the American Rheumatism Association," *Arthritis Rheum,* vol. 29, pp. 1039-49, Aug 1986.
[51] Z. Zhu, L. L. Laslett, X. Jin, W. Han, B. Antony, X. Wang, *et al.*, "Association between MRI-detected osteophytes and changes in knee structures and pain in older adults: a cohort study," *Osteoarthritis Cartilage,* vol. 25, pp. 1084-1092, Jul 2017.
[52] M. Sengupta, Y. Q. Zhang, J. B. Niu, A. Guermazi, M. Grigorian, D. Gale, *et al.*, "High signal in knee osteophytes is not associated with knee pain," *Osteoarthritis Cartilage,* vol. 14, pp. 413-7, May 2006.

[53] K. M. Fischenich, J. Lewis, K. A. Kindsfater, T. S. Bailey, and T. L. Haut Donahue, "Effects of degeneration on the compressive and tensile properties of human meniscus," *J Biomech,* vol. 48, pp. 1407-11, Jun 1 2015.
[54] K. M. Fischenich, K. D. Button, G. A. Coatney, R. S. Fajardo, K. M. Leikert, R. C. Haut, *et al.*, "Chronic changes in the articular cartilage and meniscus following traumatic impact to the lapine knee," *J Biomech,* vol. 48, pp. 246-53, Jan 21 2015.
[55] K. M. Fischenich, G. A. Coatney, J. H. Haverkamp, K. D. Button, C. DeCamp, R. C. Haut, *et al.*, "Evaluation of meniscal mechanics and proteoglycan content in a modified anterior cruciate ligament transection model," *J Biomech Eng,* vol. 136, Jul 2014.
[56] B. B. Wheatley, K. M. Fischenich, K. D. Button, R. C. Haut, and T. L. Haut Donahue, "An optimized transversely isotropic, hyper-poro-viscoelastic finite element model of the meniscus to evaluate mechanical degradation following traumatic loading," *J Biomech,* vol. 48, pp. 1454-60, Jun 1 2015.
[57] R. C. Appleyard, D. Burkhardt, P. Ghosh, R. Read, M. Cake, M. V. Swain, *et al.*, "Topographical analysis of the structural, biochemical and dynamic biomechanical properties of cartilage in an ovine model of osteoarthritis," *Osteoarthritis Cartilage,* vol. 11, pp. 65-77, Jan 2003.
[58] C. I. f. H. Information. (2015, Hip and Knee Replacements in Canada, 2014-2015.
[59] From Wikimedia Commons: By J. Lengerke - Praxis Dr. Jochen Lengerke, CC BY-SA 3.0 Germany, https://commons.wikimedia.org/wiki/File:Roe-Gonarthrose.jpg.
[60] J. H. Kellgren and J. S. Lawrence, "Radiological assessment of osteo-arthrosis," *Ann Rheum Dis,* vol. 16, pp. 494-502, Dec 1957.
[61] C. G. Peterfy, A. Guermazi, S. Zaim, P. F. Tirman, Y. Miaux, D. White, *et al.*, "Whole-Organ Magnetic Resonance Imaging Score (WORMS) of the knee in osteoarthritis," *Osteoarthritis Cartilage,* vol. 12, pp. 177-90, Mar 2004.
[62] D. J. Hunter, A. Guermazi, G. H. Lo, A. J. Grainger, P. G. Conaghan, R. M. Boudreau, *et al.*, "Evolution of semi-quantitative whole joint assessment of knee OA: MOAKS (MRI Osteoarthritis Knee Score)," *Osteoarthritis Cartilage,* vol. 19, pp. 990-1002, Aug 2011.
[63] D. T. Felson, J. Lynch, A. Guermazi, F. W. Roemer, J. Niu, T. McAlindon, *et al.*, "Comparison of BLOKS and WORMS scoring systems part II. Longitudinal assessment of knee MRIs for osteoarthritis and suggested approach based on their performance: data from the Osteoarthritis Initiative," *Osteoarthritis Cartilage,* vol. 18, pp. 1402-7, Nov 2010.
[64] From Wikimedia Commons: By Test21, CC BY-SA3.0 Unported, https://commons.wikimedia.org/wiki/File:Knie_mr.jpg.
[65] R. Stahl, G. Blumenkrantz, J. Carballido-Gamio, S. Zhao, T. Munoz, M. P. Hellio Le Graverand-Gastineau, *et al.*, "MRI-derived T2 relaxation times and cartilage morphometry of the tibio-femoral joint in subjects with and without osteoarthritis during a 1-year follow-up," *Osteoarthritis Cartilage,* vol. 15, pp. 1225-34, Nov 2007.
[66] X. Li, C. Benjamin Ma, T. M. Link, D. D. Castillo, G. Blumenkrantz, J. Lozano, *et al.*, "In vivo T(1rho) and T(2) mapping of articular cartilage in osteoarthritis of the knee using 3 T MRI," *Osteoarthritis Cartilage,* vol. 15, pp. 789-97, Jul 2007.
[67] A. Williams, B. Mikulis, N. Krishnan, M. Gray, C. McKenzie, and D. Burstein, "Suitability of T(1Gd) as the dGEMRIC index at 1.5T and 3.0T," *Magn Reson Med,* vol. 58, pp. 830-4, Oct 2007.
[68] B. Bittersohl, C. Zilkens, Y. J. Kim, S. Werlen, K. A. Siebenrock, T. C. Mamisch, *et al.*, "Delayed gadolinium-enhanced magnetic resonance imaging of hip joint cartilage: pearls and pitfalls," *Orthop Rev (Pavia),* vol. 3, p. e11, 2011.
[69] R. D. Newbould, S. R. Miller, N. Upadhyay, A. W. Rao, P. Swann, G. E. Gold, *et al.*, "T1-weighted sodium MRI of the articulator cartilage in osteoarthritis: a cross sectional and longitudinal study," *PLoS One,* vol. 8, p. e73067, 2013.

[70] C. D. Jordan, E. J. McWalter, U. D. Monu, R. D. Watkins, W. Chen, N. K. Bangerter, *et al.*, "Variability of CubeQuant T1rho, quantitative DESS T2, and cones sodium MRI in knee cartilage," *Osteoarthritis Cartilage,* vol. 22, pp. 1559-67, Oct 2014.

[71] M. T. Nieminen, J. Rieppo, J. Toyras, J. M. Hakumaki, J. Silvennoinen, M. M. Hyttinen, *et al.*, "T2 relaxation reveals spatial collagen architecture in articular cartilage: a comparative quantitative MRI and polarized light microscopic study," *Magn Reson Med,* vol. 46, pp. 487-93, Sep 2001.

[72] S. Lusse, H. Claassen, T. Gehrke, J. Hassenpflug, M. Schunke, M. Heller, *et al.*, "Evaluation of water content by spatially resolved transverse relaxation times of human articular cartilage," *Magn Reson Imaging,* vol. 18, pp. 423-30, May 2000.

[73] M. C. Chou, P. H. Tsai, G. S. Huang, H. S. Lee, C. H. Lee, M. H. Lin, *et al.*, "Correlation between the MR T2 value at 4.7 T and relative water content in articular cartilage in experimental osteoarthritis induced by ACL transection," *Osteoarthritis Cartilage,* vol. 17, pp. 441-7, Apr 2009.

[74] C. S. Wong, C. H. Yan, N. J. Gong, T. Li, Q. Chan, and Y. C. Chu, "Imaging biomarker with T1rho and T2 mappings in osteoarthritis - in vivo human articular cartilage study," *Eur J Radiol,* vol. 82, pp. 647-50, Apr 2013.

[75] H. Nishioka, J. Hirose, E. Nakamura, Y. Oniki, K. Takada, Y. Yamashita, *et al.*, "T1rho and T2 mapping reveal the in vivo extracellular matrix of articular cartilage," *J Magn Reson Imaging,* vol. 35, pp. 147-55, Jan 2012.

[76] H. Li, S. Chen, H. Tao, and S. Chen, "Quantitative MRI T2 relaxation time evaluation of knee cartilage: comparison of meniscus-intact and -injured knees after anterior cruciate ligament reconstruction," *Am J Sports Med,* vol. 43, pp. 865-72, Apr 2015.

[77] T. C. Dunn, Y. Lu, H. Jin, M. D. Ries, and S. Majumdar, "T2 relaxation time of cartilage at MR imaging: comparison with severity of knee osteoarthritis," *Radiology,* vol. 232, pp. 592-8, Aug 2004.

[78] A. M. Ellingson, T. M. Nagel, D. W. Polly, J. Ellermann, and D. J. Nuckley, "Quantitative T2* (T2 star) relaxation times predict site specific proteoglycan content and residual mechanics of the intervertebral disc throughout degeneration," *J Orthop Res,* vol. 32, pp. 1083-9, Aug 2014.

[79] A. Williams, Y. Qian, S. Golla, and C. R. Chu, "UTE-T2 * mapping detects sub-clinical meniscus injury after anterior cruciate ligament tear," *Osteoarthritis Cartilage,* vol. 20, pp. 486-94, Jun 2012.

[80] R. R. Regatte, S. V. Akella, A. Borthakur, J. B. Kneeland, and R. Reddy, "Proteoglycan depletion-induced changes in transverse relaxation maps of cartilage: comparison of T2 and T1rho," *Acad Radiol,* vol. 9, pp. 1388-94, Dec 2002.

[81] M. T. Nieminen, J. Rieppo, J. Silvennoinen, J. Toyras, J. M. Hakumaki, M. M. Hyttinen, *et al.*, "Spatial assessment of articular cartilage proteoglycans with Gd-DTPA-enhanced T1 imaging," *Magn Reson Med,* vol. 48, pp. 640-8, Oct 2002.

[82] A. Borthakur, E. M. Shapiro, J. Beers, S. Kudchodkar, J. B. Kneeland, and R. Reddy, "Sensitivity of MRI to proteoglycan depletion in cartilage: comparison of sodium and proton MRI," *Osteoarthritis Cartilage,* vol. 8, pp. 288-93, Jul 2000.

[83] K. E. Keenan, T. F. Besier, J. M. Pauly, R. L. Smith, S. L. Delp, G. S. Beaupre, *et al.*, "T1rho Dispersion in Articular Cartilage: Relationship to Material Properties and Macromolecular Content," *Cartilage,* vol. 6, pp. 113-22, Apr 2015.

[84] S. Miyata, K. Homma, T. Numano, T. Tateishi, and T. Ushida, "Evaluation of negative fixed-charge density in tissue-engineered cartilage by quantitative MRI and relationship with biomechanical properties," *J Biomech Eng,* vol. 132, p. 071014, Jul 2010.

[85] S. Miyata, T. Numano, K. Homma, T. Tateishi, and T. Ushida, "Feasibility of noninvasive evaluation of biophysical properties of tissue-engineered cartilage by using quantitative MRI," *J Biomech,* vol. 40, pp. 2990-8, 2007.

[86] A. M. Nguyen, W. Johannessen, J. H. Yoder, A. J. Wheaton, E. J. Vresilovic, A. Borthakur, *et al.*, "Noninvasive quantification of human nucleus pulposus pressure with use of T1rho-weighted magnetic resonance imaging," *J Bone Joint Surg Am*, vol. 90, pp. 796-802, Apr 2008.
[87] D. Perie, J. C. Iatridis, C. N. Demers, T. Goswami, G. Beaudoin, F. Mwale, *et al.*, "Assessment of compressive modulus, hydraulic permeability and matrix content of trypsin-treated nucleus pulposus using quantitative MRI," *J Biomech*, vol. 39, pp. 1392-400, 2006.
[88] R. M. Henkelman, G. J. Stanisz, and S. J. Graham, "Magnetization transfer in MRI: a review," *NMR Biomed*, vol. 14, pp. 57-64, Apr 2001. Permission to use figures received.
[89] M. Simard, "Quantitative Magnetization Transfer Evaluation of the Knee Joint in Magnetic Resonance Imaging," Master of Science, McGill University, 2016.
[90] M. M. Gonzalez, *Atlas of Biomarkers for Alzheimer's Disease*, 2011.
[91] G. Giulietti, M. Bozzali, V. Figura, B. Spano, R. Perri, C. Marra, *et al.*, "Quantitative magnetization transfer provides information complementary to grey matter atrophy in Alzheimer's disease brains," *Neuroimage*, vol. 59, pp. 1114-22, Jan 16 2012.
[92] N. Stikov, K. E. Keenan, J. M. Pauly, R. L. Smith, R. F. Dougherty, and G. E. Gold, "Cross-relaxation imaging of human articular cartilage," *Magn Reson Med*, vol. 66, pp. 725-34, Sep 2011.
[93] N. Sritanyaratana, A. Samsonov, P. Mossahebi, J. J. Wilson, W. F. Block, and R. Kijowski, "Cross-relaxation imaging of human patellar cartilage in vivo at 3.0T," *Osteoarthritis Cartilage*, vol. 22, pp. 1568-76, Oct 2014.
[94] M. Simard, E. J. McWalter, G. Gold, and I. Levesque, "Quantitative Magnetization Transfer MRI of In-Situ and Ex-Situ Meniscus," 2016.
[95] A. Abdelgaied, M. Stanley, M. Galfe, H. Berry, E. Ingham, and J. Fisher, "Comparison of the biomechanical tensile and compressive properties of decellularised and natural porcine meniscus," *J Biomech*, vol. 48, pp. 1389-96, Jun 1 2015.
[96] H. C. Chin, G. Khayat, and T. M. Quinn, "Improved characterization of cartilage mechanical properties using a combination of stress relaxation and creep," *J Biomech*, vol. 44, pp. 198-201, Jan 4 2011.
[97] S. A. Hunter, F. R. Noyes, B. Haridas, M. S. Levy, and D. L. Butler, "Meniscal material properties are minimally affected by matrix stabilization using glutaraldehyde and glycation with ribose," *J Orthop Res*, vol. 23, pp. 555-61, May 2005.
[98] S. H. Andrews, J. B. Rattner, N. G. Shrive, and J. L. Ronsky, "Swelling significantly affects the material properties of the menisci in compression," *J Biomech*, vol. 48, pp. 1485-9, Jun 1 2015.
[99] G. A. Ateshian, W. H. Warden, J. J. Kim, R. P. Grelsamer, and V. C. Mow, "Finite deformation biphasic material properties of bovine articular cartilage from confined compression experiments," *J Biomech*, vol. 30, pp. 1157-64, Nov-Dec 1997.
[100] J. J. Ballyns, T. M. Wright, and L. J. Bonassar, "Effect of media mixing on ECM assembly and mechanical properties of anatomically-shaped tissue engineered meniscus," *Biomaterials*, vol. 31, pp. 6756-63, Sep 2010.
[101] J. M. Deneweth, K. E. Newman, S. M. Sylvia, S. G. McLean, and E. M. Arruda, "Heterogeneity of tibial plateau cartilage in response to a physiological compressive strain rate," *J Orthop Res*, vol. 31, pp. 370-5, Mar 2013.
[102] R. K. Korhonen, M. S. Laasanen, J. Toyras, J. Rieppo, J. Hirvonen, H. J. Helminen, *et al.*, "Comparison of the equilibrium response of articular cartilage in unconfined compression, confined compression and indentation," *J Biomech*, vol. 35, pp. 903-9, Jul 2002.
[103] A. M. Nguyen and M. E. Levenston, "Comparison of osmotic swelling influences on meniscal fibrocartilage and articular cartilage tissue mechanics in compression and shear," *J Orthop Res*, vol. 30, pp. 95-102, Jan 2012.
[104] A. M. Seitz, F. Galbusera, C. Krais, A. Ignatius, and L. Durselen, "Stress-relaxation response of human menisci under confined compression conditions (vol 26, pg 68, 2013)," *Journal of the Mechanical Behavior of Biomedical Materials*, vol. 28, pp. 511-511, Dec 2013.

[105] A. K. Williamson, A. C. Chen, and R. L. Sah, "Compressive properties and function-composition relationships of developing bovine articular cartilage," *J Orthop Res,* vol. 19, pp. 1113-21, Nov 2001.
[106] R. E. Wilusz, S. Zauscher, and F. Guilak, "Micromechanical mapping of early osteoarthritic changes in the pericellular matrix of human articular cartilage," *Osteoarthritis Cartilage,* vol. 21, pp. 1895-903, Dec 2013.
[107] D. Perie, D. Korda, and J. C. Iatridis, "Confined compression experiments on bovine nucleus pulposus and annulus fibrosus: sensitivity of the experiment in the determination of compressive modulus and hydraulic permeability," *J Biomech,* vol. 38, pp. 2164-71, Nov 2005.
[108] P. M. Bursac, T. W. Obitz, S. R. Eisenberg, and D. Stamenovic, "Confined and unconfined stress relaxation of cartilage: appropriateness of a transversely isotropic analysis," *J Biomech,* vol. 32, pp. 1125-30, Oct 1999.
[109] M. K. Kwan, S. A. Hacker, S. L. Woo, and J. S. Wayne, "The effect of storage on the biomechanical behavior of articular cartilage--a large strain study," *J Biomech Eng,* vol. 114, pp. 149-53, Feb 1992.
[110] M. P. Hellio Le Graverand, E. Vignon, I. G. Otterness, and D. A. Hart, "Early changes in lapine menisci during osteoarthritis development: Part I: cellular and matrix alterations," *Osteoarthritis Cartilage,* vol. 9, pp. 56-64, Jan 2001.
[111] X. Li, A. Pai, G. Blumenkrantz, J. Carballido-Gamio, T. Link, B. Ma, *et al.*, "Spatial distribution and relationship of T1rho and T2 relaxation times in knee cartilage with osteoarthritis," *Magn Reson Med,* vol. 61, pp. 1310-8, Jun 2009.
[112] M. C. Gallo, C. Wyatt, V. Pedoia, D. Kumar, S. Lee, L. Nardo, *et al.*, "T1rho and T2 relaxation times are associated with progression of hip osteoarthritis," *Osteoarthritis Cartilage,* vol. 24, pp. 1399-407, Aug 2016.
[113] W. Yao, N. Qu, Z. Lu, and S. Yang, "The application of T1 and T2 relaxation time and magnetization transfer ratios to the early diagnosis of patellar cartilage osteoarthritis," *Skeletal Radiol,* vol. 38, pp. 1055-62, Nov 2009.
[114] E. J. McWalter, G. Gold, M. T. Alley, and B. A. Hargreaves, "T2 and T2* Relaxometry in the Meniscus using a Novel, Rapid Multi-Echo Steady State Sequence," *Proceedings of the International Society for Magnetic Resonance in Medicine,* vol. 21, 2013.
[115] S. C. Deoni, T. M. Peters, and B. K. Rutt, "High-resolution T1 and T2 mapping of the brain in a clinically acceptable time with DESPOT1 and DESPOT2," *Magn Reson Med,* vol. 53, pp. 237-41, Jan 2005.
[116] A. Ramani, C. Dalton, D. H. Miller, P. S. Tofts, and G. J. Barker, "Precise estimate of fundamental in-vivo MT parameters in human brain in clinically feasible times," *Magn Reson Imaging,* vol. 20, pp. 721-31, Dec 2002.
[117] C. D. Sinclair, R. S. Samson, D. L. Thomas, N. Weiskopf, A. Lutti, J. S. Thornton, *et al.*, "Quantitative magnetization transfer in in vivo healthy human skeletal muscle at 3 T," *Magn Reson Med,* vol. 64, pp. 1739-48, Dec 2010.
[118] J. G. Sled and G. B. Pike, "Quantitative imaging of magnetization transfer exchange and relaxation properties in vivo using MRI," *Magn Reson Med,* vol. 46, pp. 923-31, Nov 2001.
[119] B. L. Insko E., "Mapping of the Radiofrequency Field," 1993.
[120] E. G. Baylon, "Isn't it Swell? The Effect of Osmotic Swelling on Articular Cartilage and Meniscal Fibrocartilage Mechanics and Diagnostic Approaches," Doctor of Philosophy, Mechanical Engineering, Stanford University, 2018.
[121] M. Freutel, A. M. Seitz, F. Galbusera, A. Bornstedt, V. Rasche, M. L. Knothe Tate, *et al.*, "Medial meniscal displacement and strain in three dimensions under compressive loads: MR assessment," *J Magn Reson Imaging,* vol. 40, pp. 1181-8, Nov 2014.
[122] T. Masuda, K. Sakuaue, and N. Yokoya, "Registration and Integration of Multiple Range Images for 3-D Model Construction," in *IEEE Computer Society Conference on Computer Vision and Pattern Recognition*, 1996.

[123] P. J. Besl and N. D. McKay, "A method for registration of 3-D shapes," *IEEE Transactions on Pattern Analysis and Machine Intelligence,* vol. 14, pp. 239-259, 1992.
[124] C. C. Gluer, G. Blake, Y. Lu, B. A. Blunt, M. Jergas, and H. K. Genant, "Accurate assessment of precision errors: how to measure the reproducibility of bone densitometry techniques," *Osteoporos Int,* vol. 5, pp. 262-70, 1995.
[125] A. Wang, V. Pedoia, F. Su, E. Abramson, M. Kretzschmar, L. Nardo, *et al.*, "MR T1rho and T2 of meniscus after acute anterior cruciate ligament injuries," *Osteoarthritis Cartilage,* vol. 24, pp. 631-9, Apr 2016.
[126] Z. A. Zarins, R. I. Bolbos, J. B. Pialat, T. M. Link, X. Li, R. B. Souza, *et al.*, "Cartilage and meniscus assessment using T1rho and T2 measurements in healthy subjects and patients with osteoarthritis," *Osteoarthritis Cartilage,* vol. 18, pp. 1408-16, Nov 2010.
[127] S. Nebelung, M. Tingart, T. Pufe, C. Kuhl, H. Jahr, and D. Truhn, "Ex vivo quantitative multiparametric MRI mapping of human meniscus degeneration," *Skeletal Radiol,* vol. 45, pp. 1649-1660, Dec 2016.
[128] S. E. Gullbrand, B. G. Ashinsky, J. T. Martin, S. Pickup, L. J. Smith, R. L. Mauck, *et al.*, "Correlations between quantitative T2 and T1rho MRI, mechanical properties and biochemical composition in a rabbit lumbar intervertebral disc degeneration model," *J Orthop Res,* vol. 34, pp. 1382-8, Aug 2016.
[129] M. A. Sweigart, C. F. Zhu, D. M. Burt, P. D. DeHoll, C. M. Agrawal, T. O. Clanton, *et al.*, "Intraspecies and interspecies comparison of the compressive properties of the medial meniscus," *Ann Biomed Eng,* vol. 32, pp. 1569-79, Nov 2004.
[130] M. D. Joshi, J. K. Suh, T. Marui, and S. L. Woo, "Interspecies variation of compressive biomechanical properties of the meniscus," *J Biomed Mater Res,* vol. 29, pp. 823-8, Jul 1995.
[131] S. A. Hacker, Woo, S.L., Wayne, J.S., Kwan, M.K., "Compressive Properties of the Human Meniscus," ed. Annual Meeting of the Orthopaedic Research Society, 1992, p. 627.
[132] C. S. Proctor, M. B. Schmidt, R. R. Whipple, M. A. Kelly, and V. C. Mow, "Material properties of the normal medial bovine meniscus," *J Orthop Res,* vol. 7, pp. 771-82, 1989.
[133] E. K. Danso, P. Julkunen, and R. K. Korhonen, "Poisson's ratio of bovine meniscus determined combining unconfined and confined compression," *J Biomech,* vol. 77, pp. 233-237, Aug 22 2018.
[134] R. S. Adler, S. D. Swanson, K. Doi, J. G. Craig, and A. M. Aisen, "The effect of magnetization transfer in meniscal fibrocartilage," *Magn Reson Med,* vol. 35, pp. 591-5, Apr 1996.
[135] K. Siorpaes, A. Wenger, K. Bloecker, W. Wirth, M. Hudelmaier, and F. Eckstein, "Interobserver reproducibility of quantitative meniscus analysis using coronal multiplanar DESS and IWTSE MR imaging," *Magn Reson Med,* vol. 67, pp. 1419-26, May 2012.

Appendix A – qMT Sequence

Table A.1 - qMT Sequence (Table Created by Lumeng Cui)

Sequence						
0 - Localizer						
1 - GRE_Fatsat						
2 - T1 map (qMT) Start	***No.***	***MTC***	***Flip angle***			
	2.1	OFF	30°			
	2.2	OFF	5°			
	2.3	OFF	10°			
	2.4	OFF	20°			
3 - qMT	***No.***	***MTC***	***MT duration***	***MT flip angle***	***MT frequency offset***	
	3.1	OFF	10.24 ms	N/A	N/A	
	3.2	ON	10.24 ms	142°	433 Hz	
	3.3	ON	10.24 ms	426°	433 Hz	
	3.4	ON	10.24 ms	142°	1087 Hz	
	3.5	ON	10.24 ms	426°	1087 Hz	
	3.6	ON	10.24 ms	142°	2732 Hz	
	3.7	OFF	10.24 ms	N/A	N/A	
	3.8	ON	10.24 ms	426°	2732 Hz	
	3.9	ON	10.24 ms	142°	6862 Hz	
	3.10	ON	10.24 ms	426°	6862 Hz	
	3.11	ON	10.24 ms	142°	17235 Hz	
	3.12	ON	10.24 ms	426°	17235 Hz	
	3.13	OFF	10.24 ms	N/A	N/A	
4 - T1 map (qMT) End	***No.***	***MTC***	***Flip angle***			
	4.1	OFF	30°			
	4.2	OFF	5°			
	4.3	OFF	10°			
	4.4	OFF	20°			
5 - B1 map (qMT)	***No.***	***MTC***	***Flip angle***			
	5.1	OFF	60°			
	5.2	OFF	120°			
6 - T2 map (MEDESS)	***No.***	***MTC***	***TR***	***TEs***		***ΔTE***
	6.1	OFF	17.85 ms	3.03, 6.92, 8.88, 12.72 ms		2 ms

Appendix B – Other Models for Curve Fitting

The models in section 3.4 were the ones that were seriously considered for use in this study, but below are other models that were investigated.

B.1 Ateshian Model [99]

The Ateshian model is one that is rooted in Mow's biphasic theory.

$$\sigma = 0.5H_{A0}\left(\frac{\lambda^2 - 1}{\lambda^{2\beta+1}}\right)e^{\beta(\lambda^2-1)}$$

Where H_{A0} = zero-strain aggregate modulus, λ = tissue stretch, and β = non-linear stiffening coefficient.

The Ateshian model includes measures of tissue stiffness, but is lacking in a permeability parameter, with perhaps β being the closest thing related to it. It also does not include the applied strain rate. These key parameters being missing eliminated this model from consideration.

B.2 Kwan Model [109]

This model also has its roots in Mow's biphasic theory, but it focuses on large strain values in excess of 40%.

$$\sigma = 0.25H_A(1 + 0.9\varepsilon)\left(\frac{(1+\varepsilon)^4 - 1}{(1+\varepsilon)^3}\right)$$

This model is notably missing both the applied strain rate and permeability parameters, and was therefore not used. I had also decided to go with lower strain tests which ruled out this model.

B.3 Périé Model [107]

The Périé model is a more in depth version of the Ateshian model, taking permeability into consideration.

$$\sigma = 0.5H_{A0}\frac{\lambda^2 - 1^2}{\lambda^{2\beta+1}}\ e^{\beta(\lambda^2-1)}$$

$$k_p = k_0\left(\frac{\lambda - \phi_0^s}{1 - \phi_0^s}\right)^2 e^{\frac{M(\lambda^2-1)}{2}}$$

Where k_0 = zero-strain permeability, ϕ_0^s = tissue's solid-volume fraction, and M = permeability coefficient.

The down-side of this approach is that it also neglects to implement the applied strain rate, but also that it requires measures of porosity, which would be difficult to measure.

B.4 Chin Model [96]

The Chin model has its origins in Mow's biphasic theory as well, but it is unclear as to what all of the terms in it represent.

$$\sigma = \sigma_\infty + H_A B_1 e^{-\frac{t}{\tau_1}}$$

$$\tau_1 = \frac{{h_0}^2}{\pi^2 D_M}$$

$$D_M = (H_A k_p (1 - \varepsilon))_{eq}$$

Where the author gave no indication as to what B_1 represents, and D_M = mechanical diffusivity.

This model neglects the applied strain rate as well, but it is also very difficult to get a proper fit using it.

B.5 Viscoelastic Models

Viscoelastic models include the Maxwell model, Kelvin-Voigt model, and SLS model. I was unable to get a fit using any of these models, and it is likely that they are over-simplifying what is physically occurring in stress-relaxation tests.

Appendix C – Curve Fitting Results

In this appendix I am showing the curve fits with the highest and lowest R-square values, as well as one curve fit from each meniscus. The curve fits shown should give the reader a good sense of the quality of curve fits for all of the data.

Highest and Lowest R-Square Fits:

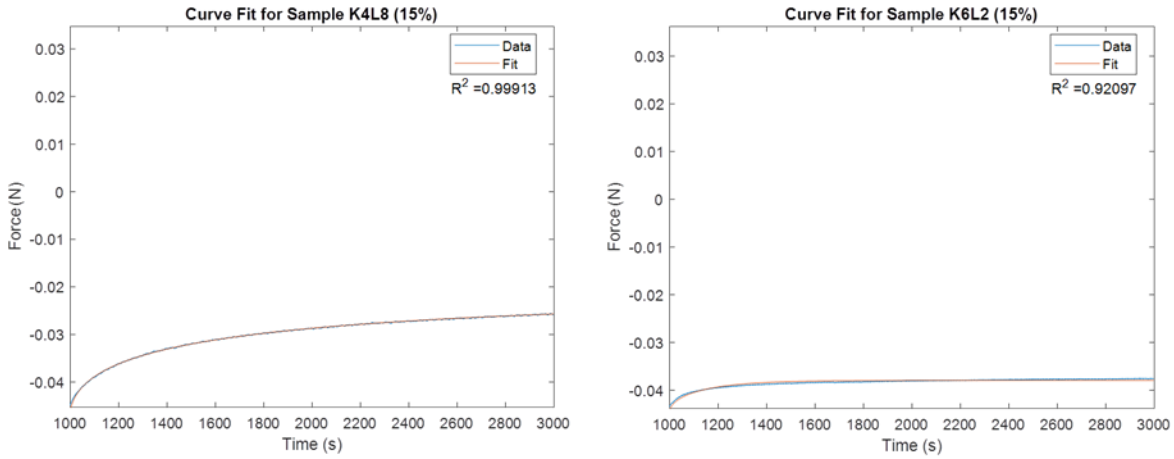

Figure C.1 - Highest and Lowest R-Square Fits

Other fits:

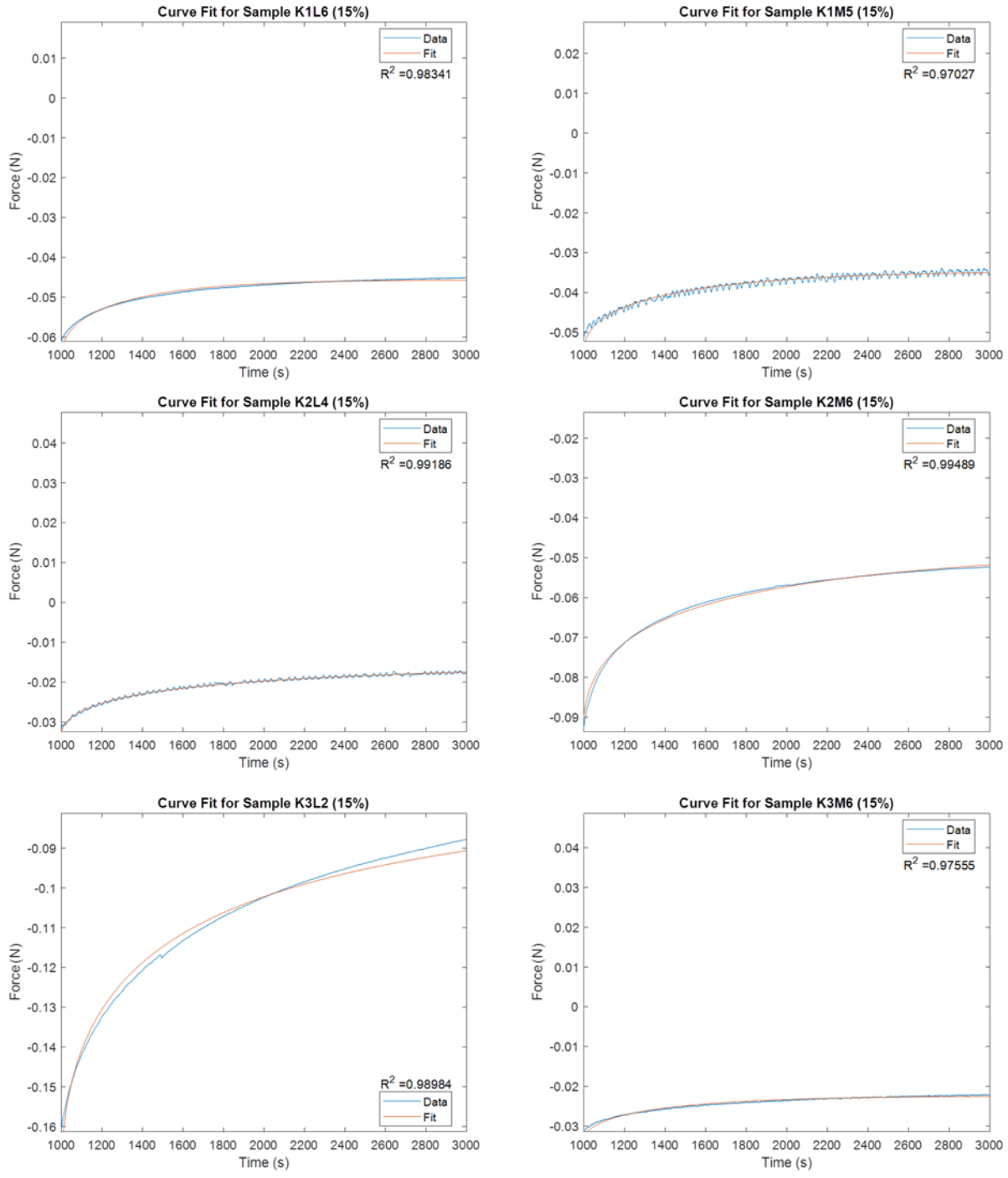

Figure C.2 - Example Curve Fits for Knees 1-3

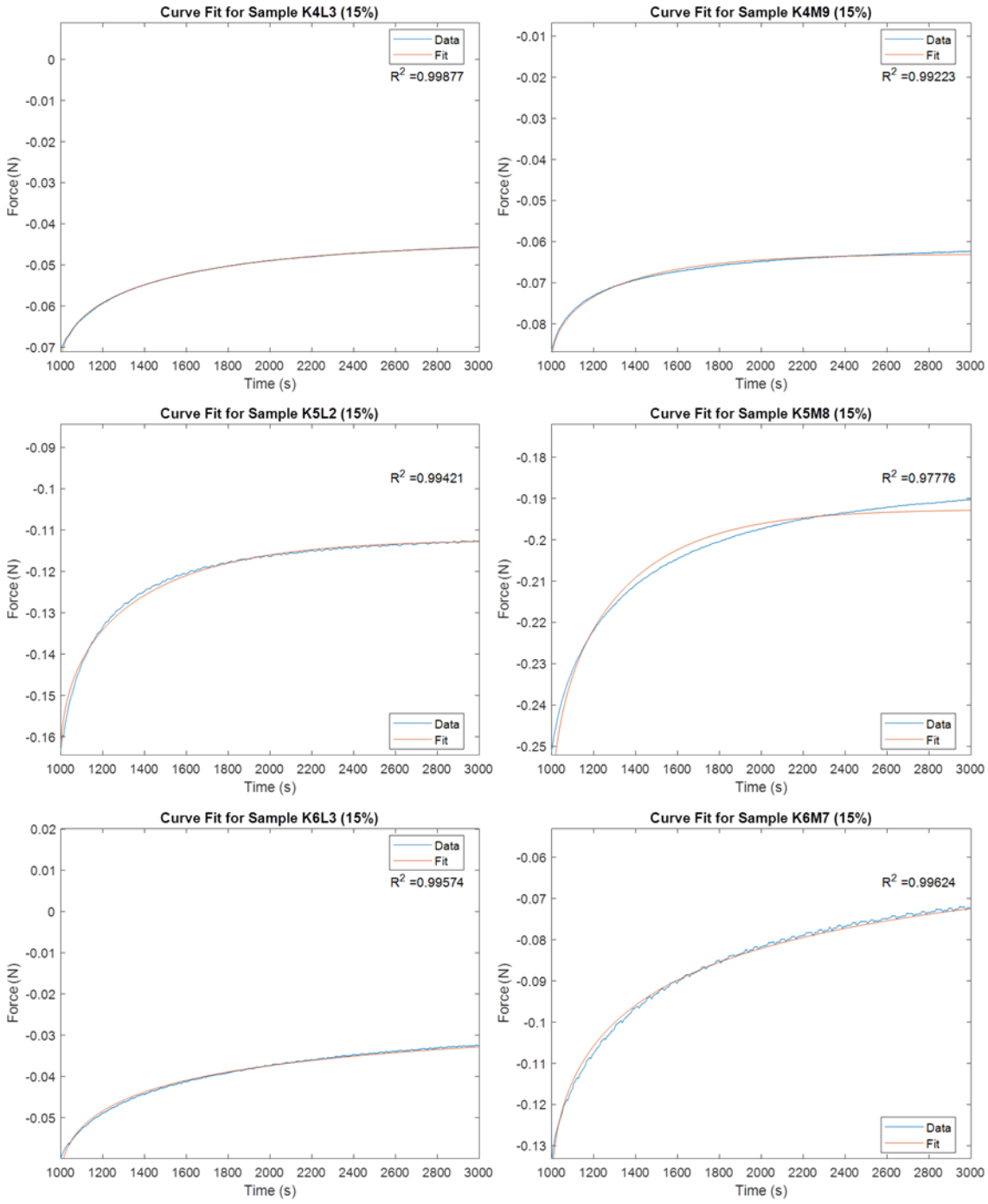

Figure C.3 - Example Curve Fits for Knees 4-6

Appendix D – Bursac Model's Sensitivity to Parameter n

$$\sigma = H_A \dot{\varepsilon}_0 t_0 - \frac{2\dot{\varepsilon}_0 h_0^2}{\pi^2 k_p} \sum_{n=1}^{\infty} \frac{e^{-\frac{nt}{\tau'}} - e^{-\frac{n^2(t-t_0)}{\tau'}}}{n^2}$$

$$\tau' = \frac{h_0^2}{\pi^2 H_A k_p}$$

The Bursac model shown above was implemented to model the experimental data in this study. It has a summation term, when n = 1 to infinity. This needed to be simplified to be useful in modeling the data. I modeled practice experimental data that was performed on bovine specimens where I sum up from n = 1 to increasing values until convergence was reached. I determined convergence when the R Square value did not change with increasing n with a precision of up to 4 decimal points. I have shown three example tests below and it can be seen that all of the R Square values converge by 25 terms. Some tests would show convergence sooner than others, but none needed more than 25 terms to converge. 25 terms was also the amount used in Bursac's study [108].

Table D.1 - Bursac Model n Sensitivity Example 1 (Note: A fit was not achieved for n=19 in this test.)

n	Sample	Date Tested	Material	h0 (mm)	diameter (mm)	Ha (kPa)	kp	R Square (n)	R Square (n) - R Square (n-1)	Computation Time (s)
1	BL4	14-Jun-18	Bovine Meniscus	2.56	4	33.166	2.48E-14	0.8293	-	2.04
2	BL4	14-Jun-18	Bovine Meniscus	2.56	4	31.594	2.16E-14	0.9447	0.1154	10.39
3	BL4	14-Jun-18	Bovine Meniscus	2.56	4	31.167	2.09E-14	0.9718	0.0271	9.09
4	BL4	14-Jun-18	Bovine Meniscus	2.56	4	31.03	2.07E-14	0.9811	0.0093	17.97
5	BL4	14-Jun-18	Bovine Meniscus	2.56	4	31.047	2.08E-14	0.985	0.0039	20.74
6	BL4	14-Jun-18	Bovine Meniscus	2.56	4	31.036	2.08E-14	0.987	0.002	24.86
7	BL4	14-Jun-18	Bovine Meniscus	2.56	4	31.111	2.10E-14	0.988	0.001	26.9
8	BL4	14-Jun-18	Bovine Meniscus	2.56	4	30.943	2.06E-14	0.9889	0.0009	34.79
9	BL4	14-Jun-18	Bovine Meniscus	2.56	4	31.064	2.09E-14	0.9892	0.0003	34.38
10	BL4	14-Jun-18	Bovine Meniscus	2.56	4	31.062	2.09E-14	0.9894	0.0002	37.17
11	BL4	14-Jun-18	Bovine Meniscus	2.56	4	31.061	2.09E-14	0.9896	0.0002	42.13
12	BL4	14-Jun-18	Bovine Meniscus	2.56	4	31.101	2.10E-14	0.9897	1E-04	44.56
13	BL4	14-Jun-18	Bovine Meniscus	2.56	4	30.936	2.06E-14	0.99	0.0003	52.51
14	BL4	14-Jun-18	Bovine Meniscus	2.56	4	30.936	2.06E-14	0.9901	1E-04	56.33
15	BL4	14-Jun-18	Bovine Meniscus	2.56	4	30.935	2.06E-14	0.9901	0	58.18
16	BL4	14-Jun-18	Bovine Meniscus	2.56	4	30.935	2.06E-14	0.9902	1E-04	63.74
17	BL4	14-Jun-18	Bovine Meniscus	2.56	4	30.935	2.06E-14	0.9902	0	67.45
18	BL4	14-Jun-18	Bovine Meniscus	2.56	4	30.935	2.06E-14	0.9902	0	70.41
19	BL4	14-Jun-18	Bovine Meniscus	2.56	4	-	-	-	#VALUE!	-
20	BL4	14-Jun-18	Bovine Meniscus	2.56	4	30.934	2.06E-14	0.9902	#VALUE!	76.97
21	BL4	14-Jun-18	Bovine Meniscus	2.56	4	30.934	2.06E-14	0.9903	1E-04	80.13
22	BL4	14-Jun-18	Bovine Meniscus	2.56	4	30.934	2.06E-14	0.9903	0	80.49
23	BL4	14-Jun-18	Bovine Meniscus	2.56	4	30.934	2.06E-14	0.9903	0	84.05
24	BL4	14-Jun-18	Bovine Meniscus	2.56	4	30.934	2.06E-14	0.9903	0	87.34
25	BL4	14-Jun-18	Bovine Meniscus	2.56	4	30.934	2.06E-14	0.9903	0	92.28

Table D.2 - Bursac Model n Sensitivity Example 2

n	Sample	Date Tested	Material	h0 (mm)	diameter (mm)	Ha (kPa)	kp	R Square (n)	R Square (n) - R Square (n-1)	Computation Time (s)
1	B2M2	8-Jul-18	Bovine Meniscus	2.84	4	13.828	2.03E-13	0.942	-	2.69
2	B2M2	8-Jul-18	Bovine Meniscus	2.84	4	13.855	2.03E-13	0.9468	0.0048	2.18
3	B2M2	8-Jul-18	Bovine Meniscus	2.84	4	13.861	2.22E-13	0.9472	0.0004	2.71
4	B2M2	8-Jul-18	Bovine Meniscus	2.84	4	13.863	2.23E-13	0.9472	0	3.17
5	B2M2	8-Jul-18	Bovine Meniscus	2.84	4	13.864	2.23E-13	0.9471	-1E-04	5.92
6	B2M2	8-Jul-18	Bovine Meniscus	2.84	4	13.865	2.24E-13	0.9471	0	4.06
7	B2M2	8-Jul-18	Bovine Meniscus	2.84	4	13.865	2.24E-13	0.9471	0	4.5
8	B2M2	8-Jul-18	Bovine Meniscus	2.84	4	13.865	2.24E-13	0.947	-0.0001	4.91
9	B2M2	8-Jul-18	Bovine Meniscus	2.84	4	13.866	2.24E-13	0.947	0	5.95
10	B2M2	8-Jul-18	Bovine Meniscus	2.84	4	13.866	2.24E-13	0.947	0	9.83
11	B2M2	8-Jul-18	Bovine Meniscus	2.84	4	13.866	2.24E-13	0.947	0	6.41
12	B2M2	8-Jul-18	Bovine Meniscus	2.84	4	13.866	2.24E-13	0.947	0	7.18
13	B2M2	8-Jul-18	Bovine Meniscus	2.84	4	13.866	2.24E-13	0.947	0	7.6
14	B2M2	8-Jul-18	Bovine Meniscus	2.84	4	13.866	2.24E-13	0.947	0	7.74
15	B2M2	8-Jul-18	Bovine Meniscus	2.84	4	13.866	2.24E-13	0.947	0	13.12
16	B2M2	8-Jul-18	Bovine Meniscus	2.84	4	13.866	2.24E-13	0.947	0	8.16
17	B2M2	8-Jul-18	Bovine Meniscus	2.84	4	13.866	2.24E-13	0.947	0	8.56
18	B2M2	8-Jul-18	Bovine Meniscus	2.84	4	13.866	2.24E-13	0.947	0	8.87
19	B2M2	8-Jul-18	Bovine Meniscus	2.84	4	13.866	2.24E-13	0.947	0	9.26
20	B2M2	8-Jul-18	Bovine Meniscus	2.84	4	13.866	2.24E-13	0.947	0	16.44
21	B2M2	8-Jul-18	Bovine Meniscus	2.84	4	13.866	2.24E-13	0.9469	-1E-04	9.79
22	B2M2	8-Jul-18	Bovine Meniscus	2.84	4	13.866	2.24E-13	0.9469	0	9.78
23	B2M2	8-Jul-18	Bovine Meniscus	2.84	4	13.866	2.24E-13	0.9469	0	10.13
24	B2M2	8-Jul-18	Bovine Meniscus	2.84	4	13.866	2.24E-13	0.9469	0	17.62
25	B2M2	8-Jul-18	Bovine Meniscus	2.84	4	13.866	2.24E-13	0.9469	0	17.88

Table D.3 - Bursac Model n Sensitivity Example 3

n	Sample	Date Tested	Material	h0 (mm)	diameter (mm)	Ha (kPa)	kp	R Square (n)	R Square (n) - R Square (n-1)	Computation Time (s)
1	B1L3	5-Jul-18	Bovine Meniscus	2.89	4	34.434	4.18E-14	0.946	-	1.72
2	B1L3	5-Jul-18	Bovine Meniscus	2.89	4	35.558	4.51E-14	0.9893	0.0433	2.64
3	B1L3	5-Jul-18	Bovine Meniscus	2.89	4	35.61	4.60E-14	0.9961	0.0068	3.23
4	B1L3	5-Jul-18	Bovine Meniscus	2.89	4	35.627	4.63E-14	0.9979	0.0018	3.81
5	B1L3	5-Jul-18	Bovine Meniscus	2.89	4	35.642	4.65E-14	0.9985	0.0006	4.64
6	B1L3	5-Jul-18	Bovine Meniscus	2.89	4	35.639	4.65E-14	0.9988	0.0003	5.34
7	B1L3	5-Jul-18	Bovine Meniscus	2.89	4	35.648	4.66E-14	0.9989	1E-04	6.04
8	B1L3	5-Jul-18	Bovine Meniscus	2.89	4	35.658	4.67E-14	0.9989	0	7.18
9	B1L3	5-Jul-18	Bovine Meniscus	2.89	4	35.657	4.67E-14	0.999	1E-04	8.54
10	B1L3	5-Jul-18	Bovine Meniscus	2.89	4	35.657	4.67E-14	0.999	0	8.13
11	B1L3	5-Jul-18	Bovine Meniscus	2.89	4	35.657	4.67E-14	0.999	0	8.87
12	B1L3	5-Jul-18	Bovine Meniscus	2.89	4	35.656	4.67E-14	0.999	0	9.63
13	B1L3	5-Jul-18	Bovine Meniscus	2.89	4	35.656	4.67E-14	0.999	0	10.36
14	B1L3	5-Jul-18	Bovine Meniscus	2.89	4	35.656	4.67E-14	0.999	0	11.12
15	B1L3	5-Jul-18	Bovine Meniscus	2.89	4	35.656	4.67E-14	0.999	0	11.28
16	B1L3	5-Jul-18	Bovine Meniscus	2.89	4	35.656	4.67E-14	0.999	0	11.63
17	B1L3	5-Jul-18	Bovine Meniscus	2.89	4	35.666	4.68E-14	0.999	0	12.05
18	B1L3	5-Jul-18	Bovine Meniscus	2.89	4	35.666	4.68E-14	0.999	0	12.01
19	B1L3	5-Jul-18	Bovine Meniscus	2.89	4	35.666	4.68E-14	0.999	0	13.03
20	B1L3	5-Jul-18	Bovine Meniscus	2.89	4	35.666	4.68E-14	0.999	0	12.24
21	B1L3	5-Jul-18	Bovine Meniscus	2.89	4	35.666	4.68E-14	0.999	0	13.36
22	B1L3	5-Jul-18	Bovine Meniscus	2.89	4	35.666	4.68E-14	0.999	0	14.41
23	B1L3	5-Jul-18	Bovine Meniscus	2.89	4	35.666	4.68E-14	0.999	0	15.28
24	B1L3	5-Jul-18	Bovine Meniscus	2.89	4	35.666	4.68E-14	0.999	0	14.4
25	B1L3	5-Jul-18	Bovine Meniscus	2.89	4	35.666	4.68E-14	0.999	0	13.45

Appendix E – Additional Correlation Scatter Plots

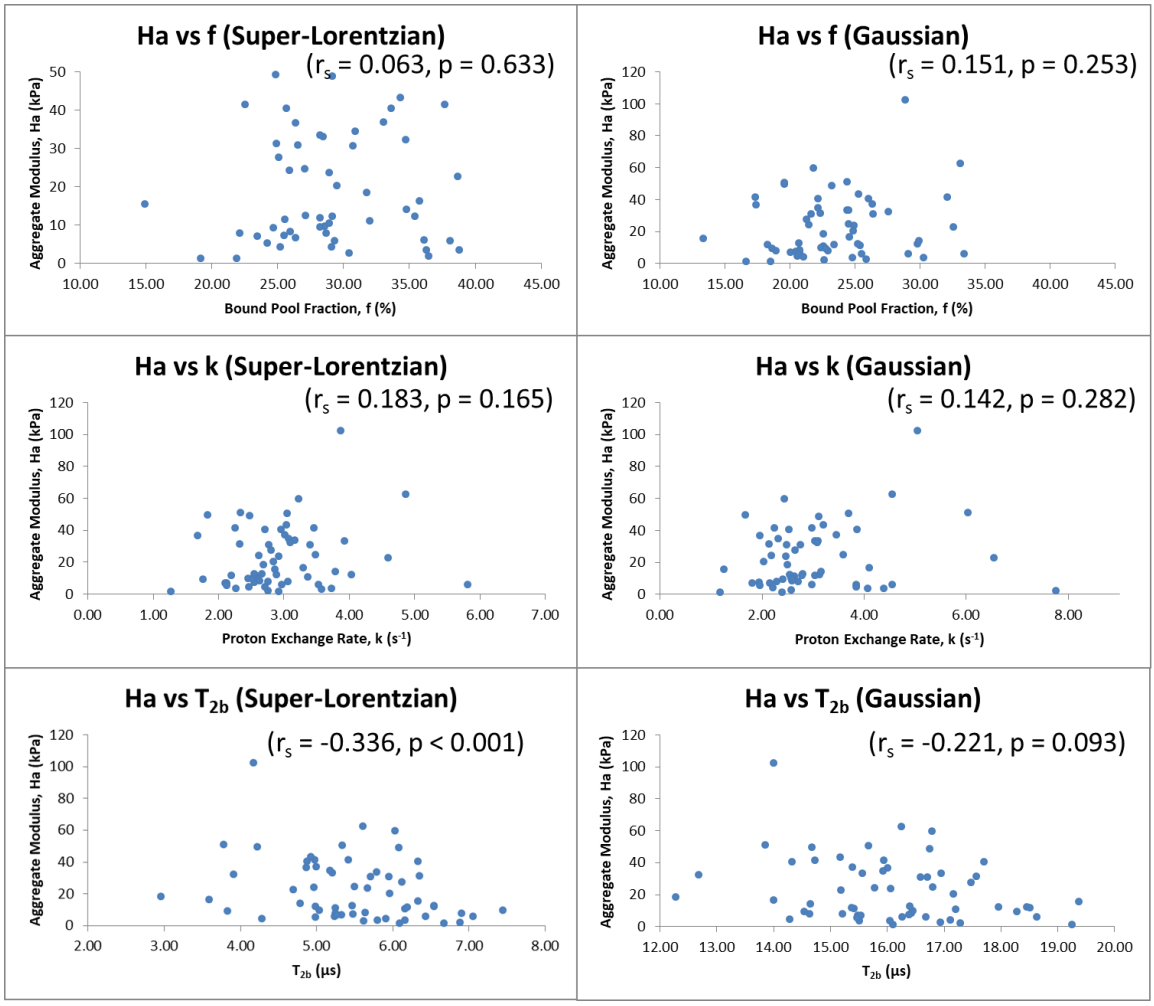

Figure E.1 - qMT Metrics Predicting Aggregate Modulus

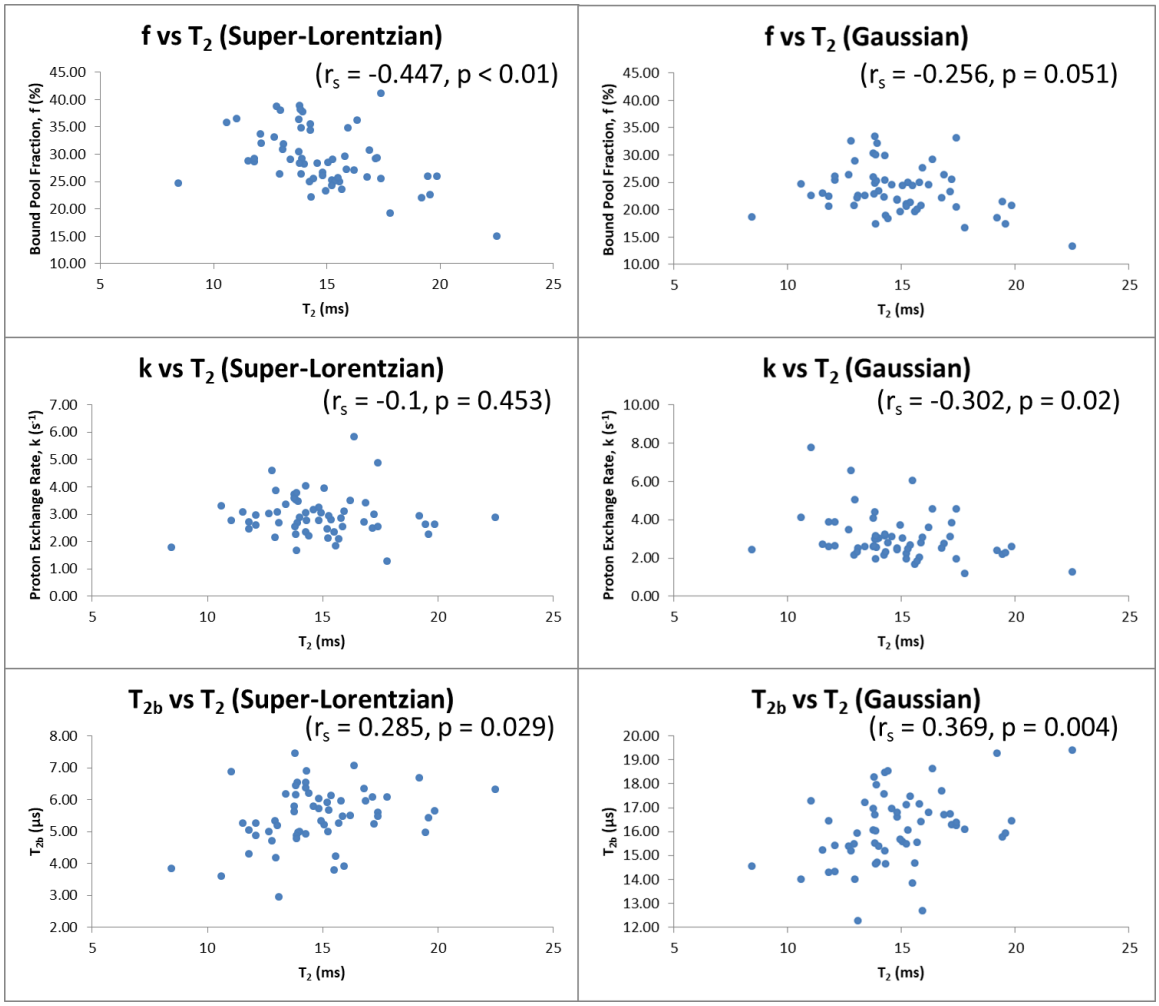

Figure E.2 - T2 Correlating with qMT Parameters

Appendix F – qMT Maps of Each Knee

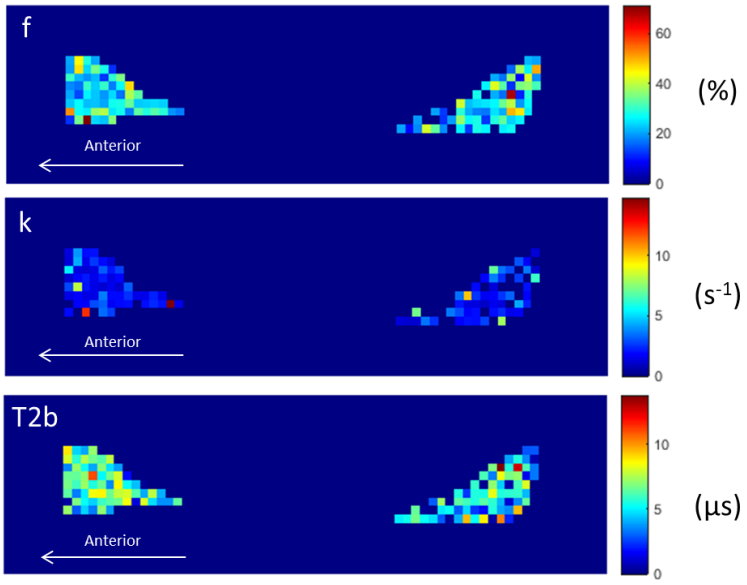

Figure F.1 - qMT Parameter Maps (Super-Lorentzian Line Shape) of the Lateral Meniscus of specimen K01 viewed in the sagittal direction.

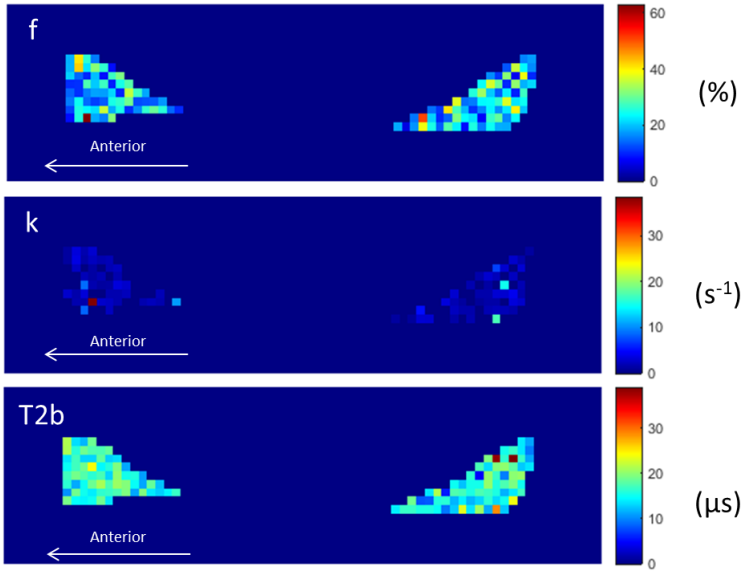

Figure F.2 - qMT Parameter Maps (Gaussian Line Shape) of the Lateral Meniscus of Specimen K01 viewed in the sagittal direction.

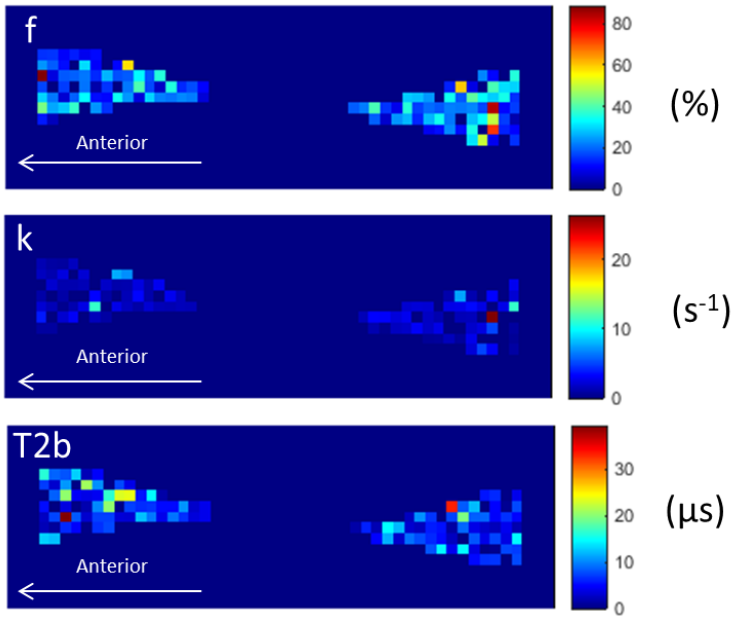

Figure F.3 - qMT Parameter Maps (Super-Lorentzian Line Shape) of the Lateral Meniscus of specimen K02 viewed in the sagittal direction.

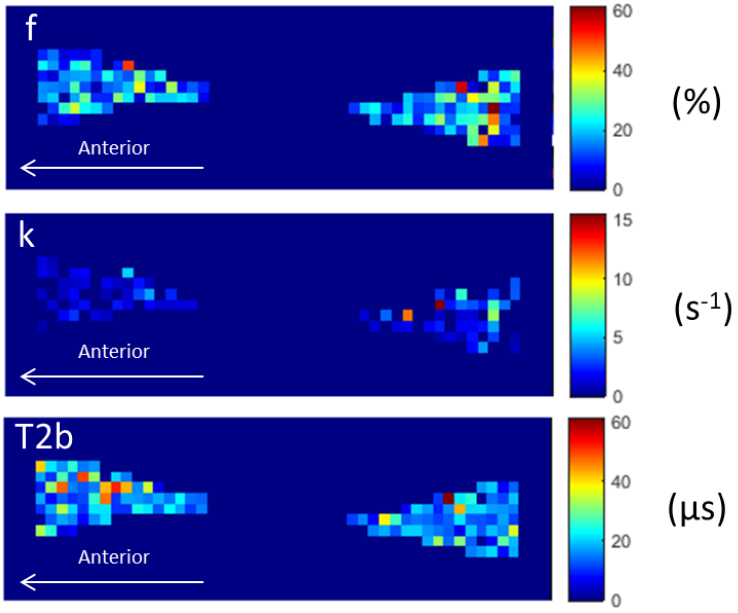

Figure F.4 - qMT Parameter Maps (Gaussian Line Shape) of the Lateral Meniscus of specimen K02 viewed in the sagittal direction.

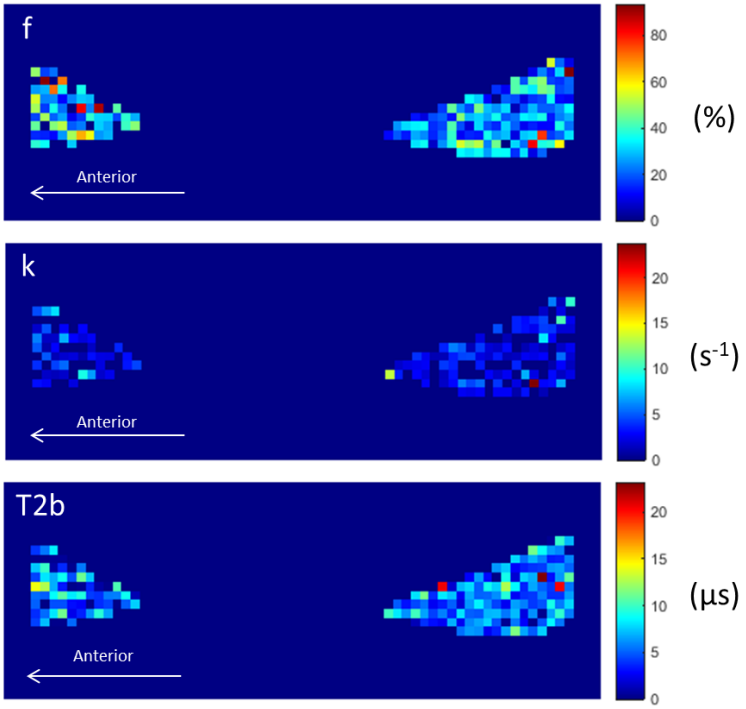

Figure F.5 - qMT Parameter Maps (Super-Lorentzian Line Shape) of the Medial Meniscus of specimen K03 viewed in the sagittal direction.

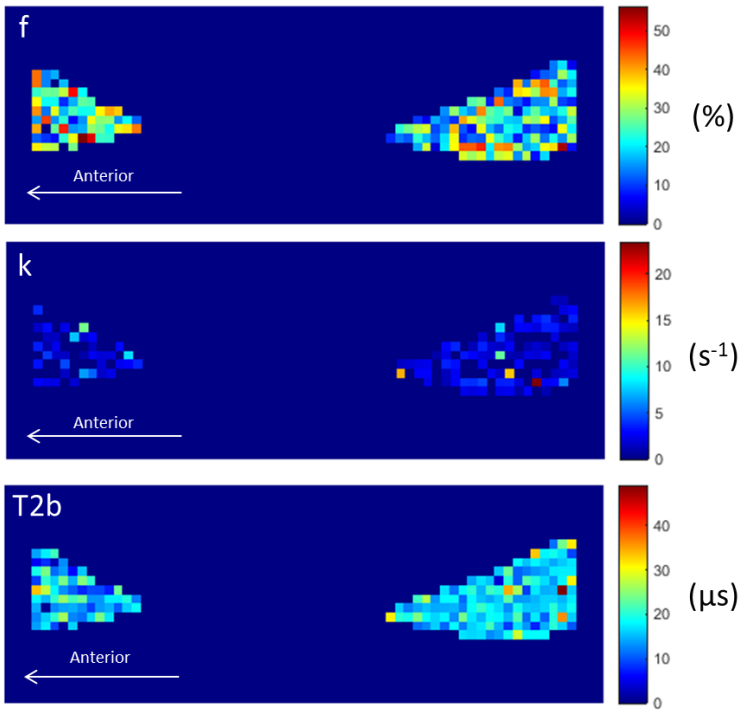

Figure F.6 - qMT Parameter Maps (Gaussian Line Shape) of the Medial Meniscus of specimen K03 viewed in the sagittal direction.

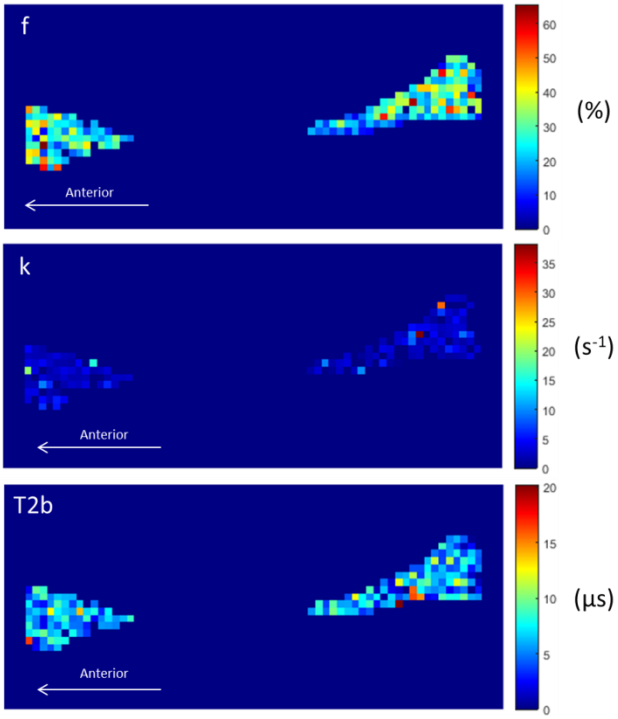

Figure F.7 - qMT Parameter Maps (Super-Lorentzian Line Shape) of the Medial Meniscus of specimen K04 viewed in the sagittal direction.

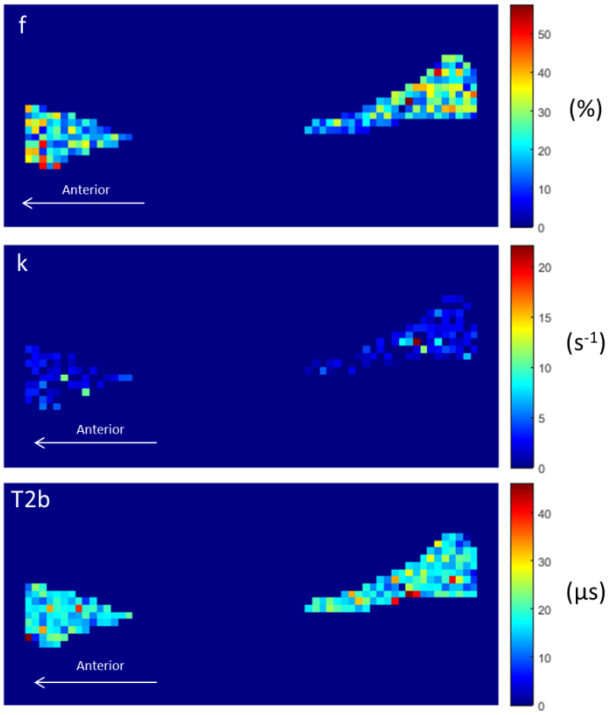

Figure F.8 - qMT Parameter Maps (Gaussian Line Shape) of the Medial Meniscus of specimen K04 viewed in the sagittal direction.

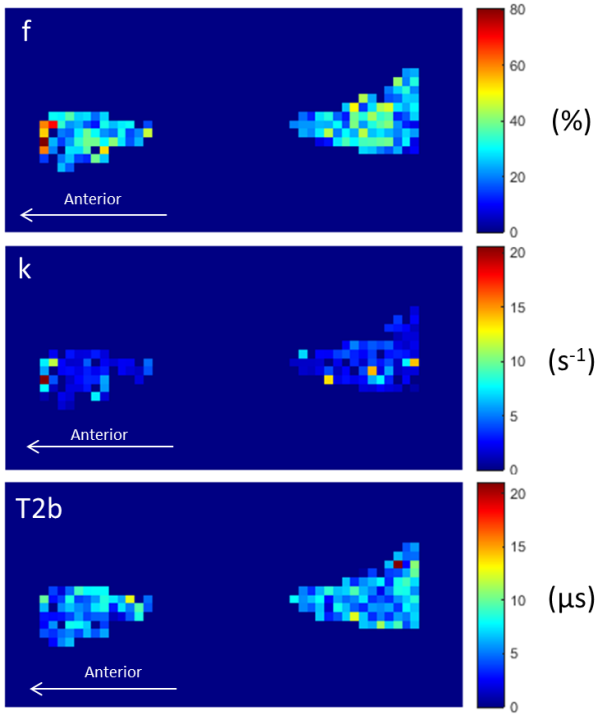

Figure F.9 - qMT Parameter Maps (Super-Lorentzian Line Shape) of the Lateral Meniscus of specimen K05 viewed in the sagittal direction.

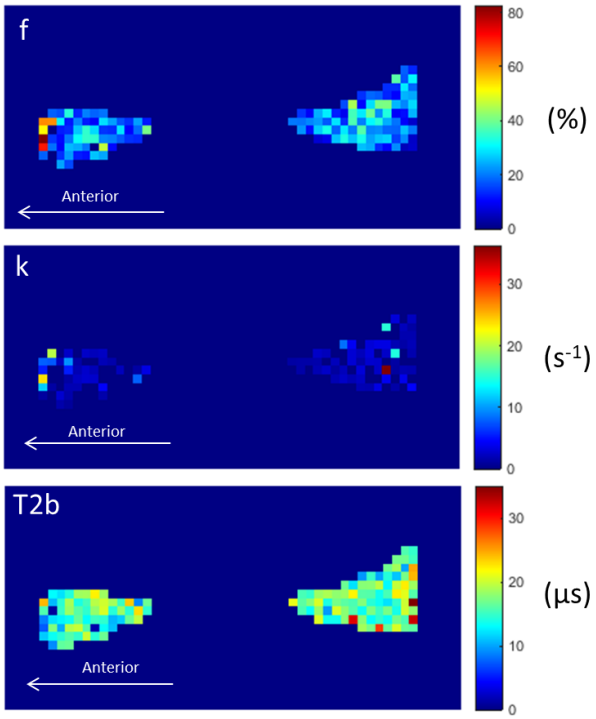

Figure F.10 - qMT Parameter Maps (Gaussian Line Shape) of the Lateral Meniscus of specimen K05 viewed in the sagittal direction.

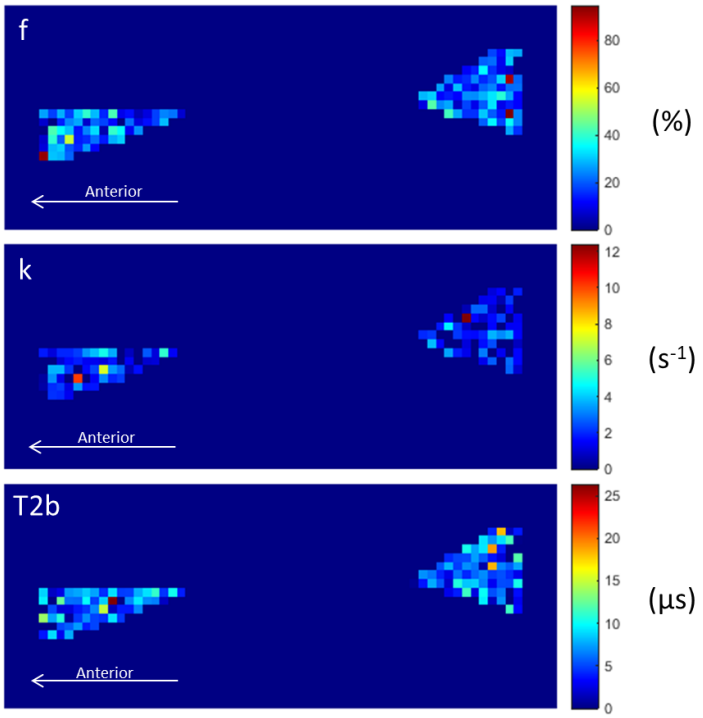

Figure F.11 - qMT Parameter Maps (Super-Lorentzian Line Shape) of the Lateral Meniscus of specimen K06 viewed in the sagittal direction.

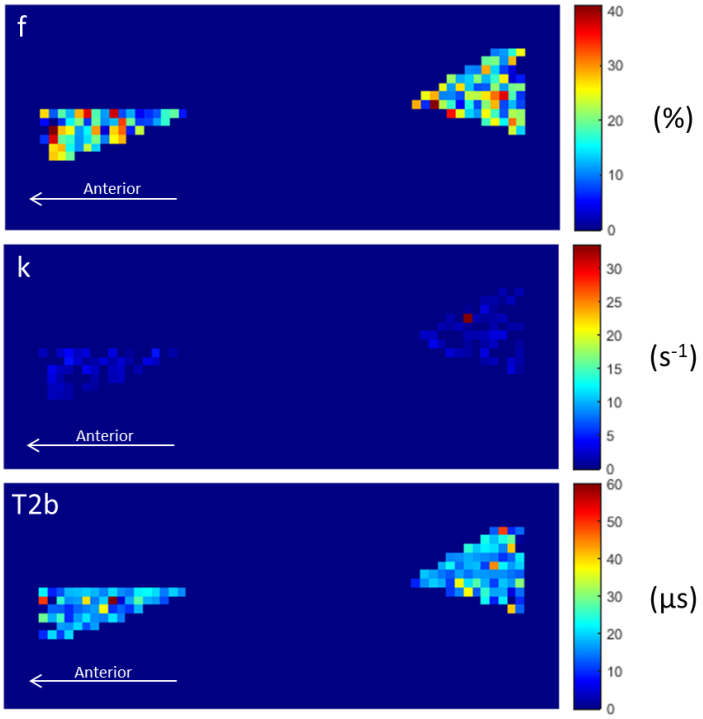

Figure F.12 - qMT Parameter Maps (Gaussian Line Shape) of the Lateral Meniscus of specimen K06 viewed in the sagittal direction.

Appendix G – qMT Line Shapes

Gaussian Line Shape [116]:

$$R = \omega^2 \sqrt{\frac{\pi}{2}} T_{2b} \left(e^{\frac{(-2\pi \Delta f T_{2b})^2}{2}} \right)$$

Where R = the rate of loss of magnetization,

ω = MT flip angle, and

Δf = offset frequency.

Super-Lorentzian Line Shape [116]:

$$R = \omega^2 \pi \left(\int_0^{\frac{\pi}{2}} d\theta sin\theta \sqrt{\frac{2}{\pi}} \frac{T_2}{3cos^2\theta - 1} e^{-2\left(\frac{2\pi \Delta f T_2}{3cos^2\theta - 1}\right)^2} \right)$$

Where θ = the angle between the external magnetic field and the axis of molecular orientation.

Appendix H – Ethics Certificate

UNIVERSITY OF SASKATCHEWAN

Biomedical Research Ethics Board (Bio-REB) 24-Jul-2020

Certificate of Re-Approval

Ethics Number:	16-158
Principal Investigator:	Emily McWalter
Department:	Department of Mechanical Engineering
Locations Where Research Activities are Conducted:	Canadian Light Source, Canada College of Kinesiology, Canada Royal University Hospital, Saskatoon, Canada
Student(s):	Alvaro Espinosa Maldonado Brennan Berryman Chelsey Thorson Ibukunoluwa Elebute Kirstin Olsen Lumeng Cui Madeline Martel
Funder(s):	Canada Foundation for Innovation College of Engineering Innovation Saskatchewan Natural Sciences and Engineering Research Council of Canada Office of the Vice-Provost, Faculty Relations
Sponsor:	
Title:	MRI and Mechanical Testing of Cadaver Knee Specimens
Protocol Number:	
Approval Effective Date:	16/07/2020
Expiry Date:	16/07/2021
Acknowledgment Of:	
Review Type:	Delegated Review
IRB Registration Number:	

* This study, inclusive of all previously approved documents, has been re-approved until the expiry date noted above

CERTIFICATION

The University of Saskatchewan Biomedical Research Ethics Board (Bio-REB) has reviewed the above-named project.The project is acceptable on scientific and ethical grounds. The principal investigator has the responsibility for any other administrative or regulatory approvals that may pertain to this project, and for ensuring that the authorized project is carried out according to governing law. This approval is valid for the specified period provided there is no change to the approved project.

FIRST TIME REVIEW AND CONTINUING APPROVAL

The University of Saskatchewan Research Ethics Boards review above minimal projects at a full-board (face-to-face) meeting. If a project has been reviewed at a full board meeting, a subsequent project of the same protocol may be reviewed through the delegated review process. Any research classified as minimal risk is reviewed through the delegated (subcommittee) review process. The initial Certificate of Approval includes the approval period the REB has assigned to a study. The Status Report form must be submitted within one month prior to the assigned expiry date. The researcher shall indicate to the REB any specific requirements of the sponsoring organizations (e.g. requirement for full-board review and approval) for the continuing review process deemed necessary for that project.

REB ATTESTATION

In respect to clinical trials, the University of Saskatchewan Research Ethics Board complies with the membership requirements for Research Ethics Boards defined in Part 4 of the Natural Health Products Regulations and Part C Division 5 of the Food and Drug Regulations and carries out its functions in a manner consistent with Good Clinical Practices. Members of the Bio-REB who are named as investigators, do not participate in the discussion related to, nor vote on such studies when presented to the Bio-REB. This approval and the views of this REB have been documented in writing. The University of Saskatchewan Biomedical Research Ethics Board is constituted and operates in accordance with the current version of the Tri-Council Policy Statement: Ethical Conduct for Research Involving Humans (TCPS 2 2018).

Digitally Approved by Dr. Gordon McKay, Ph.D.
Chair, Biomedical Research Ethics Board
University of Saskatchewan